CHANNEL MODELING, ESTIMATION AND EQUALIZATION IN WIRELESS COMMUNICATION

A Dissertation

presented to

the Faculty of the Graduate School

University of Missouri-Columbia

In Partial Fulfillment

of the Requirements for the Degree

Doctor of Philosophy

by

SANG-YICK LEONG

Dr. Chengshan Xiao, Dissertation Supervisor

MAY 2005

The undersigned, appointed by the Dean of the Graduate School, have examined the dissertation entitled

CHANNEL MODELING, ESTIMATION AND EQUALIZATION IN WIRELESS COMMUNICATION

presented by Sang-Yick Leong

a candidate for the degree of Doctor of Philosophy

and hereby certify that in their opinion it is worth acceptance.
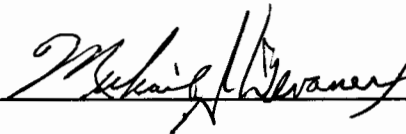
Dr. Chengshan Xiao

Dr. Curt H. Davis

Dr. Dominic K.C. Ho

Dr. Michael J. Devaney

Dr. Yunxin Zhao

ACKNOWLEDGMENTS

I extend my gratitude to the following person and parties for the completion of this dissertation:

Academically, I am indebted to my advisor, Dr. Chengshan Xiao, for providing me the opportunity to do research under his guidance. I would like to sincerely thank for his intellectual guidance and generous encouragement. I would also acknowledge my thanks to my Ph. D dissertation examining committee members, Dr. Curt Davis, Dr. Michael Devaney, Dr. Dominic K.C. Ho and Dr. Yunxin Zhao for their effort and valuable advices in reviewing my dissertation.

I would also like to thank Dr. J.C. Olivier and Dr. Zheng (Rosa) for their many valuable comments in reviewing the journal and conference papers.

I would like to thank Mrs. Betty Barfield, Mrs. Tami Beatty and Mrs. Kelly Scott for always lending a helping hand.

I would like to thank all the students in the Communication Lab for their assistances in facilitating the research.

Finally, I wish to acknowledge my thanks to both sides of my family for all their love and support. I particularly would like to thank my dearest parents for their guidance and support in my entire life and what they have done for me that I cannot possibly count them all. I would also like to thank my wife Kah-Ping Lee for enduring these last few years with generous love and support.

CHANNEL MODELING, ESTIMATION AND EQUALIZATION IN WIRELESS COMMUNICATION

Sang-Yick Leong

Dr. Chengshan Xiao, Dissertation Supervisor

ABSTRACT

Channel modeling, estimation and equalization are discussed throughout this dissertation. Relevant research topics are first studied at the beginning of each chapter and the new methods are proposed to improve the system performance. MLSE is an optimum equalizer for all the case. However, due to its computational complexity, it is impractical for today technologies in third generation wireless communication. Thus, a suboptimum equalizer so-called perturbation equalizer is proposed, which outperforms the RSSE equalizer in the sense of bit error rate or computational complexity. In order to improve the system performance dramatically, the iterative equalization algorithm is implemented. It has been shown that the turbo equalization using the trellis based *Maximum A Posteriori* equalizer is a powerful receiver that yielding the optimum system performance. Unfortunately, due to its exhausted computational complexity, a suboptimal equalizer is required. An improved DFE algorithm, which only requires low computational complexity, is proposed for turbo equalization. The promising simulation results indicate that the proposed equalizer provides significant improvement in bit error rate while compared to the conventional DFE algorithm. Prior to channel equalization, channel estimation enable us to extract the necessary channel information from the pilot symbols for equalizers. Least-squares algorithm is a promising estimation algorithm providing the channel is time-invariant in a given period. Based on the derivations, we show that the channel is no longer constant and a new least-squares based algorithm is proposed to estimate the channel accurately. Simulation results convince us that the

new algorithm provides the equalizer more reliable information. Besides, antenna diversity is another promising technique implemented practically to improve the system performance provided that the channels of antennas are not correlated. A new three dimensional multiple-input multiple-output abstract model is proposed for the investigation and understanding of the correlation of fading channel. The new model allows us to consider the channel correlation of which the mobile stations receive the incoming waves from any directions and angle spreads. Based on this abstract model, the closed form and mathematical tractable formula is derived for space-time correlation function. The new function can be further simplified other known special cases.

LIST OF TABLES

LIST OF FIGURES

TABLE OF CONTENTS

To the memory of my father Kwang Fong Leong,

my mum Ai Mui Tan, my wife Kah Ping Lee,

and our child Yick Ren Leong

Chapter 1

Introduction

In early 1980s, the first generation cellular and cordless phone systems were introduced where analog FM technology is implemented to carry voice services only. Then, the second generation digital cellular radio networks were introduced to improve the spectral efficiency and voice quality in early 1990s. Basically, the cellular networks on air can be divided into two major categories given as Time Division Multiple Access (TDMA) and Code Division Multiple Access (CDMA). The European standard Global System for Mobile Communication (GSM), which is the world leader of second generation communication systems, is designed based on TDMA concept operating at 900 MHz, 1800 MHz and 1900 MHz. In addition, the digital PCS IS-136 which is the extension of IS-54 in United States, and Personal Digital Cellular (PDC) in Japan are also based on TDMA [3]. Since the introduction of digital cellular radios networks, the service providers were facing the exponential growth of subscriber numbers in wireless communication systems. Predicted from the trend of growth, the evolution of second-generation cellular systems is necessary. Based on the 2-G background, the third generation wireless systems were introduced that allowing the mobile users to have larger bandwidth for new features such as web browsing, video, image and other multimedia services. Intend to provide quality of service in all types of requirements for future wireless communications, extensive researches are in progress for fourth and later generation of communication systems.

The wireless communication channels consist of various types of impairments such

as delay spread, fading and Doppler spread etc. Because of the multipath propagation in the channel, it introduces the delay spread that causing interference between the adjacent symbols known as intersymbol interference (ISI). Thus, an equalizer is employed at the receiver to mitigate the combined effect of ISI and noise. According to the literatures in the past, there are two broad categories of equalizers; symbol-by-symbol equalizers and sequence estimators. The symbol-by-symbol equalizers make the decision on the received sequence symbol-by-symbol, while the sequence estimators make decisions on the sequences after a period of observation on the received sequence. In general, the sequence estimators has higher computational complexity than symbol-by-symbol equalizer but offer better performance. The chapter starts by a brief introduction on maximum likelihood sequence estimation (MLSE), delayed decision feedback sequence estimation (DDFSE) and reduced-state sequence estimation (RSSE). The MLSE proposed by Forney is recognized as the optimum equalizer for the detection of digital signals corrupted by ISI and additive white Gaussian noise. However, its complexity grows exponentially with the size of signal constellation and the length of channel impulse response. Thereby, research of reduce complexity sequence estimators are undertaken to retain most of the MLSE performance. Duel-Hallen [8] and Eyuboglu [6], respectively proposed the DDFSE and reduced state sequence estimation (RSSE). The reduced-state equalizers truncate the channel impulse response into a manageable length for Viterbi algorithm to search the branch metrics throughout the sequence. Next, we introduce the structure of third generation EDGE cellular system where 8-PSK modulation is employed, and conclude that the MLSE is prohibited due to its computational complexity. An alternative method is proposed to reduce complexity through iteratively minimizing the Euclidean distance between the detected signal sequence and the received signal sequence with neighbor symbol perturbation. Then, the simulation results comparing our method with RSSE method are presented.

In 1993, the concept of turbo coding was proposed by Berrou,Glavieux and Thiti-majashima, who reported that the coding gain approaches to Shannon limit prediction. Due to this reason, the research of "Turbo Principle" was carried out in the area of channel equalization in order to improve the system performance. In chapter 3, the so-called "Turbo Equalization" concept is introduced. At the beginning of the chapter, the definition of the system model and the principle of turbo equalization are given. Using a trellis-based channel equalizer and channel decoder, turbo equalization improves the bit error rate (BER) performance tremendously. However, given that large alphabet modulation is employed in the system with multipath channels causing significant inter-symbol interference, the optimal maximum *a posteriori* probability (MAP) equalizer is prohibitively complex, and thus the sub-optimum equalizers such as decision feedback equalizer (DFE) have to be considered. We firstly show that the gain in BER offered by the iterative receiver when using a conventional DFE is however limited by the error propagation. To minimize the error propagation and increase the reliability of the ex-trinsic information, an improved decision feedback equalizer algorithm is introduced for turbo equalization. The novel low complexity DFE algorithm detects the symbols using the extra metric and the feedback symbol from previous iteration. This simple method is accomplished by extracting and delivering more reliable *extrinsic* information as *a priori* information for the detection and decoding steps. Both the analytical and simulation results indicate that the improved DFE algorithm has better BER performance (about 1dB improvement) over the conventional DFE in turbo equalization.

As described above, ISI caused by multipath propagation can be mitigated by the channel equalizer providing the receiver has the knowledge of the channel. Therefore, the system performance is also mainly determined by the accuracy of the channel esti-mation. In a conventional GSM receiver, the known training sequence is inserted in the middle of each slot are used to extract the channel impulse response with the received se-quence. Chapter 4, the derivation of least-squares estimation is provided at the beginning

to show that when large number of information are provided, least-squares estimation approaches the optimum Wiener solution [24]. Furthermore, a recursive least-squares estimation algorithm is introduced to update the estimated channel parameters while new information is available. Next, we presents the channel estimation in 8-PSK with time-varying and frequency-selective fading channels. It is shown that the fast fading channel during a selected slot in the EDGE system can be modeled as a linear function of time, and a least-squares based algorithm is proposed and combined with a modified slot structure to estimate the fading channel. For typical channel profiles of the EDGE system, the channel impulse response is not in its minimum phase form, thus cannot be directly used in computationally efficient equalizers, such as delayed decision feedback sequence estimation or reduced state sequence estimation. To overcome this problem, a Cholesky decomposition based method is introduced to transform the estimated channel impulse response energy to the first few taps.

In previous chapters, the system performance is improved by channel estimation and equalization in single base station and single mobile station antennas system. Unlike equalization and estimation, diversity is a low cost powerful receiver technique that improves the link significantly. For instance, there are two antennas separated by a distance at the base station. While the transmitted signal is distorted by the multi-path Rayleigh fading channels, one radio path might undergo a deep fade and another independent path might have a strong signal. Thus, the average signal to noise ratio (SNR) at the receiver are improved. It is important to note that, the diversity technique assumes that the transmitted signals undergo independent radio paths to two separated antennas. However, in practice, the optimum relative antenna separation and placement may not feasible due to space limitations and other practical constraints. Consequently, the channels of the antennas are correlated and the improvement of the performance degrades. In Chapter 5, we investigate the correlation of channels in multiple trans-mit and receive antennas in details. An overview of various Rayleigh fading channel

model is given at the beginning of the chapter. Clarke's model is a commonly used two dimensional isotropic scattering that the mobile station antenna receives the arriving plane wave from all directions with equal probability. Base on the one-ring scattering, Shiu proposed a two dimensional multiple-input multiple output (MIMO) model and derived a new correlation functions for the subchannels based on this model. In paper [63], the authors argued that the waves are not necessarily transmitted on two-dimensional. Thereby, a 3-D cylinder model was proposed to describe the scattering environment that encloses the mobile station. Based on this background, a space-time correlation functions between the links of MIMO Rayleigh fading channels are derived using a new three-dimensional (3-D) cylinder scattering model. Closed form, mathematically tractable formulas are obtained for the space-time correlation functions for general MIMO systems where the base station and mobile station antennas may be arranged in 3-D space. In the discussion of special cases such as 2-D Clarke's model, single input multiple output (SIMO) and multiple-input single-output (MISO) in two dimensional and three dimensional, the new correlated function is simplified to others known formulas from the literatures. Moreover, it is shown that the correlation functions computed by the 3-D cylinder model are of significant difference than those of the conventional 2-D Clarke's isotropic scattering model for vertically placed antennas. Finally, the summary of the research and future works are provided in Chapter 6.

Chapter 2

Perturbation Equalization for
8-PSK EDGE Cellular System

2.1   Introduction

Recently, there are two major approaches to third-generation (3G) mobile communication systems. The first one is universal mobile telecommunications service (UMTS), which is based on wideband code division multiple access (WCDMA), while the other one is Enhanced Data rates for GSM Evolution, which is an evolution of the existing time-division multiple access (TDMA) standards GSM and Industry Standard 136 (IS-136) [2]. In order to keep backward compatibility with the worldwide successful second generation GSM and IS-136 mobile systems, EDGE has an almost identical time frame and slot structure as GSM, but it can achieve significantly higher data rates and spectral efficiency compared to existing data services in GSM and TDMA IS-136, because it improves the spectral efficiency by employing the 8-PSK modulation. A simplified baseband system block diagram of EDGE with 8-PSK modulation is given in Fig. 2.1.

As depicted in Fig. 2.1, when the modulated data and training symbols are transmitted to the receiver, the transmitted signals will be distorted by multipath multiplicative fading and additive noise in the mobile radio channel. To take a close look at the mobile channel, the typical EDGE channel propagation models for Typical Urban (TU) and
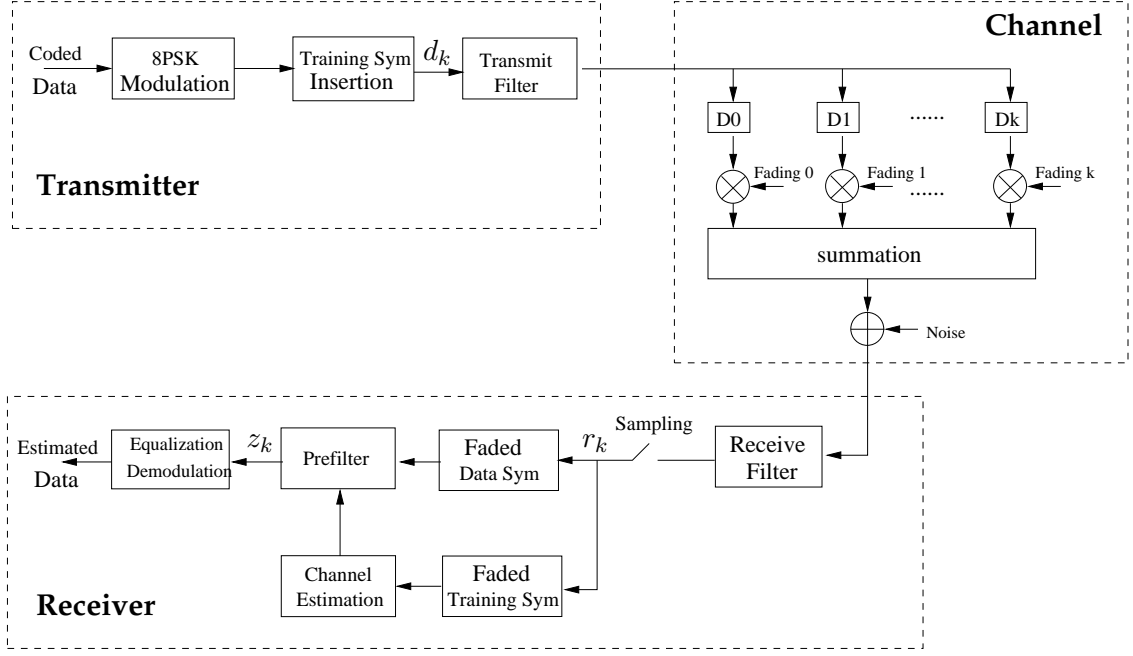
Figure 2.1: Baseband system block diagram

Hilly Terrain (HT) environments are depicted in Fig. 2.2 and 2.3, respectively, which shows individual path delay and its average power. Assume that there is no line-of-sight (LOS) case, each path represents an independent Rayleigh fading. Given that the EDGE symbol interval to be 3.69μs, we can conclude that the transmitted signals undergo severe intersymbol interference (ISI) in the HT and LU environments. As a consequence, a reliable and effective channel estimation and channel equalizer must be reside in both base stations and mobile handsets for successful detection of the information data.

2.2 Channel Equalizer

The channel equalizer is designed to jointly eliminate the ISI and estimate the transmitted symbol sequence at the receiver. Optimum equalization, i.e., maximum-likelihood sequence estimation (MLSE) [5] based on Viterbi algorithm (VA) is a promising technique used in GSM with binary Gaussian minimum-shift keying (GMSK) modulation scheme. Nevertheless, the optimum algorithm, which minimizing the probability of
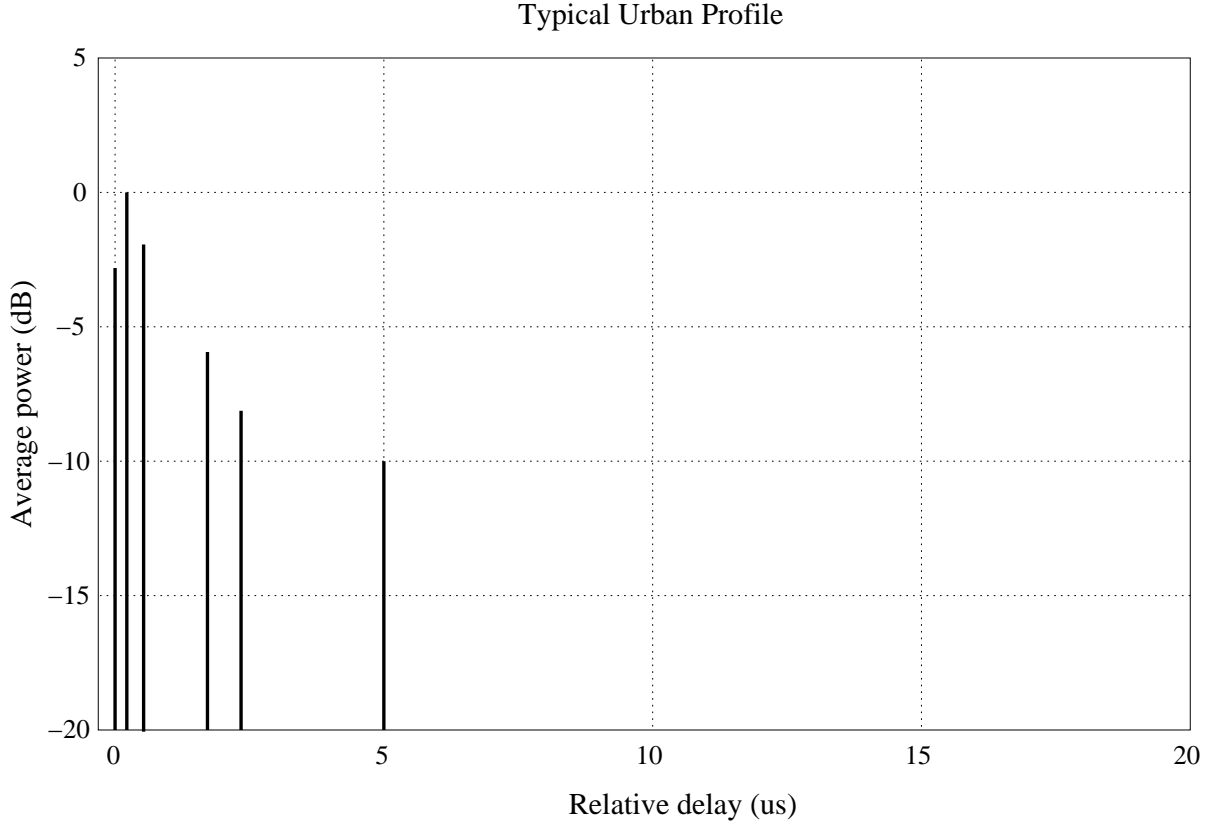
Figure 2.2: Typical Urban propagation model

sequence error provided the channel impulse response is estimated accurately, would require an excessive computational complexity and is prohibited with currently available digital signal processors (DSPs). According to the typical channel profiles of GSM, the HT channel model requires the channel impulse response (CIR) length of 7. Therefore, the computational complexity of the equalization in 8-PSK EDGE system is given by 8^6 per received data system.

To limit the computational complexity and eliminate the ISI in the received samples, some alternatively methods were proposed in the literature. An example is Decision Feedback Equalizer (DFE) and Linear Equalizer (LE) [73] which employ various adaptive algorithms to find the optimum equalizer weights. However, the DFE tends to perform poorly for 8-PSK since the signal constellation is fairly dense causing the algorithm to become overly sensitive to noise. Due-Hallen introduced a delayed decision feedback
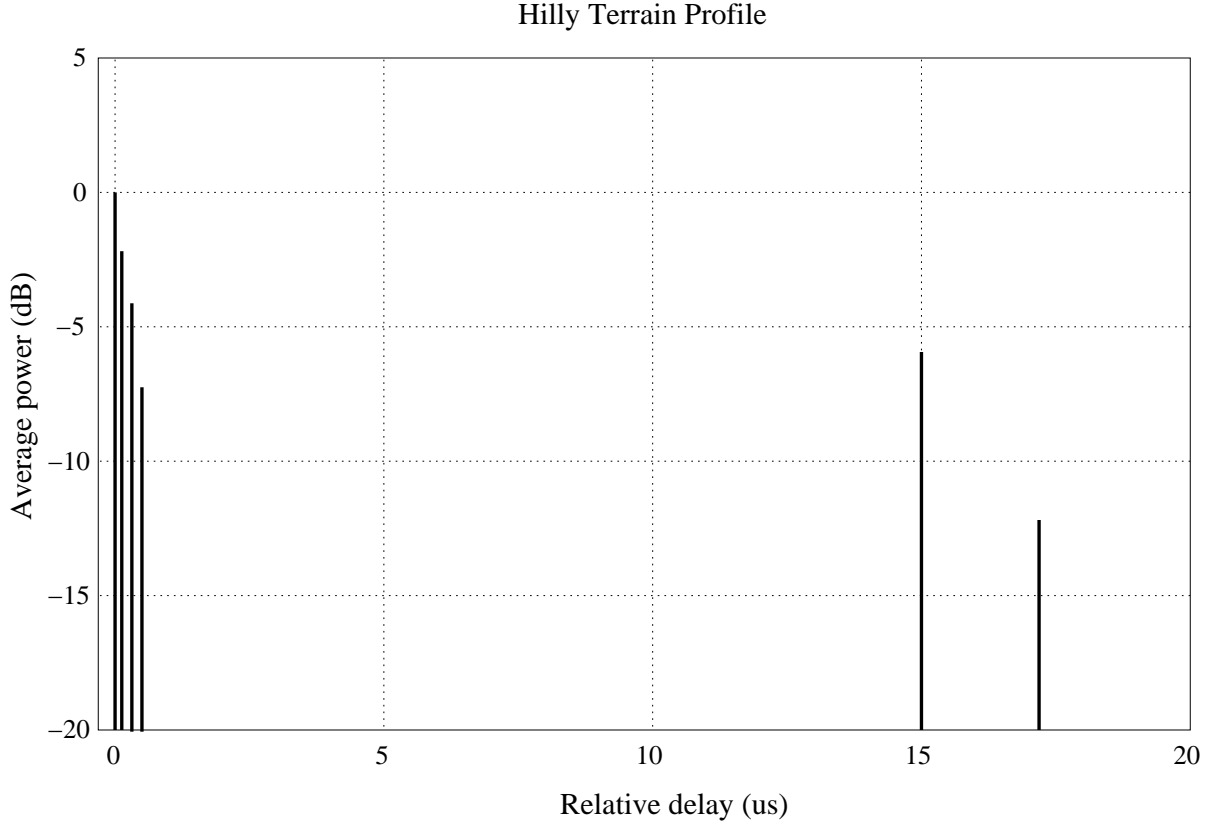
Figure 2.3: Hilly Terrain propagation model

sequence estimation [8] which truncate the channel impulse response to a manageable length for MLSE. This algorithm belonging to the class of suboptimum equalizer. In general, the suboptimum DDFSE has advantageous tradeoff between performance and computational complexity providing the channel impulse response that has to be equalized has a minimum-phase characteristic. Eyuboglu proposed a reduced-stated sequence estimation which can further simplify DDFSE to less computational complexity. In the following subsections, we introduce the commonly used equalizers MLSE, DDFSE and RSSE in brief details. In proceed, we propose a new efficient equalization method, which is shown to be a suboptimum equalizer and provides a good performance in the sense of bit error rate.

2.2.1 Maximum-Likelihood Sequence Estimation (MLSE)

When the transmitted signal has memory, i.e, the received signals are distorted by the ISI channel, MLSE is an optimum equalizer that make the decision on the symbol based on observation of a sequence of received signals over successive signal intervals. It searches the minimum Euclidean distance path through the trellis that characterizes the memory in transmitted signal.

To illustrate the maximum-likelihood sequence detection algorithm clear to the reader, we consider the system as follow. Denote a transmitted sequence $\mathbf{d} = [d_0 d_1 \cdots d_{K-1}]$, where K is total number of signals transmitted. If we assume that the channel has $L-1$ memory, the received sequence at the receiver is given by

$$y_k = \sum_{l=0}^{L-1} d_{k-l} h(l) + n_k \tag{2.1}$$

where y_k is the received signal at kth signal interval, $h(l)$ for $l = 0, 1, \cdots, L-1$ is the channel impulse response and $n_k \sim \mathbb{N}(0, \sigma^2)$ is a zero-mean Gaussian random variable. Given that we know the channel information $\{g(l)\}_{l=0}^{L-1}$ perfectly, the conditional probability density function (pdf) for the transmitted signal is

$$P(y_k | d_k, d_{k-1}, \cdots, d_{k-L+1}) = \frac{1}{\sqrt{2\pi\sigma^2}} \exp\left(-\frac{1}{2\sigma^2}\left|y_k - \sum_{l=0}^{L-1} h(l) d_{k-l}\right|^2\right) \tag{2.2}$$

After receiving the sequence $\{y_k\}_{k=0}^{K-1}$, the equalizer decides in favor of the sequence $\{d_k\}_{k=0}^{K-1}$ that maximizes the **likelihood function**

$$P(y_{K-1}, y_{K-2}, \cdots, y_0 | d_{K-1}, d_{K-2}, \cdots, d_0). \tag{2.3}$$

Denote the branch metric

$$\tilde{\varepsilon}_k = -\left|y_k - \sum_{l=0}^{L-1} h(l) d_{k-l}\right|^2. \tag{2.4}$$

Based on the recursion in (2.2) and the branch metric (2.4), we can implement the well-known Viterbi algorithm searching through the $N_s = 2^{nL}$ states, where 2^n is the size of

signal constellation, for the most likely transmitted sequence $\mathbf{d}$. This searching process is known as maximum likelihood sequence estimation. In follow, we give a very brief outline of the Viterbi algorithm. Denote the state at node k as

$$\varrho_k = (d_{k-1}, d_{k-2}, \cdots, d_{k-L+1}), \tag{2.5}$$

we have N_s surviving sequences $\check{\mathbf{d}}(\varrho_k^{(i)})$ along with their associated path metrics $\Gamma(\varrho_k^{(i)})$ that terminate at that $\varrho_k^{(i)}$, where $i = 0, 1, \cdots, N_s - 1$. The path metric is defined as total of the branch metric $\tilde{\varepsilon}_k$ along the surviving path is given by

$$\Gamma(\varrho_k^{(i)}) = \sum_{\{k\}} \tilde{\varepsilon}_k. \tag{2.6}$$

While the received signal arrives at the receiver, the MLSE start the search process as following steps,

1. Compute the path metrics $\Gamma(\varrho_k^{(i)} \rightarrow \varrho_{k+1}^{(j)})$ from state i to state j for all possible paths through the trellis that terminate in state $\varrho_{k+1}^{(j)}$, $j = 0, 1, \cdots, N_s - 1$.

2. At each state j, find the maximum $\Gamma(\varrho_k^{(i)} \rightarrow \varrho_{k+1}^{(j)})$ among all possible paths that terminate in state $\varrho_{k+1}^{(j)}$.

3. Store the maximum $\Gamma(\varrho_k^{(i)} \rightarrow \varrho_{k+1}^{(j)})$ and its associated surviving sequence $\check{\mathbf{d}}(\varrho_{k+1}^{(j)})$ and discard other paths.

After all the states have been processed, the time index k is incremented by one and the entire process is repeated again. The recursive algorithm is terminated until the entire sequence $\{y_k\}_{k=0}^{K-1}$ has been processed. The maximum path metric $\Gamma(\varrho_{K-1}^{(i)})$ is found among all possible N_s states and its associated surviving sequence $\check{\mathbf{d}}(\varrho_{K-1}^{(i)})$ is the estimated received sequence output by the equalizer.

2.2.2 Delayed Decision-Feedback Sequence Estimation (DDFSE)

As we mention before, the computational complexity of the MLSE grows exponentially with the channel memory length and signal constellation size. For instance, with 8-PSK

constellation in EDGE system, the channel memory length is 6 and the total number of states computed in the trellis is $8^6 = 262144$ states. Therefore the MLSE becomes impractical. In order to limit the computational complexity, Due-Hallen truncated channel memory to μ terms, where μ is an integer that can be varied from 0 to $L-1$. Thus, the computational complexity of the suboptimum equalizer controlled by th parameter μ and this suboptimum equalizer is so-called the delayed decision feedback sequence estimation.

Since the DDFSE equalizer is based on the parameter μ and μ falls into the range of 0 to $L-1$. Thus, the DDFSE itself can be viewed as the combination of Viterbi algorithm and decision feedback equalizer. When $\mu = 0$, the DDFSE equalizer is equivalent to the DFE receiver, which using a single unreliable decision for feedback. When $\mu = L - 1$, the DDFSE equalizer is equivalent to MLSE.

Assume that μ is chosen as the truncation length of DDFSE equalizer, the received sample at time index k is given by

$$y_k = \sum_{l=0}^{\mu} h(l)d_{k-l} + \sum_{l=\mu+1}^{L-1} g(l)d_{k-l}. \tag{2.7}$$

Thereby, the state at node k can be decomposed into the following two states, one is given by

$$\varrho_k^\mu = (d_{k-1}, d_{k-2}, \cdots, d_{k-\mu}), \tag{2.8}$$

and the partial state is

$$\tilde{\varrho}_k = (d_{k-\mu-1}, d_{k-\mu-2}, \cdots, d_{L-1}). \tag{2.9}$$

Based on (2.8), the Viterbi algorithm searching through the $N_\mu = 2^{n\mu}$ states for the most likely transmitted sequence $\mathbf{d}$. The DDFSE equalizer implement the same recursive algorithm of MLSE given in Section 2.2.1, except it computes the branch metric for each

state transition $\varrho_k^{\mu(i)} \rightarrow \varrho_{k+1}^{\mu(j)}$ as follows,

$$
\tilde{\varepsilon}_k(\varrho_k^{\mu(i)} \rightarrow \varrho_{k+1}^{\mu(j)}) = - \left| y_k - h(0)d_k(\varrho_k^{\mu(i)} \rightarrow \varrho_{k+1}^{\mu(j)}) \right.
$$

$$
\left. - \sum_{l=0}^{\mu} h(l)d_{k-l}(\varrho_k^{\mu(i)}) - \sum_{l=\mu+1}^{L-1} h(l)\check{d}(\varrho_k^{\mu(i)}) \right|^2 \quad (2.10)
$$

where $\check{d}(\varrho_k^{\mu(i)})$ is the lth component of the surviving sequence $\check{\mathbf{d}}(\varrho_k^{\mu(i)})$.

Apparently, the DDFSE equalizer estimates the sequence based on the μ most recent symbols. Hence, it is important that the signal energy is contained in these μ signals. So a noise whitening filter is carefully selected to produce the overall channel in minimum phase form.

2.2.3 Reduced-State Sequence Estimation (RSSE)

When large signal constellation is employed, the number of states associated with DDFSE is still substantial even for small μ. For instance, 16-QAM consists of 2^4 symbols and $\mu = 4$ is given, the number of states searched by the VA in DDFSE is 2^{16}. Thus, we can use one possible remedy is so-called Ungerboeck-like set partitioning principles to further simplify the computational complexity.

Define a set partitioning $\Omega(i)$, where $1 \leq i \leq \mu \leq L - 1$ where the signal set is partitioned into J_i subsets in a way of increasing intrasubset minimum Euclidean distance [6]. Denote the subset in the partitioning $\Omega(i)$ as $c_i(x_{k-i})$ that consists of elements x_{k-i}. The subset partitioning is also defined in a way such that $\Omega(i)$ is a finer partitioned of $\Omega(i+1)$ and $J_1 \geq J_2 \geq \cdots \geq J_\mu$. Consequently, the RSSE does not specify the μ most recent symbols $\{x_{k-i}\}_{i=1}^{\mu}$ but only specify the subsets to which these symbols belong. Note that when $J_1 = J_2 = \cdots = J_\mu$, RSSE becomes DDFSE. In Fig. 2.4 and 2.5, we depict the set partitioning for 16-QAM and 8-PSK, respectively.

The Viterbi algorithm in MLSE is used to search the subset trellis for different branch metrics associated with the subset-transitions. Note that the branch metric of RSSE is not uniquely determined by the associated pair subset-states. A decision feedback

13
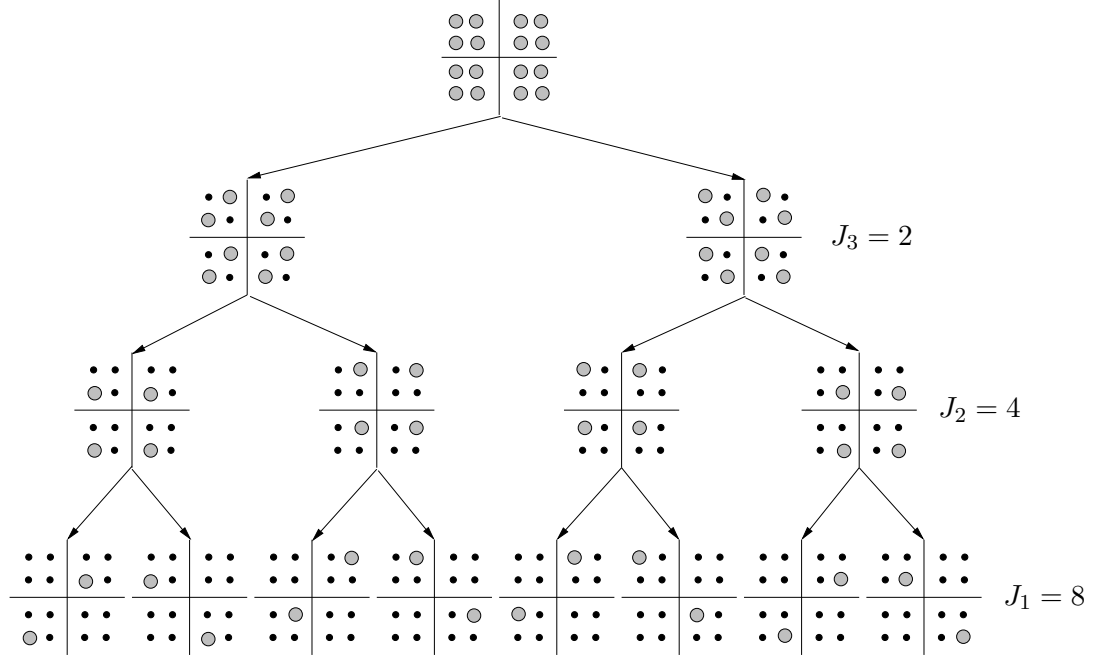
Figure 2.4: Ungerboeck partition tree for the rectangular 16-QAM signal set

mechanism in DDFSE is also implemented for branch metric calculation. Define the subset state as follows

$$\varrho_k^\mu = [c_1(x_{k-1}, c_2(x_{k-2}), \cdots, c_\mu(x_{k-\mu})]. \tag{2.11}$$

The RSSE branch metric for a particular parallel transition associated with the subset transition $(\varrho_k^{\mu(i)} \to \varrho_{k+1}^{\mu(j)})$ is written as

$$\tilde{\varepsilon}_k(\varrho_k^{\mu(i)} \to \varrho_{k+1}^{\mu(j)}) = - \left| y_k - h(0) x_k(\varrho_k^{\mu(i)} \to \varrho_{k+1}^{\mu(j)}) - \sum_{l=\mu+1}^{L-1} h(l) \check{x}_{k-l}(\varrho_k^{\mu(i)}) \right|^2 \tag{2.12}$$

where $\check{x}_{k-l}(\varrho_k^{\mu(i)})$ is the lth component of the surviving path $\check{\mathbf{x}}(\varrho_k^{\mu(i)})$ leading to the subset $\varrho_k^{\mu(i)}$.

2.3   Minimum Phase Noise Whitening Filter

As mentioned before, the reduced-state equalizers truncate the channel impulse response to a manageable length. Therefore, the sequence estimations are only concentrated on

14
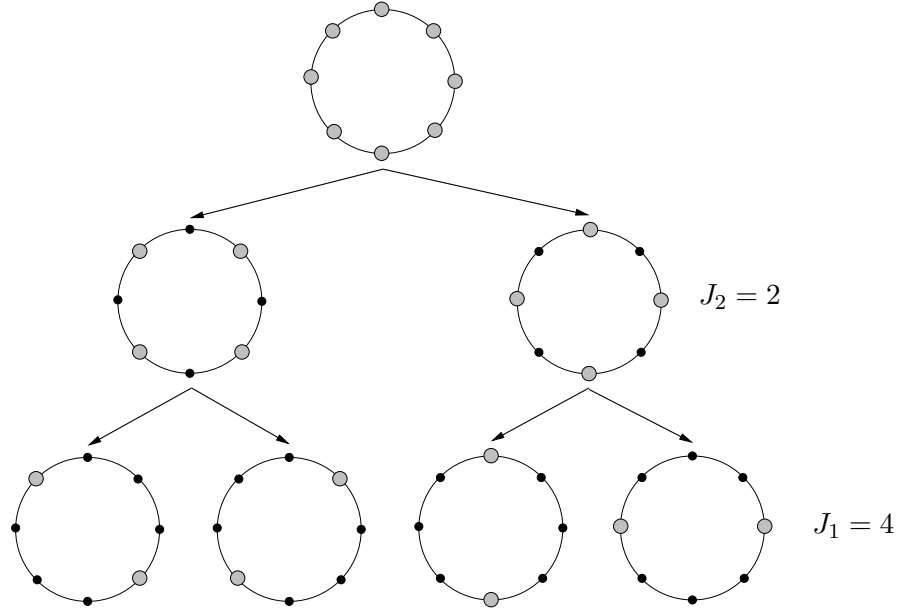
Figure 2.5: Ungerboeck partition tree for 8-PSK signal set

the first few taps. As a result, we need to carefully designed a noise whitening filter so that the overall response will be in minimum phase. In Fig. 2.3, a system consists of transmitting filter $P_{tr}(t)$, ISI rayleigh fading channel $g(t)$ and receiving filter $P_r(t)$ is depicted. The channel impulse response $\mathbf{h}$ is the convolution of $P_{tr}(t)$, $P_r(t)$ and $g(t)$.
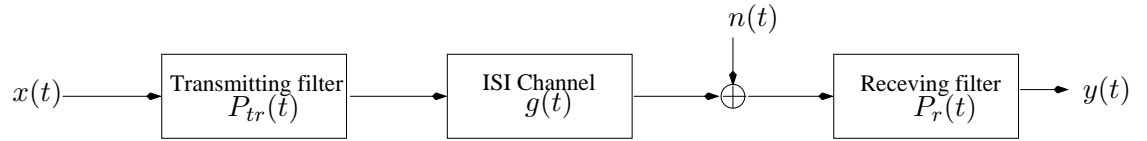
Figure 2.6: ISI channel system

The z-transform of the vector $\mathbf{h}$ is given as

$$H(z) = \sum_{l=-L}^{L} h(l)z^{-n} \tag{2.13}$$

Given that the ISI coefficient $\mathbf{h}$ has the property of $h(l) = h^h(-l)$, where $[\cdot]^h$ is the complex conjugate operator. We can write

$$H^h(1/z^h) = H(z). \tag{2.14}$$

15
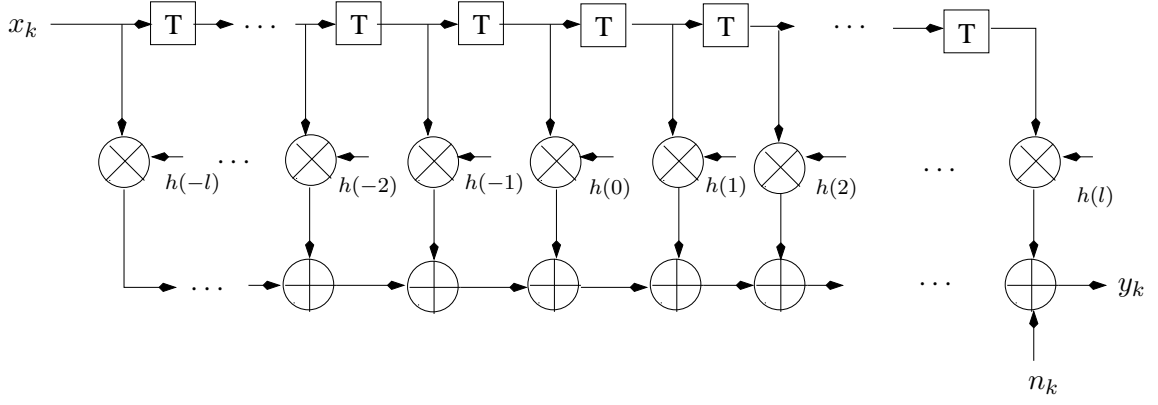
Figure 2.7: Discrete-time model for ISI channel

Follows, $H(z)$ can be factorized to

$$H(z) = G(z)G^h(1/z^h) \tag{2.15}$$

where $G(z)$ and $G^h(1/z^h)$ are polynomials of degree L [73]. Based on the polynomials, there are 2^L possible choices for the roots of $G^h(1/z^h)$ for the noise whitening filter. To produce a filter that the overall response $G(z)$ has minimum-phase for reduced state equalizers, we have to choose the unique $G(z)$ has all its roots fall inside the unit circle and noise whitening filter $G^h(1/z^h)$ is a stable but noncausal filter. Finally, the filter output is

$$\begin{aligned} V(z) &= (X(z)H(z) + \tilde{n}(z))\frac{1}{G^h(1/z^h)} \tag{2.16} \\ &= X(z)G(z) + \tilde{n}(z)\frac{1}{G^h(1/z^h)} \tag{2.17} \end{aligned}$$

and the whitening noise filter system is shown in Fig.
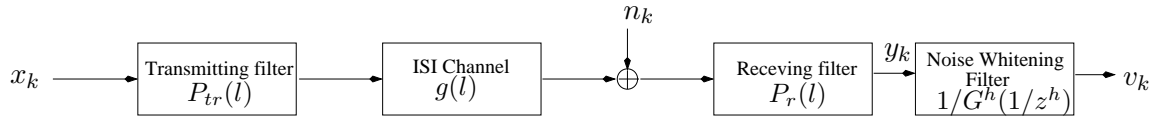
Figure 2.8: ISI channel system followed by a discrete-time noise whitening filter

16

2.4 Perturbation Equalization and Symbol Detection

In this section, a new approach is presented for 8-PSK EDGE channel equalization. The method is suboptimal but can achieve good bit error rate (BER) performance with low computational complexity. The algorithm iteratively minimizes the Euclidean distance between the detected signal sequence and the received signal sequence, with good initial conditions provided. The detected hard symbols are then used to cancel ISI when computing zero delay form of the symbol (bit) probabilities for soft decision decoding.

2.4.1 Baseband System Parameters

We assume that the system transmits the signal in burst mode. In Fig. 2.1, the transmitted data bits are modulated to 8-PSK symbols $a_k \in \{\exp(j\frac{2\pi i}{8}); \ i = 0, 1, 2, \cdots, 7\}$, where $j = \sqrt{-1}$ and placed in a short slot depicted in Fig. 2.9. Next, the 26 training symbols are inserted in the middle of the slot as pilot symbols. Assume that there is no timing error and frequency offset at the receiver, the baseband of the EDGE system shown in Fig. 2.1 can be written as

$$y_k = \sum_{l=0}^{L-1} h(l) d_{k-l} + n_k, \tag{2.18}$$

where $k = 0, 1, \cdots, 147$, d_k is the transmitted 8-PSK symbol, y_k is the symbol rate sampled output of the receive filter, n_k is the additive white Gaussian noise (AWGN), and $h(l)$, $0 \leq l \leq L - 1$, is the time-invariant CIR of the fading channel. $h(l)$ is the symbol rate sampled version of the composite channel impulse response that is the convolution of the transmit filter, the receive filter, and the physical channel impulse response.

At the receiver depicted in bottom part of Fig. 2.1, the received signal is then separated into two streams: one stream is for data symbols, and the other stream is for
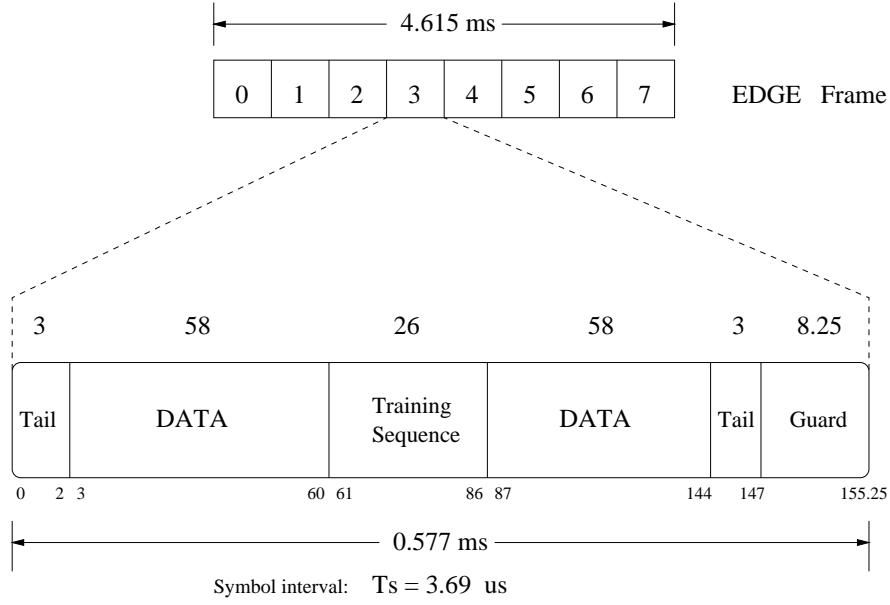
Figure 2.9: Transmitted slot structure

the training symbols which channel fading information is extracted. Due to its short duration of each time slot and low or moderate mobile speeds, it is reasonable to assume that the CIR is time-invariant within a time slot. Hence, the preceding or the next slot will have different CIR implying the equalization will be done slot by slot. Based on least-squares (LS) algorithm, we are able to estimate the overall channel impulse response vector $\mathbf{h} = [h(0), h(1), \cdots, h(L-1)]$.

As shown in Fig. 2.2 and 2.3, the power of the Rayleigh fading at the path delay $\tau = 0$ is small. As a result, the average power of the first CIR $E[|h(0)|^2]$ is significantly small while we compare to the CIRs $E[|h(1)|^2]$ and $E[|h(2)|^2]$. Therefore, the system is not in minimum phase and it would lead to numerical instability if we estimate the data symbols based on $\mathbf{h}$. With reference to Fig. 2.1 we indicate the need for a prefilter [13]. The prefilter transform the Rayleigh fading vector $\mathbf{h}$ to a minimum phase form $\mathbf{b}$ where the leading taps are dominant. Denote the prefiltered received sequence by a colum vector $\mathbf{z} \in \mathbb{C}^{1 \times 148}$, we have the compact form received sequence as follows,

$$\mathbf{z} = \mathbf{Bd} + \tilde{\mathbf{n}} \tag{2.19}$$

18

where column vectors $\mathbf{d} \in \mathbb{C}^{1\times 148}$ and $\tilde{\mathbf{n}} \in \mathbb{C}^{1\times 148}$ are the unknown transmitted burst to be estimated and additive noise, respectively. The matrix $\mathbf{B} \in \mathbb{C}^{148\times 148}$ is a lower triangular and banded, with rows containing the post prefilter impulse response (IR) as

$$\mathbf{B} = \begin{bmatrix} b(0) & 0 & \cdots & & & & \\ b(1) & b(0) & 0 & \cdots & & & \\ b(2) & b(1) & b(0) & 0 & \cdots & & \\ b(L) & \cdots & b(1) & b(0) & 0 & \cdots & \\ 0 & b(L) & \cdots & b(1) & b(0) & 0 & \cdots \\ \vdots & \vdots & \vdots & \vdots & \vdots & \vdots & \end{bmatrix}. \tag{2.20}$$

Note that $\mathbf{B}$ is a diagonally dominant matrix and full rank. In proceed, a computationally algorithm can be developed to detect the transmitted symbol vector $\mathbf{d}$ by minimizing $\varepsilon^2 = \|\mathbf{z} - \mathbf{B}\mathbf{d}\|^2$ with respect to $\mathbf{d}$. If we define $\mathbf{v} = \mathbf{z} - \mathbf{T}\mathbf{d}$, then $\varepsilon^2 = \|\mathbf{v}\|^2 = \sum_{i=0}^{57} |v(i)|^2$. As shown in Fig. 2.9, the data symbol streams are located at two separated blocks and each of them consists of 58 data symbols. We now propose a two step optimization procedure to find the symbol vector $\mathbf{d}$ that will minimize the sequence error ε^2.

2.4.2   Equalization and Hard Symbol Detection Algorithm

Step 1: Let $\mathbf{d} = 0$. Starting d_n with $n = 1$ select the 8-PSK alphabet hard symbol d_n that yields the least value for $\|z(n) - b(0)d_n - \sum_{i=1}^{L} b(i)d(n-i)\|^2$. Repeat the search for the next symbol d_{n+1} using previously detected symbols $d_n, d_{n-1,\cdots}$ and so on until the end of the burst is reached. The result of this hard symbol search is denoted $\mathbf{d}^*$.

Step 2: Using the obtained $\mathbf{d}^*$ as an initial solution, starting from the end of the burst test the 2 nearest neighbors of d_n^* in the 8-PSK constellation for a possible reduction in the sequence error ε^2. If the sequence error ε^2 is reduced (or reduced most) by one of the two neighbors, then update d_n^* with that neighbor. Repeat the procedure for the next symbol d_{n-1}^* and so on until $n = 1$ is reached. This is **one iteration**. Repeat the

procedure above until the sequence error ε^2 is no longer reduced by additional iterations or until the iteration number reaches a pre-set value. Then this updated $\mathbf{d}^*$ is the final estimate of the transmitted hard symbol vector in the sequence sense denoted by $\mathbf{d}_{sq}$. The idea of nearest neighbor perturbation is shown in Fig. 2.10.

PSfrag replacements
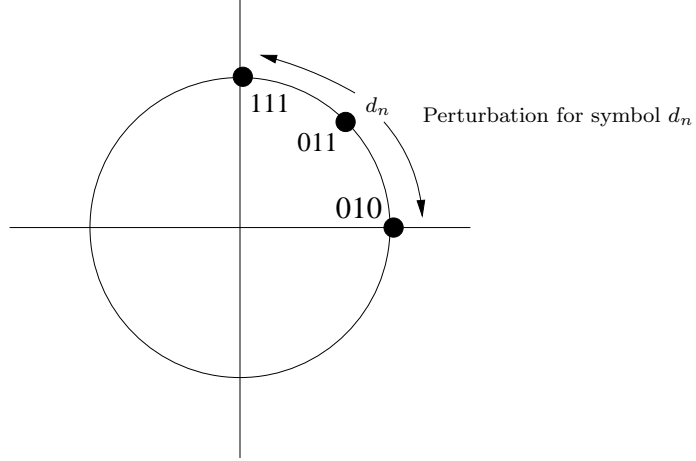
Figure 2.10: The idea of nearest neighbor perturbation.

2.4.3 Soft Bits Estimation

The algorithm given above provided a hard sequence $\mathbf{d}_{sq}$ that minimized the sequence error. From these hard symbols we may derive hard bits denoted by $\bar{\boldsymbol{x}}$ directly given the symbol to bit map, shown in Fig. 2.11. However, for soft decision decoding, we need soft bits, defined as

$$soft_i = \left| \ln \left(\frac{P_i}{1 - P_i} \right) \right| \bar{x}_i \tag{2.21}$$

where P_i denotes the probability that the i th bipolar bit is a logical 1. It is straightforward to find the zero delay form of these probabilities [1] as is done for the DFE method, except that we substitute the hard sequence $\mathbf{d}_{sq}$ when we perform the decision feedback part, thus enhancing the quality of the bit probabilities significantly.

---

[1]Symbol probabilities are computed, then converted to bit probabilities using the symbol to bit map.

20

M=1
1 1 1
(0+j1)

M=8
1 1 0
$\sqrt{\frac{1}{2}}$ (-1+j1)

M=2
0 1 1
$\sqrt{\frac{1}{2}}$ (1+j1)

M=7
1 0 0
(-1+j0)

M=3
0 1 0
(1+j0)

M=6
1 0 1
$\sqrt{\frac{1}{2}}$ (-1-j1)

M=4
0 0 0
$\sqrt{\frac{1}{2}}$ (1-j1)

(0-j1)
0 0 1
M=5
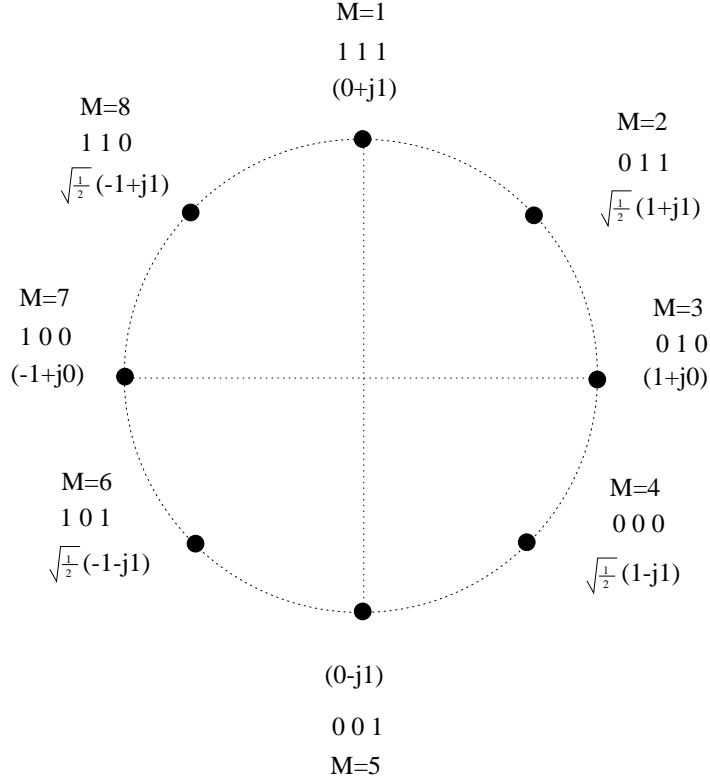
Figure 2.11: The 8PSK symbol to bit mapping.

2.5 Simulation Results

In this section we show the results obtained with the equalization and soft bit estimation presented in Section 2.4.3. Each ray in the dispersive channel is assumed to undergo Rayleigh fading independently of other rays. The transmission filter is Gaussian as defined in GSM and causes ISI of three symbols. Additive white Gaussian noise (AWGN) is added to the received symbols. The amount of noise added is determined by the desired E_b/N_o ratio. The CIR length is chosen as $L = 7$, and a SRC receiver filter with normalized bandwidth of 1 and roll-off 0.5 is used.

In our simulations, it has been observed that the first two iterations provide significant reduction for the bit error rate (BER), and there is little change to the estimated symbol sequence$\mathbf{d}_{sq}$ after 3 iterations. To gain the most benefit with paying the least cost, we choose to fix $N_{\text{iteration}} = 2$ in Step 2 of the equalizer in our simulation results

presented in this section.

2.5.1   Typically Urban Channel

Our equalizer with $N_{\text{iteration}} = 2$ is compared to RSSE with four way (2 state) set partitioning (RSSE2) since the complexity of the two methods are the same, as well as to RSSE8 where no set partitioning is used, and the complexity is four times as high as our method. The four way set partitioning prevents the trellis from producing trellis based soft bits as is possible in the 8 state RSSE and DDFSE equalizers. This causes the decoded BER (from [12]) to be suboptimal in the RSSE2 method. For the RSSE8 method and the TU channel that is essentially a two tap channel after the prefilter, the RSSE8 equalizer achieves a near optimal decoded BER that can be expected for the TU channel as all soft bits are computed from the 8 state (two tap) trellis.

The bit error rate (BER) after channel decoding versus E_b/N_0 for the TU3 profile with mobile speed being 3 km/h is shown in Figure 2.12 for MCS-5 and MCS-7 coding schemes as well as the uncoded scheme.

As can be seen, our equalizer has almost the same BER performance as the RSSE2 equalizer for uncoded scheme under TU3. However, our equalizer well outperforms the RSSE2 equalizer for MCS-5 scheme where the soft bits are important. For the computational complexity, the RSSE2 needs to calculate 16 metrics per symbol, and our algorithm, for the choices made here in these simulations with $N_{\text{iteration}} = 2$ we need to calculate 18 metrics per symbol when producing soft bit information to aid the soft decision decoder. The RSSE8 method shows gain over both our method and the RSSE2 method, but requires 64 metrics per detected symbol (3 bits).

2.5.2   Hilly Terrain Channel

As a second example, we select the Hilly Terrain (HT) channel model, at a mobile velocity of 50 km/h, and we select to use the RSSE method without any set partitioning
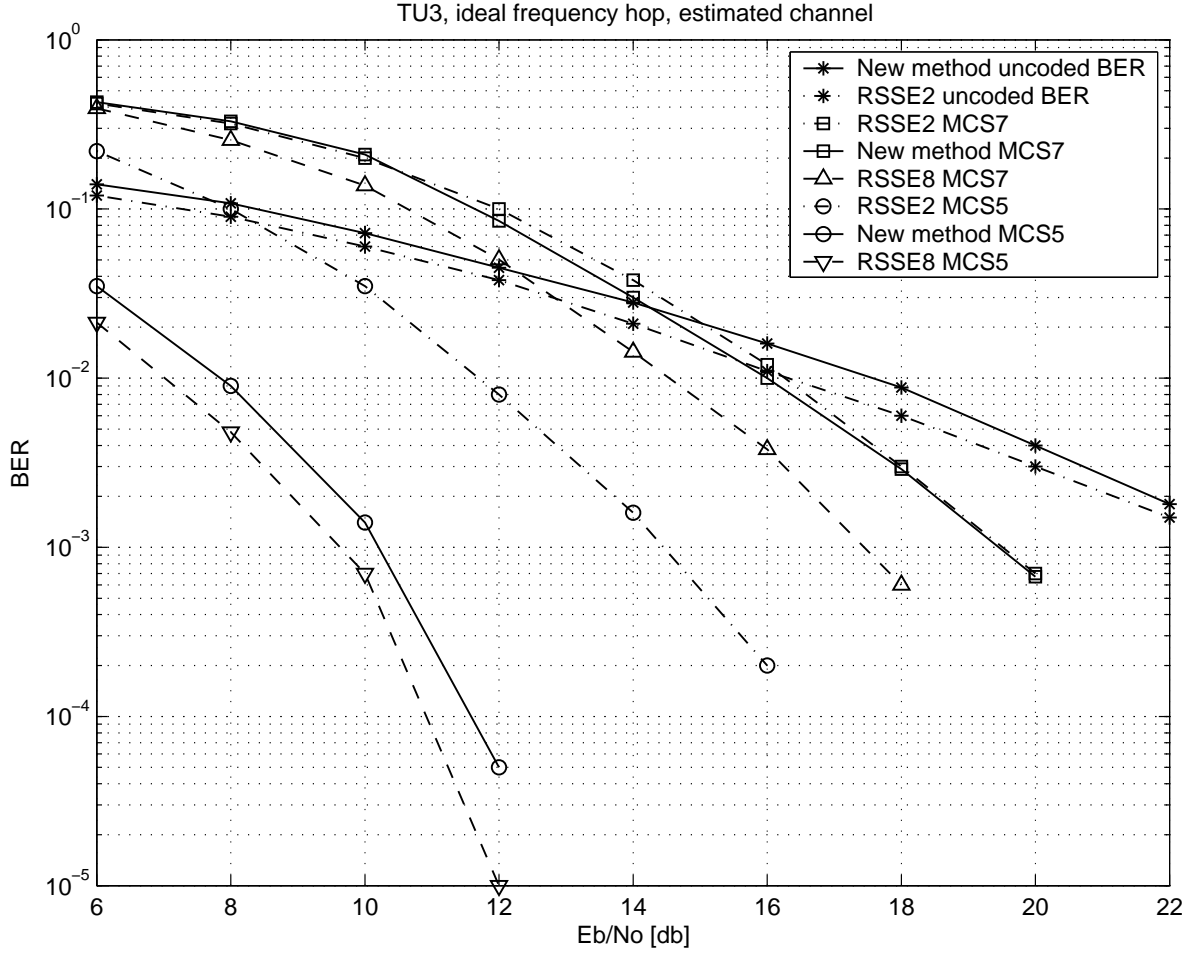
Figure 2.12: Comparison of BER vs E_b/N_o for our new algorithm with RSSE2 and RSSE8 under Typical Urban Profile with mobile speed being 3 km/h.

with an 8 state trellis producing trellis based soft bits. We consider here only decoded BER, as indicated in Figure 2.13. Even though the 8 state RSSE method requires 64 metrics to be computed per detected symbol, versus our equalizer requiring only 18 metrics, the gain over our method in decoded BER is small in MCS5, on the order of 0.5 dB. For MCS7 the 8 state RSSE method gains around 1 dB.

The fact that the RSSE8 method shows less gain over our method for the HT channel is due to the fact that after the prefilter the HT channel still shows 5 significant taps in the impulse response, and thus the 8 state trellis is not able to produce optimal soft bits as was the case for the TU channel.
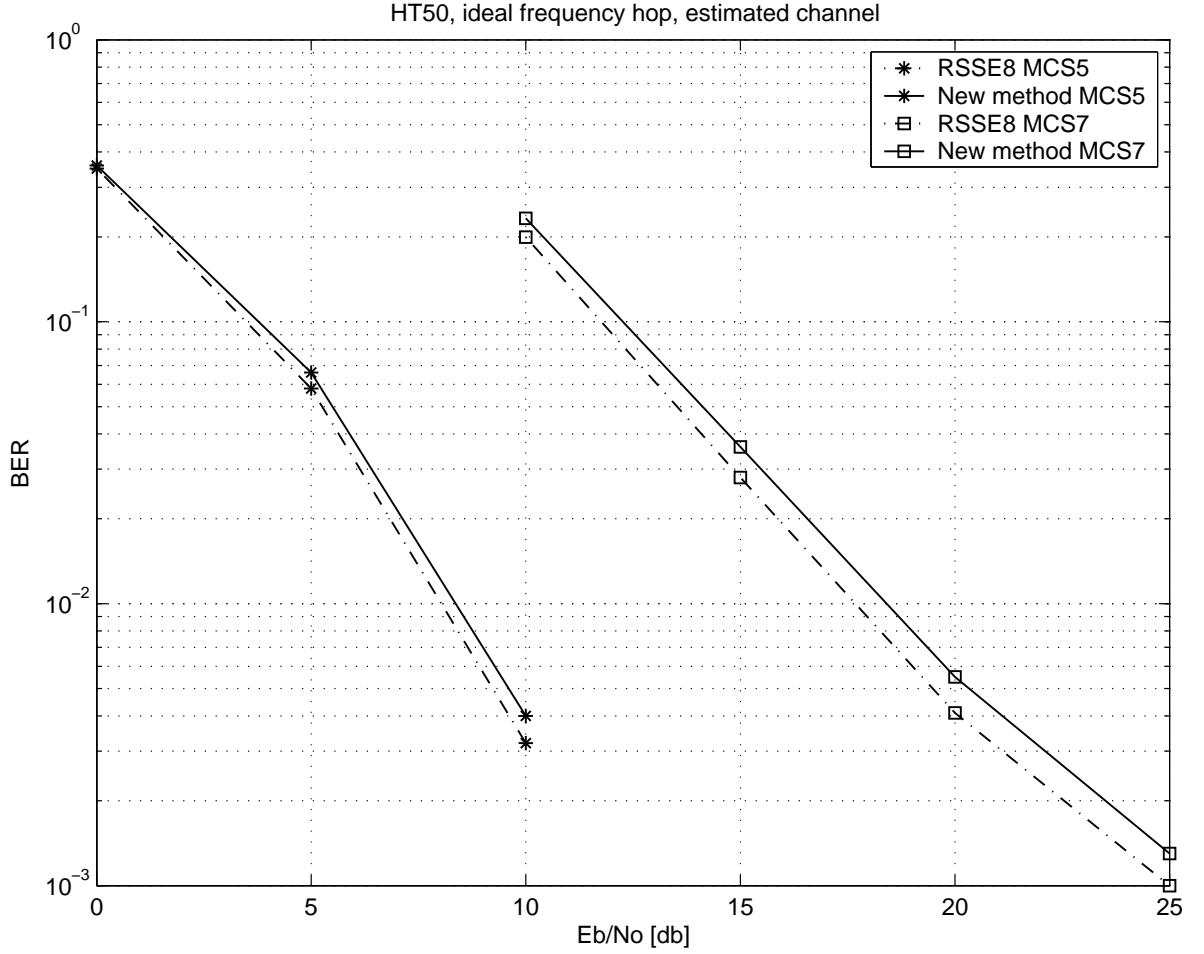
Figure 2.13: Comparison of BER vs E_b/N_o for our new algorithm with 8 state RSSE under Hilly Terrain model with mobile speed being 50 km/h.

2.6 Conclusions

In this chapter, an iterative method is presented for 8-PSK EDGE equalization and symbol detection. The proposed method is based on minimizing the Euclidean distance between the detected signal sequence and the received signal sequence, with neighbor symbol perturbation to reduce the computational complexity. Given the detected symbol sequence, we may compute the zero delay bit probabilities by feeding back the detected sequence to cancel ISI. These in turn are used to produce soft bits. Simulation results were performed by comparing the performance of our equalizer versus the RSSE detector. We presented both the cases where four way set partitioning is used (2 state RSSE) and

where no set partitioning is used (8 state RSSE). For 2 state RSSE the complexity is similar to our method, but is was shown that our method is able to produce better decoded BER when coding is strong. For 8 state RSSE, our equalizer performance shows a small loss, but it requires only a quarter (approximately) of the computational complexity. The proposed method can easily be extended to other high-level modulation schemes as long as the effective channel impulse response can be estimated.

Chapter 3

Improved Decision Feedback Equalization Using *A Priori* Information

3.1   Introduction

Turbo equalization is a powerful iterative receiver which employs trellis-based channel equalization and decoding methods [28]. At the transmitter, the data is first protected by an error correction code and then followed by an interleaver to mitigate bursty errors. At the receiver, the encoder and the discrete-time equivalent channel is treated as the serial concatenation of two codes. Hence, the so-called *Turbo-principle* [29] can easily be applied. The performance of the system is improved in the fashion of exchanging the *extrinsic* information iteratively among the soft-input/soft-output (SISO) equalizer and SISO channel decoder until convergence is achieved. To achieve optimal equalization, we may use a symbol by symbol MAP algorithm [30] or soft MLSE detector minimizing the sequence error via maximum likelihood estimation [5, 41, 42]. In [28], the first proposed turbo equalization implements the soft-output Viterbi algorithm (SOVA) exclusively for both equalization and decoding, as in [40]. Unfortunately, these optimum algorithms are not usually applicable to many practical communication systems in use today due

to their high computational complexity. For large constellation size M modulation used with long discrete-time equivalent channel length L results in high computational complexity of $\mathcal{O}(M^L)$ that is intractable for equalization. As a consequence, an efficient reduced complexity SISO equalizer is required for sub-optimal turbo equalization, with very little performance degradation.

Due to this reason, the low complexity SISO equalizers have been investigated by many authors in the recent literature. In [31], Wang and Poor developed an iterative receiver structure for decoding multiuser information data in code division multiple access (CDMA). The minimum mean square error (MMSE) linear equalizer (LE) implemented in turbo equalization cancels the inter-symbol interference and multi-access interference (MAI) successfully. Ariyavisitakul and Li [45] proposed a joint convolutional coding and DFE in an iterative equalization scheme. The DFE uses a combination of soft decisions and tentative decisions obtained from the Viterbi decoder to cancel ISI. Tuchler showed that MMSE-based LE performs well compared with a MAP equalizer while only low computational complexity is needed [33]. The equalization was extended to multilevel modulation in [32].

In this chapter, we specifically focus on the DFE algorithm. We address the drawback of the conventional DFE algorithm in turbo equalization, which has error propagation. The effects of error propagation are observed clearly from the simulation results of [32, 33], where the turbo equalizer does not produce significant improvement in multipath channels throughout the iterations. Besides, the gain in BER offered by the conventional DFE diminished dramatically after several iterations. Therefore, a new approach is proposed to mitigate the error propagation in the DFE algorithm when used in turbo equalization while retaining low computational complexity. It estimates the data using the *a priori* information from the SISO channel decoder and also the *a priori* detected data from previous iteration to minimize error propagation. From the simulation results, we show that the bit error rate (BER) performance of the improved DFE algorithm

provides significant improvement when compared with the conventional DFE algorithm.

3.2   System Model

We consider the system model shown in Fig. 3.1. All other approaches presented in this chapter use the same structure except the type of equalizer. Prior to transmission, a frame of binary data $b_i \in \{0, 1\}$ with length K_d is encoded through a convolutional encoder with constraint length K and rate r. The output encoded bits $c_k \in \{-1, +1\}$, where $k = 1, 2, \cdots, K_c$, are interleaved into a block of different ordering data $x_k \in \{-1, +1\}$ using a random permutation function. The interleaver operation is denoted as $x_n = \Pi(c_k)$ and its reverse operator (de-interleaver) is denoted as $\Pi^{-1}(\cdot)$. To simplify the derivation of algorithms, the interleaved code bits x_k are partitioned into $M \cdot Q$ sequences given as $\mathbf{x} \triangleq [\mathbf{x}_0 \mathbf{x}_1 \cdots \mathbf{x}_{M-1}]$, where $M = K_c/Q$ and the subsequence $\mathbf{x}_i \triangleq [x_{i,1} \ x_{i,2} \ \cdots \ x_{i,Q}]$. Next, the transmitted symbol d_i is generated by mapping each subsequence $\mathbf{x}_i$ to a modulated signal $s_i \in \mathcal{S} = \{s_1, s_2, \cdots, s_{2Q}\}$ that corresponds to the 2^Q-ary bit pattern $\mathbf{z}_i \triangleq [z_{i,1} \ z_{i,2} \ \cdots \ z_{i,Q}]$. The phase shift keying (PSK) constellation shown in Fig. 3.2 is used throughout this chapter for simulation and analysis.

Assume that the data sequence $\mathbf{d} = [d_0 d_1 \cdots d_{M-1}]$, $d_i \in \mathcal{S}$, is transmitted in burst mode to the receiver. The transmitted data is distorted by the ISI channel and additive white Gaussian noise (AWGN). For the sake of simplicity, we assume that there is no timing error and frequency offset at the coherent symbol-spaced receiver. The baseband representation of the system at the receiver shown in Fig. 3.1 can be written as

$$y_n = \sum_{l=0}^{L-1} h_l d_{n-l} + w_n, \quad 0 \leq n \leq M-1 \tag{3.1}$$

where y_n is the symbol-rate received sample at the receiver, d_n is the transmitted symbol and $w_n \sim \mathbb{N}(0, \sigma^2)$ is the additive white Gaussian noise. h_l, $0 \leq l \leq L-1$, is a discrete time composite (overall) channel impulse response (CIR) that is the cascade of the transmit filter, the physical channel and the receive filter. The CIR is assumed

time-invariant within a burst, but will vary from burst to burst, a situation commonly assumed valid in burst mode communication systems.
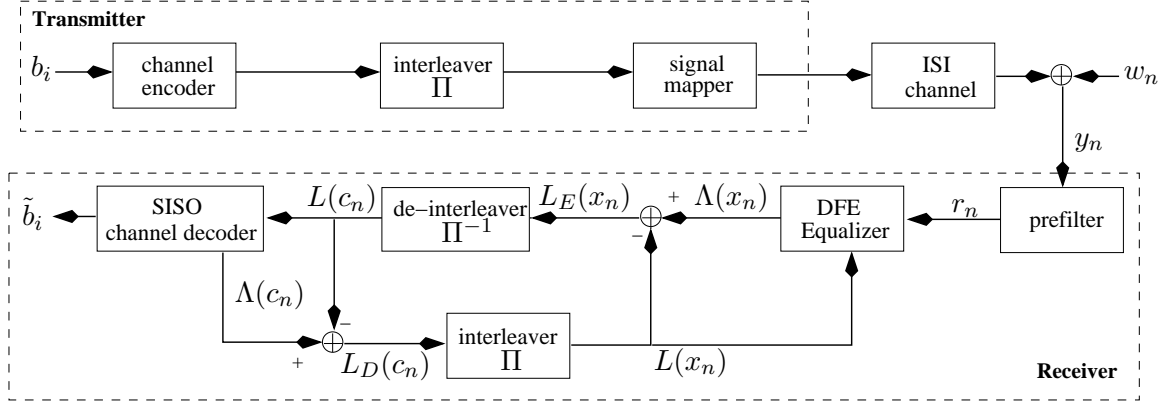
Figure 3.1: Turbo Equalization system model consists of SISO equalizer and channel decoder
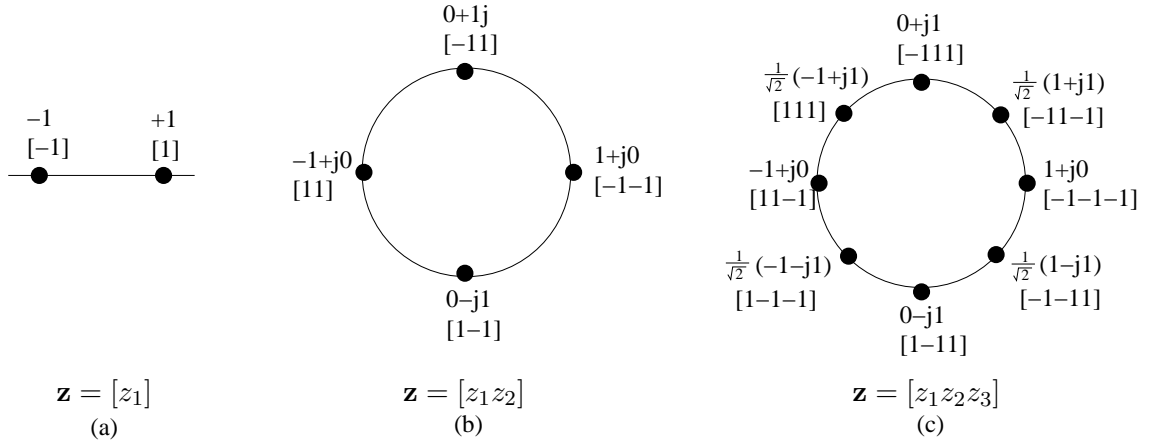
Figure 3.2: 2^Q-ary phase shift keying (PSK) symbols and bit patterns

Note that an anti-causal prefilter updated using the MMSE criterion [21] is added before the equalizer in Fig. 3.1 to transform the estimated CIR into the minimum phase form so that the leading taps will dominate the post prefilter CIR. In some channel profiles, such as typical urban and hilly terrain of the GSM/EDGE system, the channel impulse is not necessarily in the minimum phase form before the prefilter is applied. This leads to numerical instability and degradation of BER performance in reduced state equalization. Denote the output prefiltered received sequence as $\mathbf{r} = [r_0 r_1 \cdots r_{M-1}]$, the

input-output relationship of the received sample after the prefilter is given as follows

$$r_n = \sum_{l=0}^{L-1} u_l d_{n-l} + v_n \qquad (3.2)$$

where u_l, $0 \leq l \leq L-1$, is the minimum phase form feedback filter and v_n is additive white Gaussian noise. In the multipath channel where $L \geq 2$, ISI channel itself can be treated as a convolutional encoder with rate 1. Hence, the combination of ISI channel and a convolution encoder at the transmitter forms a serial concatenated 'coding' scheme, which can be iteratively decoded as shown in Fig. 3.1.

3.3   Principle of Turbo Equalization

The iterative receiver in the lower part of Fig. 3.1 is presented. For the sake of simplicity, the system model implements BPSK modulation is discussed in this section whereas higher modulation signals will be described in the section where the new equalizer is presented. The system model consists of two stages, a SISO equalizer following by a SISO channel decoder. They are separated by an interleaver $\Pi(\cdot)$ and a de-interleaver $\Pi^{-1}(\cdot)$ blocks. We consider only the BER-optimal MAP approach in decoding. For turbo equalization, it has been shown that the MAP-based equalizer using the BCJR algorithm (trellis-based detection) delivers the best result in simulations. It computes the *a posteriori* probabilities $P(x_n = x|\mathbf{r})$, $x \in \{-1, 1\}$, or *a posteriori* Log Likelihood Ratios (LLR) given by

$$\Lambda(x_n|\mathbf{r}) = \ln\frac{P(x_n = +1|\mathbf{r})}{P(x_n = -1|\mathbf{r})}. \qquad (3.3)$$

Using Bayes' Rule, (3.3) can be expressed as

$$\begin{aligned}
\Lambda(x_n|\mathbf{r}) &= \ln\frac{\sum_{\forall \mathbf{x}:x_n=+1} P(\mathbf{r}|\mathbf{x})P(\mathbf{x})}{\sum_{\forall \mathbf{x}:x_n=-1} P(\mathbf{r}|\mathbf{x})P(\mathbf{x})} \\
&= \ln\underbrace{\frac{\sum_{\forall \mathbf{x}:x_n=+1} P(\mathbf{r}|\mathbf{x}) \prod_{\forall n' \text{ except } n'=n} P(x_{n'})}{\sum_{\forall \mathbf{x}:x_n=-1} P(\mathbf{r}|\mathbf{x}) \prod_{\forall n' \text{ except } n'=n} P(x_{n'})}}_{L_E(x_n)} + L(x_n). \qquad (3.4)
\end{aligned}$$

$L(x_n)$ is the *a priori* information on the occurrence probability of x_n from the decoder in last iteration. In the first iteration, there is no *a priori* information available and we have $L(x_n) = 0, \forall n$. Starting from the second iteration, the existence of $L(x_n)$ may improve the information of the data x_n and further reduce the ISI. The *extrinsic* LLR $L_E(x_n)$ computed in the first term of (3.4) will be de-interleaved to $L(c_n)$ as the *a priori* information of the decoder. Based on the $L(c_n)$ and the trellis structure of the convolutional code, the MAP approach SISO channel decoder in the second stage computes the *extrinsic* LLR $L_D(c_n)$ of each code bit as follows

$$L_D(c_n) \triangleq \ln\frac{P(c_n = +1|L(c_1), \cdots, L(c_{K_c}))}{P(c_n = -1|L(c_1), \cdots, L(c_{K_c}))} - \underbrace{\ln\frac{P(c_n = +1)}{P(c_n = -1)}}_{L(c_n)} \tag{3.5}$$

where $L_D(c_n)$ is interleaved to provide the correct ordering of LLR $L(x_n)$ and fed into the equalizer as the *a priori* information in the next iteration. When arriving at the final iteration, the SISO channel decoder estimates the binary data bits $b_i \in \{0, 1\}$ using

$$\tilde{b}_i \triangleq \operatorname*{argmax}_{b \in \{0,1\}} P(b_i = b|L(c_1), \cdots, L(c_{K_c})). \tag{3.6}$$

It is important to note that the statistically independent *a priori* LLRs $L_E(x_n)$ and $L_D(c_n)$ are fed back to each other iteratively and lead to significant improvement in BER performance. This essential feature achieves the *turbo* principle, which is known as *turbo equalization*. However, after the first iteration, $L_E(x_n)$ and $L_D(c_n)$ become more correlated throughout the iterations. As a consequence, the improvement will diminish after a large number of iterations and therefore a termination criterion is required to stop the iterative process.

3.4 The MAP algorithm

The process of turbo code decoding and turbo equalization involves with the formation of *a posteriori probability* for each data bits, which is followed by choosing the data

bits that corresponds to the *maximum a posteriori* probability for that data bits. This implementation process some-what like a bi-directional Viterbi algorithm over a block of code bits. Once the state and the branch metrics for the blocks are computed, the APPS and the MAP can be obtained for each data bit represented within the block. In here, we briefly describe the formation of the state and branch metrics for the MAP algorithm. Let us denote the state of the trellis at time t as S_t and the code bits $x_t(S_{t-1}, S_t)$ is the output given by the state transition from state S_{t-1} to state S_t. Thereby, we can define the forward and backward recursions as follows

$$\mathbb{F}(S_t) = \sum_b \mathbb{F}(S_{t-1}^b) P[x_t(S_{t-1}^b, S_t)] \tag{3.7}$$

$$\mathbb{B}(S_t) = \sum_b \mathbb{B}(S_{t+1}^b) P[x_t(S_t, S_{t+1}^b)] \tag{3.8}$$

where b is the input bits. For implementation simplicity, we assume that the forward state and backward state start at the first state, which imply that $\mathbb{F}(S_0 = 0) = \mathbb{B}(S_0 = 0) = 1$ and $\mathbb{F}(S_0 \neq 0) = \mathbb{B}(S_0 \neq 0) = 0$. In equations (3.7) and (3.8), the summation is the sum of overall possible states S_{t-1} and S_{t+1}, respectively, where the transtition (S_{t-1}, S_t) and (S_t, S_{t+1}) are possible.

3.4.1 State Metric Calculation

In Fig., the graphical representation for the calculation of forward state and backward state metrics are depicted. Assume that there are two possible inputs $b = \{0, 1\}$. The equations (3.7) and (3.8) can expanded as follows,

$$\mathbb{F}(S_t) = \mathbb{F}(S_{t-1}^0) P[x_t(S_{t-1}^0, S_t)] + \mathbb{F}(S_{t-1}^1) P[x_t(S_{t-1}^1, S_t)] \tag{3.9}$$

$$\mathbb{B}(S_t) = \mathbb{B}(S_{t+1}^0) P[x_t(S_t, S_{t+1}^0)] + \mathbb{B}(S_{t+1}^0) P[x_t(S_t, S_{t+1}^0)] \tag{3.10}$$

It is important to note that a direct implementation of the equations (3.9) and (3.10) will cause the system numerically unstable, since both $\mathbb{F}(S_t)$ and $\mathbb{B}(S_t)$ drop toward zero

exponentially. In order to avoid these defect and produce a numerically stable algorithm, these quantities must be scale as the computation proceeds. Denote $\tilde{\mathbb{F}}(S_t)$ is the scaled version of $\mathbb{F}(S_t)$. Thereby, for each $t \geq 2$, we can write the following equations,

$$\mathbb{F}(S_t) = \sum_b \tilde{\mathbb{F}}(S_{t-1}^b)P[x_t(S_{t-1}^b, S_t)] \tag{3.11}$$

$$\tilde{\mathbb{F}}(S_t) = e_t \cdot \mathbb{F}(S_t) \tag{3.12}$$

$$e_t = 1 \bigg/ \sum_{S_t} \mathbb{F}(S_t) \tag{3.13}$$

Now, imply a simple induction, $\tilde{\mathbb{F}}(S_t)$ is given by

$$\tilde{\mathbb{F}}(S_{t-1}) = (\Pi_{i=1}^{t-1}e_i)\mathbb{F}(S_{t-1})$$

$$= E_{t-1}\mathbb{F}(S_{t-1}) \tag{3.14}$$

$$\tilde{\mathbb{F}}(S_t) = \frac{\sum_b E_{t-1}\mathbb{F}(S_{t-1}^b)P[x_t(S_{t-1}^b, S_t)]}{\sum_{S_t}\sum_b E_{t-1}\mathbb{F}(S_{t-1}^b)P[x_t(S_{t-1}^b, S_t)]}$$

$$= \frac{\mathbb{F}(S_t)}{\sum_{S_t}\mathbb{F}(S_t)} \tag{3.15}$$

According to (3.15), we can obtain the numerically stable $\mathbb{F}(S_t)$ by effectively scaled by the sum over all states of $\mathbb{F}(S_t)$.

In proceed, let us denote $\tilde{\mathbb{B}}(S_t)$ as the scaled version of $\mathbb{B}(S_t)$. For each $t < \tau - 1$, we compute the following expressions,

$$\mathbb{B}(S_t) = \sum_b \tilde{\mathbb{B}}(S_{t+1}^b)P[x_t(S_t, S_{t+1}^b)] \tag{3.16}$$

$$\tilde{\mathbb{B}}(S_t) = f_t \cdot \mathbb{B}(S_t) \tag{3.17}$$

$$f_t = 1 \bigg/ \sum_{S_t} \mathbb{B}(S_t) \tag{3.18}$$

Same as above, by simple induction, we can derive the following expressions,

$$\tilde{\mathbb{B}}(S_{t+1}) = (\Pi_{i=t+1}^{\tau}f_i)\mathbb{B}(S_{t+1})$$

$$= F_{t+1}\mathbb{B}(S_{t+1}) \tag{3.19}$$

$$\tilde{\mathbb{B}}(S_t) = \frac{\sum_b F_{t+1}\mathbb{B}(S_{t+1}^b)P[x_t(S_t, S_{t+1}^b)]}{\sum_{S_t}\sum_b F_{t+1}\mathbb{B}(S_{t+1}^b)P[x_t(S_t, S_{t+1}^b)]}$$

$$= \frac{\mathbb{B}(S_t)}{\sum_{S_t}\mathbb{B}(S_t)} \tag{3.20}$$

3.4.2 Branch Metric Calculation

We start with the equations

$$L(x_t) = \log\frac{P(x_t = +1)}{P(x_t = -1)} \tag{3.21}$$

$$P(x_t = +1) = 1 - P(x_t = -1). \tag{3.22}$$

Assume that $x = \{-1, +1\}$, after some mathematical manipulation, we obtain

$$
\begin{aligned}
P[x_t = x] &= \frac{\exp[xL(x_t)]}{1 + \exp[xL(x_t)]} \\
&= \frac{2\exp[\frac{x}{2}L(x_t)]}{\exp[\frac{x}{2}L(x_t)]\{\exp[-\frac{x}{2}L(x_t)] + \exp[\frac{x}{2}L(x_t)]\}} \\
&= \frac{1}{2}\frac{\cosh[\frac{1}{2}L(x_t)] + x\sinh[\frac{1}{2}L(x_t)]}{\cosh[\frac{1}{2}L(x_t)]} \\
&= \frac{1}{2}[1 + x\tanh(\frac{1}{2}L(x_t))] \tag{3.23}
\end{aligned}
$$

where $L(x_t)$ is the *a priori* information for the channel decoder or channel equalizer.

3.5 Turbo Equalization using DFE

Clearly, the MAP equalizer computes the soft information based on the trellis structure is complicated. When the large constellation symbols are distorted by a length L multipath channel, the receiver may require excessive computational power that is impractical in today's technology. In this section, we replace the MAP equalizer by an inexpensive MMSE-DFE equalizer that computes the probability on a symbol by symbol basis instead of the received sequence.

3.5.1 Conventional DFE Algorithm

After the MMSE prefilter, we will have the channel impulse response in minimum phase form. According to input-output relationship (3.2), when BPSK modulated signals are

transmitted ($d_n = x_n$), we can write the *a posteriori* probability (APP) of the BPSK signal being +1 as follows,

$$P(x_n = +1|r_n) = \frac{P\left(r_n|\tilde{\mathbf{X}}_n^{+1}\right) P(x_n = +1)}{\sum_x P\left(r_n|\tilde{\mathbf{X}}_n^x\right) P(x_n = x)}, \quad x \in \{-1, +1\} \tag{3.24}$$

where

$$\tilde{\mathbf{X}}_n^{+1} = [\tilde{x}_0 \ \tilde{x}_1 \ \cdots \ \tilde{x}_{n-1} \ +1], \tag{3.25}$$

$$P\left(r_n|\tilde{\mathbf{X}}_n^{+1}\right) = \frac{1}{\sqrt{2\pi\sigma^2}} \exp\left[-\frac{1}{2\sigma^2}\left|r_n - u_0(+1) - \sum_{l=1}^{L-1} u_l\tilde{x}_{n-l}\right|^2\right]. \tag{3.26}$$

$\tilde{x}_i$ is the feedback hard decided symbol estimated by the DFE. Similarly, define $P(x_n = -1|r_n)$. Substitute (3.26) and (3.24) into (3.3) with some mathematical manipulations, the *a posteriori* LLR of code bit is given by

$$\Lambda(x_n) = \ln \underbrace{\frac{\exp\left[-\frac{1}{2\sigma^2}\left|r_n - u_0(+1) - \sum_{l=1}^{L-1} u_l\tilde{x}_{n-l}\right|^2\right]}{\exp\left[-\frac{1}{2\sigma^2}\left|r_n - u_0(-1) - \sum_{l=1}^{L-1} u_l\tilde{x}_{n-l}\right|^2\right]}}_{L_E(x_n)} + \underbrace{\ln\frac{P(x_n = +1)}{P(x_n = -1)}}_{L(x_n)}. \tag{3.27}$$

A similar *a posteriori* LLR can be found in [36]. Based on (3.27), the hard decided code bits can be estimated and feedback to the equalizer for the next symbol estimation. Assuming that all the feedback symbols are estimated correctly, the cancellation of ISI interference results in better BER performance. Meanwhile, the *extrinsic* LLR $L_E(x_n)$, the first term of (3.27), is interleaved and delivered to the channel decoder as the *a priori* information. Unfortunately, the performance of the conventional MMSE-DFE is poor in turbo equalization due to the residual interference in the presence of the severely multipath channels and incorrect symbols are being feedback during equalization. In [32, 33], the simulation results indicate that MMSE-DFE is not an effective equalizer and it has only small improvement throughout the iterations when compared with a MMSE linear equalizer.

3.5.2 Improved DFE Algorithm

Here we proceed to a novel DFE algorithm for the iterative receiver to improve BER performance over an ISI channel. The key idea is increasing the reliability of the *extrinsic* LLR by computing an extra metric. Let us define $\tilde{x}_n^{(k)}$ as the nth symbol estimated at kth iteration from the equalizer. In the first iteration of turbo equalization, the *a posteriori* LLR is calculated based on equation (3.27) and there is no *a priori* LLR available from the channel decoder. Starting from the second iteration, we define a new *a posteriori* probability of the code bit as follows,

$$
P(x_n^{(k)} = +1 | r_n, r_{n+1}) \triangleq
$$
$$
\frac{P\left(r_n, r_{n+1} | \tilde{x}_{n+1}^{(k-1)}, \tilde{\mathbf{X}}_n^{+1}\right) P(x_n^{(k)} = +1)}{\sum_x P\left(r_n, r_{n+1} | \tilde{x}_{n+1}^{(k-1)}, \tilde{\mathbf{X}}_n^x\right) P(x_n^{(k)} = x)}, \quad x \in \{-1, +1\} \tag{3.28}
$$

where $k = 2, 3, \cdots, \infty$ denotes the number of iteration and $x_n^{(k)}$ is the code bit estimated in kth iteration. Similarly define $P(x_n^{(k)} = -1 | r_n, r_{n+1})$. Given that the received samples are independent, the probability of received samples r_n and r_{n+1} at kth iteration is obtained using (3.26) and given as

$$
\begin{aligned}
P\left(r_n, r_{n+1} | \tilde{x}_{n+1}^{(k-1)}, \tilde{\mathbf{X}}_n^{+1}\right) &= P\left(r_n | \tilde{\mathbf{X}}_n^{+1}\right) P\left(r_{n+1} | \tilde{x}_{n+1}^{(k-1)}, \tilde{\mathbf{X}}_n^{+1}\right) \\
&= \frac{1}{\sqrt{2\pi\sigma^2}} \exp\left[-\frac{1}{2\sigma^2}\left\{g_0(x_n = +1) + g_1(x_n = +1)\right\}\right] \tag{3.29}
\end{aligned}
$$

where

$$
\begin{aligned}
g_0(x_n = x) &= \left| r_n - u_0 \cdot x - \sum_{l=1}^{L-1} u_l \tilde{x}_{n-l}^{(k)} \right|^2, \\
g_1(x_n = x) &= \left| r_{n+1} - u_1 \cdot x - \left(u_0 \tilde{x}_{n+1}^{(k-1)} + \sum_{l=2}^{L-1} u_l \tilde{x}_{n-l+1}^{(k)} \right) \right|^2, \quad x \in \{-1, +1\}.
\end{aligned}
$$

Define a new *a posteriori* LLR $\Lambda(x_n^{(k)}) = \ln\frac{P(x_n^{(k)}=+1|r_n, r_{n+1})}{P(x_n^{(k)}=-1|r_n, r_{n+1})}$, we substitute (3.29) into (3.28) and after some mathematical manipulations, we obtain the new *a posteriori* LLR

of code bit at kth iteration as follows

$$\Lambda(x_n^{(k)}) = \ln\underbrace{\frac{\exp\left[-\frac{1}{2\sigma^2}\left\{g_0(x_n=+1)+g_1(x_n=+1)\right\}\right]}{\exp\left[-\frac{1}{2\sigma^2}\left\{g_0(x_n=-1)+g_1(x_n=-1)\right\}\right]}}_{L_E(x_n^{(k)})}+\ln\underbrace{\frac{P(x_n^{(k)}=+1)}{P(x_n^{(k)}=-1)}}_{L(x_n^{(k)})}. \quad (3.30)$$

Comparing the first term in equations (3.27) and (3.30), it is clear that the new algorithm considers the extra metric r_{n+1} in the process of computing $L_E(x_n^{(k)})$. It is important to note that in the first iteration, when the DFE computes $L_E(x_n^{(1)})$, neither $L(x_n^{(1)})$ nor symbol $\tilde{x}_{n+1}^{(0)}$ information is available. Therefore, the computation of metric r_{n+1} is discarded and the new algorithm (3.30) is simplified to the conventional DFE algorithm given in (3.27) in the first iteration. The conventional DFE discards the estimated symbol set $\tilde{\mathbf{x}}$ at the end of process. On the other hand, the improved DFE algorithm not only has the estimated set of symbols $\tilde{\mathbf{x}}^{(k)} = [\tilde{x}_0^{(k)}\tilde{x}_1^{(k)}\cdots\tilde{x}_{M-1}^{(k)}]$, fed back to the equalizer for ISI cancellation, it also keeps the data in memory for the estimation in the next iteration $(k+1)$. Hence, the new algorithm treats the detected symbol $\tilde{\mathbf{x}}$ from the last iteration as another set of *a priori* information besides $L(x_n)$ that is delivered from the channel decoder. In short, the metric of the received sample r_{n+1} is computed based on the *a priori* data $\tilde{x}_{n+1}^{(k-1)}$ and the feedback data $\tilde{x}_i^{(k)}$ from the DFE starting from the second iteration onward.

Remark: The new *a posteriori* probability can be computed using L number of received samples. For instance, $P(x_n^{(k)}=+1|r_n,r_{n+1},\cdots,r_{n+j})$, where $j=0,1,\cdots,L-1$. Given that j equals to 0 and 1, it is simplified to (3.24) and (3.28), respectively. According to the system model in Section II, prior to equalization, the CIR is first fed to the anti-causal MMSE prefilter and hence the energy of prefiltered CIR is concentrated at the first few taps. Consequently, while $j \geq 2$, the gain of the BER is thus small. Due to this reason and the tradeoff between the computational complexity and the system performance, we compute the new *a posteriori* probability using $j=1$ throughout this chapter.

3.5.3 Improved DFE in M-PSK modulation systems

When $Q > 1$, (such as QPSK and 8-PSK modulation), is employed in the system, the *extrinsic* information cannot be computed directly using the equations (3.27) and (3.30) while the estimation is based on the complex number symbols $s_i \in \mathcal{S}$. Thus, a slight modification is required to facilitate the LLR calculation of the code bits in higher constellation modulation scheme. Denote

$$\tilde{\mathbf{D}}_n^{s_i} \triangleq [\tilde{d}_0 \cdots \tilde{d}_{n-1} s_i], \tag{3.31}$$

$$\mathbb{S}_j^{+1} \triangleq \{s_i \in \mathcal{S} : z_{i,j} = +1\}, \quad j \in \{1, 2, \cdots, Q\} \tag{3.32}$$

where $\tilde{\mathbf{D}}_n^{s_i}$ is the estimated feedback sequence that has s_i at the nth sample and $\mathbb{S}_j^{+1}$ consists of a set of symbols s_i, whose jth bit $z_{i,j} = +1$. Similarly, define $\mathbb{S}_j^{-1}$. Proceeding, we define a new *a posteriori* probability of the code bit in M-PSK modulation system as follows,

$$P(x_{n,j}^{(k)} = 1 | r_n, r_{n+1}) \triangleq$$
$$\frac{\sum_{s_i \in \mathbb{S}_j^{+1}} P\left(r_n, r_{n+1} | \tilde{d}_{n+1}^{(k-1)}, \tilde{\mathbf{D}}_n^{s_i}\right) P(x_{n,j}^{(k)} = +1)}{\sum_{s_i} P\left(r_n, r_{n+1} | \tilde{d}_{n+1}^{(k-1)}, \tilde{\mathbf{D}}_n^{s_i}\right) P(x_{n,j}^{(k)} = x)}, \quad x \in \{-1, +1\}. \tag{3.33}$$

Applying the same derivation steps from previous subsection, we are able to obtain the new *a posteriori* LLR of code bit at kth iteration in M-PSK modulation system as follows

$$\Lambda(x_{n,j}^{(k)}) = \ln \underbrace{\frac{\sum_{s_p \in \mathbb{S}_j^{+1}} \exp\left[-\frac{1}{2\sigma^2}\{g_0(d_n = s_p) + g_1(d_n = s_p)\}\right]}{\sum_{s_q \in \mathbb{S}_j^{-1}} \exp\left[-\frac{1}{2\sigma^2}\{g_0(d_n = s_q) + g_1(d_n = s_q)\}\right]}}_{L_E(x_{n,j}^{(k)})}$$
$$+ \ln \underbrace{\frac{P(x_{n,j}^{(k)} = 1)}{P(x_{n,j}^{(k)} = -1)}}_{L(x_{n,j}^{(k)})}. \tag{3.34}$$

It is important to note that the new DFE computes the *a posteriori* LLR based on the feedback estimated complex modulated signals. Thus, *a posteriori* LLR are hard decided to $x \in \{-1, +1\}$ and mapped to the modulated signal $s_i \in \mathcal{S}$ before feed back

to the equalizer for next symbol estimation. Finally, we summarize the new complete DFE algorithm processing a received sequence $\mathbf{r}$ and the computation of the *a priori* information in Table 3.1. In the Section VI, the simulation results show that the new algorithm provides more reliable information for symbol detection and improves the BER performance significantly by computing the extra metric r_{n+1}.

---

1. Filter $y_n = \sum_{l=0}^{L-1} h_l d_{n-l} + w_n$ and obtain
       i. $r_n = \sum_{l=0}^{L-1} u_l d_{n-l} + v_n$
2. First iteration: $L(x_{n,j}) = 0, \forall n$
       i. Compute $L_E(x_{n,j}^{(1)})$ based on the first term in (3.27).
       ii. Make hard decision on code bits based on $\Lambda(x_{n,j}^{(1)})$.
       iii. Map code bits $[x_{n,1}^{(1)} x_{n,2}^{(1)} \cdots x_{n,Q}^{(1)}]$ to corresponding symbol.
       iv. Feedback $\tilde{d}_n^{(1)}$ for ISI cancellation.
       v. Save $\tilde{d}_n^{(1)}$ in memory.
       vi. Deliver $L_E(x_{n,j}^{(1)})$ to channel decoder for second stage process.
3. kth iteration, $k \in \{2, \cdots, \infty\}$:
       i. Compute $L_E(x_{n,j}^{(k)})$ based on the first term in (3.30).
         • Metric r_n is calculated based on feedback symbols $[\tilde{d}_{n-1}^{(k)} \tilde{d}_{n-2}^{(k)} \cdots \tilde{d}_{n-L+1}^{(k)}]$.
         • Metric r_{n+1} is calculated based on previous iteration symbol $\tilde{d}_{n+1}^{(k-1)}$ and feedback symbols $[\tilde{d}_{n-1}^{(k)} \cdots \tilde{d}_{n-L+2}^{(k)}]$.
       ii. Repeat (ii) through (vi) in step 2.

Table 3.1: Turbo equalization using new MMSE-DFE equalizer

3.6 Performance Analysis and Complexity

Assuming that we have perfect knowledge of the channel information, we may compute the mean squared error (MSE) J_n and the time average MSE $\bar{J}$ as follows

$$J_n \triangleq E\left(|y_n - \tilde{y}_n|^2\right), \tag{3.35}$$

$$\bar{J} = \frac{1}{M} \sum_{n=0}^{M-1} E\left(|y_n - \tilde{y}_n|^2\right) \tag{3.36}$$

where $\tilde{y}_n$ is the nth estimated received sample formed by the hard decided symbols given by

$$\tilde{y}_n \;=\; \sum_{l=0}^{L-1} h_l \tilde{d}_{n-l}. \tag{3.37}$$

Denote $\bar{J}_{DFE}$ and $\bar{J}_{NEW}$, respectively, are the time averaged MSE computed using the conventional and improved DFE. If all the transmitted symbols are estimated correctly, then the time-averaged MSE $\bar{J}$ becomes

$$\bar{J}_{\min} \;=\; \frac{1}{M} \sum_{n=0}^{M-1} E\left(|(\tilde{y}_n + w_n) - \tilde{y}_n)|^2 \right) \tag{3.38}$$

$$\;=\; \sigma^2. \tag{3.39}$$

In Table 3.2, we compare the $\bar{J}_{DFE}$ and $\bar{J}_{NEW}$ at 4dB in different number of iterations. Obviously, the new DFE algorithm always has the smallest MSE when compared to the conventional DFE algorithm.

Another important aspect of these SISO equalizers is their computational complexity. Table II shows the required number of real multiplications and additions per received symbol r_n in an iteration to compute the *extrinsic* LLR $L_E(x_n)$. Given that 8-PSK modulated signals are implemented in ISI channel with discrete time channel length of $L = 6$. The conventional DFE requires 105 real multiplications and 102 real additions while the improved DFE requires 209 real multiplications and 206 real additions. Though, the computational complexity of the new algorithm is about doubled that of the conventional DFE, but it still has low computational complexity when compared to the optimum equalizers (SOVA or MAP) and is easily implemented in today's technology. The simulation results in next section strongly show that the BER performance are improved more than 1dB when using the improved DFE algorithm.

Equalizer	J at 4dB		
	2nd	5th	15th
Conventional DFE	0.8562	0.8196	0.8131
Improved DFE	0.8090	0.8007	0.7966

	Complexity		
	real multiplications	real additions	metrics
Conventional DFE	$2NL + N + 1$	$2NL + N - 2$	N
Improved DFE	$4NL + 2N + 1$	$4NL + 2N - 2$	$2N$

Table 3.2: The time-averaged MSE $\bar{J}$ at SNR= 4dB and Complexity. Data length M=1024; L: Channel impulse response length; N:Alphabet size of the signal constellation

3.7 Simulation Results

In this section, we present several simulation results obtained with the SISO MMSE DFE presented in Section IV. The entire scenario of turbo equalization is depicted in Fig. 3.1. In the BPSK and 8-PSK system, the block size of the transmitted data M is 1024. The binary data is encoded through rate $r = 1/2$ and constraint length $K = 5$ convolutional encoder. The generator code in octal notation is $G = [23, 35]$. The code bits are placed into a different order within a block of data by the interleaver to mitigate bursty errors. Prior to transmission, the code bits are mapped to the M symbols based on the 2^Q-ary bit patterns shown in Fig. 2. Within a burst, we consider a static ISI channel (slow fading) with $L = 6$ and the CIR given as

$$
\begin{aligned}
h(n) &= (-0.0058 + 0.0007j)\delta(n) + (-0.1577 + 0.5639j)\delta(n-1) \\
&\quad + (-0.2282 + 0.7624j)\delta(n-2) + (-0.1303 + 0.0769j)\delta(n-3) \\
&\quad + (-0.0286 + 0.0014j)\delta(n-4) + (-0.0004 + 0.0052j)\delta(n-5)
\end{aligned}
$$

where j is $\sqrt{-1}$ and the complex path gains are normalized such that $\sum_{l=0}^{L-1} |h_l|^2 = 1$. The additive white Gaussian noise added to the received symbols is determined by the desired E_b/N_0. In the lower part of Fig. 1, the received signal y_n is first fed into the prefilter, which has the length of the anti-causal feedforward and causal feedback filters equal to 12 and 6, respectively.

According to the improved DFE algorithm derived in Section IV, it has the same

performance as the conventional DFE algorithm if *a priori* data $\tilde{x}_{n+1}^{(k-1)}$ from previous iteration and $L(x_n)$ do not exist. Obviously, the conventional DFE algorithm has only a small improvement in BER after several iterations in all the figures. In the BPSK system shown in Fig. 3, the conventional DFE has BER of 0.006 at 5 dB E_b/N_0 after 5 iterations. It has only an 1dB gain compared to the BER after the first iteration. However, using the improved DFE algorithm can achieve 2dB gain after 5 iterations. In Fig. 4, the code bits are modulated into 8-PSK. After one iteration, the receiver achieves a BER of 0.058 at 6dB E_b/N_0. Clearly, the gain of the new method is thus 2.2dB while the conventional DFE only produces the gain of 1.2dB after 5 iterations. The results indicate that the improved DFE algorithm can achieve approximate 1dB gain extra by computing the metric r_{n+1} compared to the conventional DFE algorithm. Besides, in Fig. 3.4 and 3.5, the new DFE algorithm obviously requires only 3 iterations to achieve better BER performance compared to the all BER performance (up to 15 iterations in the simulations) computed by the conventional DFE algorithm.

Note that the BER performance given above is simulated with the data block size M. A better BER can be achieved after several iterations by using a longer data block size. For instance, in Fig. 3.6, the BER performance at 4dB E_b/N_0 based on data lengths of 2^8, 2^9 and 2^{11} are depicted. 'DFE 2^8' denotes the BER performance computed by the conventional DFE using the data length 2^8. Similarly, define improved DFE. Apparently, the improved DFE improves the BER dramatically while data length is increased. After 7 iterations, the conventional DFE using data length 2^9 achieves the BER at 0.0266 but the BER offered by the improved DFE can be as good as 0.0028. Moreover, the improved DFE algorithm with data length 2^8 requires only 3 iterations to achieve better BER performance than those of conventional DFE with different data length.

3.8   Conclusion

In this chapter, the improved DFE algorithm is introduced and analyzed for turbo equalization. We address the exhaustive computational complexity of the MAP equalizer and the inefficiency of the conventional DFE algorithm in iterative equalization, especially when the higher level modulation is used with severely distorted ISI channels. The new method improves the BER performance by computing the extra metric r_{n+1} using the feedback symbols from previous iteration and combining it with *a priori* information of the symbols. After each iteration, the hard detected symbols are saved in the memory as *a priori* data for next iteration. We verified the proposed algorithm for BPSK and 8PSK modulation. The promising simulation results show that the BER performance given by the proposed low complexity DFE algorithm improved dramatically throughout the iterations when the conventional DFE has only insignificant improvement in the process of iterative equalization.

(a)

(b)
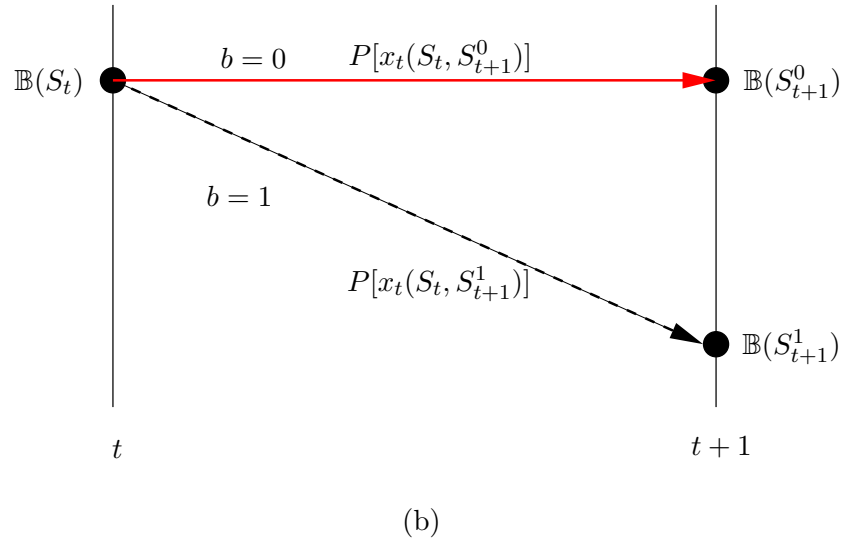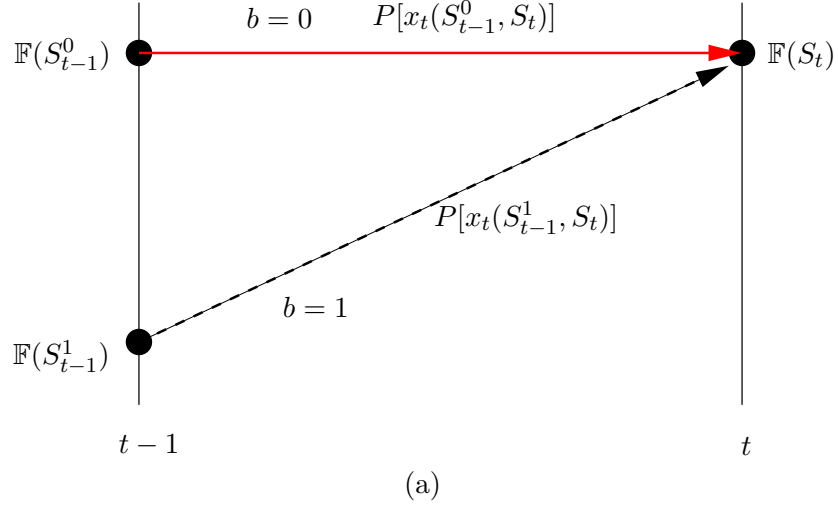
Figure 3.3: (a) Forward state metrics. (b) Backward state metrics.

44
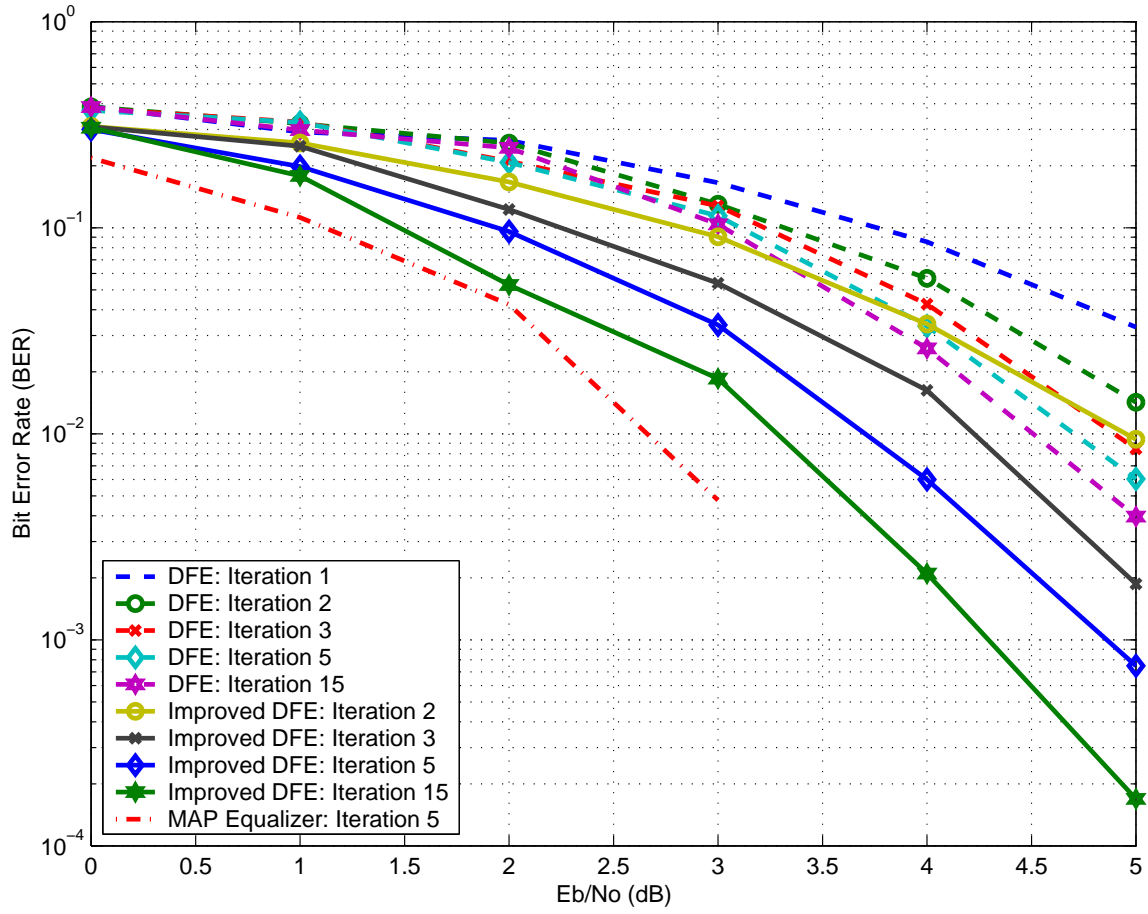
Figure 3.4: BER performance of conventional and improved DFE in BPSK modulation system.
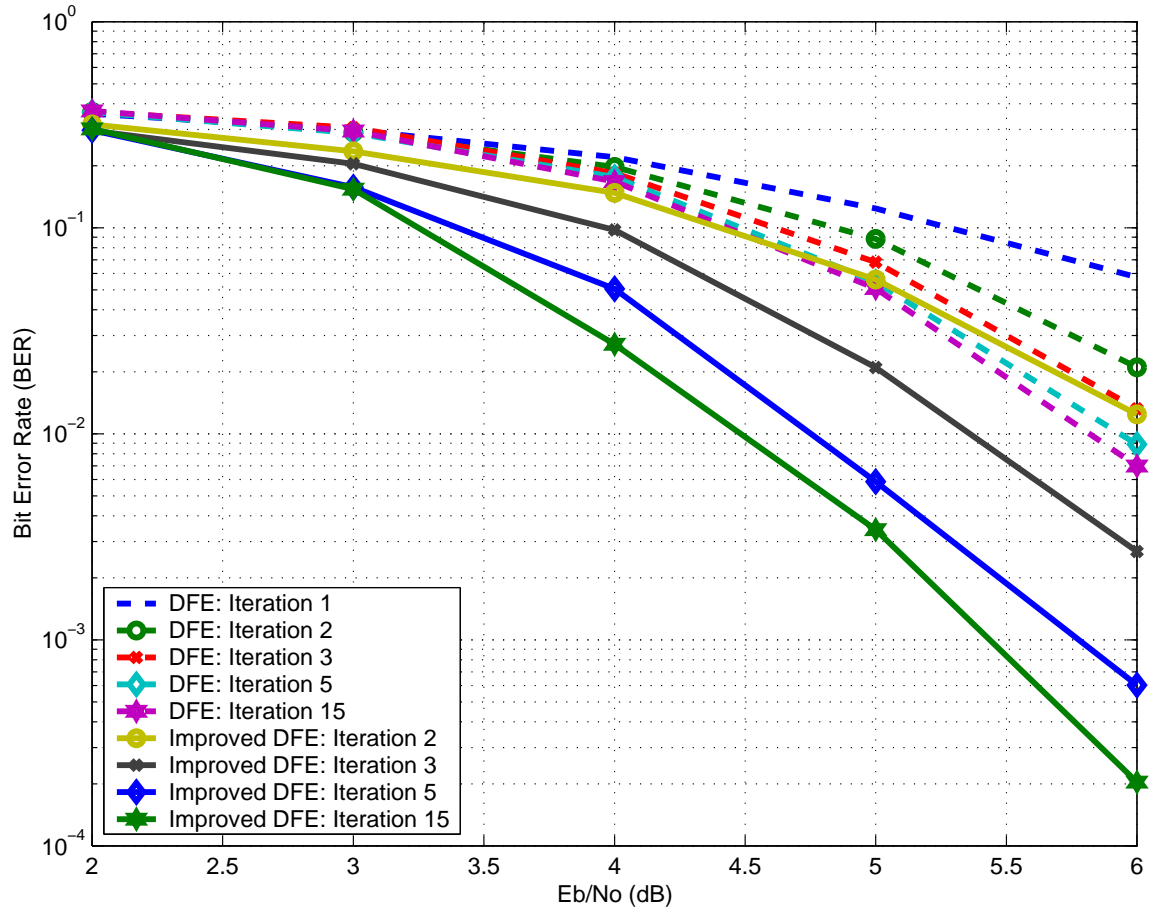
Figure 3.5: BER performance of conventional and improved DFE in 8PSK modulation system.
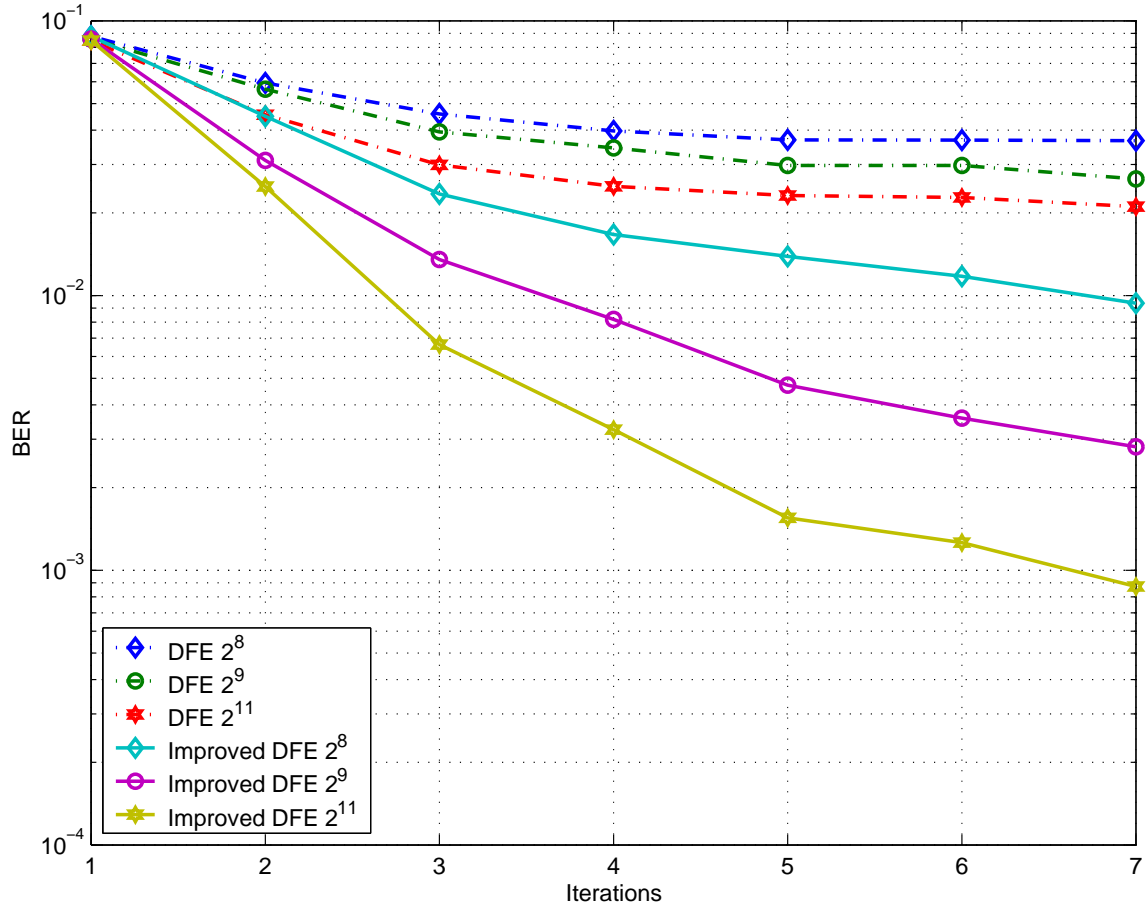
Figure 3.6: Effect of data length on performance of conventional and improved DFE at $E_b/N_o = 4$dB in turbo equalization.

Chapter 4

Fast Time-Varying Dispersive Channel Estimation and Equalization for 8-PSK Cellular System

4.1 Introduction

As described in Chapter 2, the third generation cellular system Enhanced Data Rates for GSM Evolution has similar slot structure and system parameters as GSM but has higher data rates and spectral efficiency. Time-division multiple-access is used in EDGE with the symbol period $T_s = 3.69\mu s$ and a slot length of $576.92\mu s$. Consequently, for static or slow moving communication devices, it is reasonable to assume that the fading channel is time-invariant during the period of one time slot. This assumption is adopted by us in Chapter 2 and papers [12], [21], where various channel estimation and equalization algorithms are developed or applied for EDGE system with slow fading channels. The application of the delayed decision feedback sequence estimation and reduced state sequence estimation equalizers are discussed in [12], where the time-invariant channel

was estimated with least-squares method. In [21], a computationally efficient perturbation equalizer with weighted LS channel estimation was proposed for the 8-PSK EDGE system. The simulation results obtained in these references are in good agreement with those obtained under ideal cases, *i.e.*, perfect channel estimation with maximum likelihood sequence estimation (MLSE) equalizer. However, the algorithms developed for slow fading channels cannot be directly applied to systems with high mobile speed subscribers, where the time-invariant channel assumption cannot hold.

In this chapter, the channel estimation and equalization for 8-PSK system in the typical channel profiles of EDGE system are discussed. We adopt the EDGE system parameters such as data bandwidth, 8-PSK modulation, transmit and receive filters as the simulation setup. In next, a LS based algorithm is proposed for the estimation of the time-varying channel. We first analyze the characteristics of the time-varying fading channel, and show that the time-varying property of fast fading channels of EDGE system can be modeled as a linear function of the time in the range of Doppler frequency up to 100Hz. Based on this property, we develop a novel LS based method for EDGE system with fast fading dispersive channels.

The MLSE equalizer with Viterbi algorithm is currently used in GSM systems, where binary Gaussian minimum-shift keying (GSMK) is used as the modulation scheme. In order to improve the system throughput, 8-PSK modulation is employed in EDGE system. The computational complexity of MLSE equalizer makes it prohibitive to be used in EDGE system. It is shown in [12] that DDFSE and RSSE equalization techniques provide good trade-offs between the system performance and computational complexity. It is important to note that the performance of these equalizers will degrade dramatically if the CIR is not in its minimum-phase form, as the leading taps of the CIR need to be dominant. For time-invariant channels, prefilter can be used in the system to produce a minimum-phase channel. However, the prefilter approach is not applicable to systems with time-varying CIR without resorting to complex channel tracking. To overcome this

problem, a Cholesky decomposition method is introduced in this chapter to convert the estimated CIR energy to dominant in the first few taps in the presence of a time-varying CIR.

4.2   Discrete-Time Linear Estimation

Given in Chapter 2, when channel equalization is performed to estimate the data sequence, the system is optimized if MLSE is implemented and provided that the receiver has the perfect channel information. In many practical case of interest especially in wireless communication, the channel is time-variant and unknown to the receiver. Thus, the channel estimation is performed periodically to update the channel information. In next, we introduce the estimation on the physical parameter of interest by using Wiener theory.

4.2.1   Least-Squares Estimation

According to [24], Wiener theory optimize the estimation by minimizing the mean-square value of the error signal. Consider the same system implemented in Chapter 2 where the received signal at the receiver is given by $y_k = \sum_{l=0}^{L-1} d_{k-l} h(l) + n_k$. The transmitted signals are first distorted by difference time-delay channel impulse response and then corrupted by the additive white Gaussian noise. Define an error signal or residual as

$$e_k = n_k = y_k - \sum_{l=0}^{L-1} d_{k-l} h(l), \qquad k = 0, 1, \cdots, n. \tag{4.1}$$

Given by Wiener theory, the estimation of the CIR $\mathbf{h} = [h_0 h_1 \cdots h_{L-1}]$ is performed in such a way that it minimizes the residual sum of squares that given by

$$J(n) = \sum_{k=0}^{n} e_k^2 \tag{4.2}$$

$$= \sum_{k=0}^{n} y_k^2 - 2 \sum_{l=0}^{L-1} h(l) \sum_{k=0}^{n} y_k d_{k-l} + \sum_{l=0}^{L-1} \sum_{m=0}^{L-1} h(l) h(m) \sum_{k=0}^{n} d_{k-l} d_{k-m} \tag{4.3}$$

Differentiating equation (4.3) with respect to $h(l)$, we have

$$\frac{\partial J(K)}{\partial h(l)} = -2\sum_{k=0}^{K} y_k d_{k-l} + 2\sum_{m=0}^{L-1} h(m) \sum_{k=0}^{K} d_{k-l}d_{k-m} \qquad (4.4)$$

By letting $\partial J(K)/\partial h(l) = 0$, we get a set of L simultaneous equations consists the deterministic normal equations. As a result, the estimated CIR $\hat{\mathbf{h}} = [\hat{h}_0 \hat{h}_1 \cdots \hat{h}_{L-1}]^T$, where $[\cdot]^T$ is a transpose function operator, can be easily solved from (4.4) which is known as **least-squares estimation**. We may rewrite the normal equations above in a compact form by using the following definitions. Define a row vector $\mathbf{d}_k = [d_k d_{k+1} \cdots d_{k+L-1}]$; the received sample at the receiver can be written as

$$y_k = \mathbf{d}_k * \hat{\mathbf{h}} \qquad (4.5)$$

$$\mathbf{d}_k^T y_k = \mathbf{d}_k^T \mathbf{d}_k * \hat{\mathbf{h}} \qquad (4.6)$$

where $\mathbf{d}_k^T \mathbf{d}_k \in \mathbb{C}^{L \times L}$ represents the correlation matrix of the transmitted signals and $\mathbf{d}_k^T y_k \in \mathbb{C}^{1 \times L}$ represents the cross-correlation column vector of the transmitted signals and the received sample. Assume that the $\mathbf{d}_k^T \mathbf{d}_k$ is non-singular, we solve $\hat{\mathbf{h}}$ as follows,

$$\mathbf{d}_k^T \mathbf{d}_k * \hat{\mathbf{h}} = \mathbf{d}_k^T y_k \qquad (4.7)$$

$$\hat{\mathbf{h}} = [\mathbf{d}_k^T \mathbf{d}_k]^{-1} \mathbf{d}_k^T y_k. \qquad (4.8)$$

It is important to note that the least square estimate of the coefficient vector approaches the optimum Wiener solution as the data length n approaches infinity. Moreover, the least-squares estimator is an unbiased estimator [24].

4.2.2 Recursive Least-Squares Algorithm

In this section, our goal is demonstrating a recursive algorithm for computing the least-squares estimate $\hat{\mathbf{h}}$ of the coefficient vector. The recursive least-squares (RLS) algorithm is capable of adjusting the coefficients of the channel impulse response $\hat{\mathbf{h}}$ with the arrival of each new sample. In each iteration, the RLS algorithm learns a little more about the

statistics of the relevant signals, and an improvement to current set of $\tilde{\mathbf{h}}$ is computed using this new information. In the development of RLS algorithm, in part, relies on the inverse operation of a matrix in linear algebra known as the matrix inversion lemma. Thereby, we first introduce the concept of the matrix inversion lemma and next proceed to the RLS algorithm.

A. The Matrix-Inversion Lemma

Let $\mathbf{E}$ and $\mathbf{B} \in \mathbb{C}^{L \times L}$ be two positive definite matrices related by

$$\mathbf{E} = \mathbf{B}^{-1} + \mathbf{C}\mathbf{D}^{-1}\mathbf{C}^T \tag{4.9}$$

where $\mathbf{C} \in \mathbb{C}^{L \times M}$ matrix and $\mathbf{D} \in \mathbb{C}^{M \times M}$ positive definite matrix. According to the definition of matrix inversion lemma, the inverse of matrix $\mathbf{A}$ is given by

$$\mathbf{E}^{-1} = \mathbf{B} - \mathbf{B}\mathbf{C}[\mathbf{D} + \mathbf{C}^T\mathbf{B}\mathbf{C}]^{-1}\mathbf{C}^T\mathbf{B}. \tag{4.10}$$

B. RLS algorithm

Denote

$$\mathbf{U}(n) = \mathbf{d}_n^T\mathbf{d}_n \tag{4.11}$$

$$\mathbf{V}(n) = \mathbf{d}_n^T y_n. \tag{4.12}$$

The correlation matrix $\mathbf{U}(n)$ can be updated by recursive algorithm as follows,

$$\mathbf{U}(n) = \mathbf{U}(n-1) + \mathbf{d}_n^T\mathbf{d}_n, \tag{4.13}$$

$$\mathbf{V}(n) = \mathbf{V}(n-1) + \mathbf{d}_n^T y_n. \tag{4.14}$$

Compare (4.13) to (4.9) and (4.10), we can identify the following notations $\mathbf{E}$, $\mathbf{B}$, $\mathbf{C}$ and $\mathbf{D}$ and express the inverse of the correlation matrix in the following recursive form,

$$\begin{aligned}
\mathbf{E} &= \mathbf{U}(n) \\
\mathbf{B}^{-1} &= \mathbf{U}(n-1) \\
\mathbf{C} &= \mathbf{d}_n^T \\
\mathbf{D} &= 1 \\
\mathbf{U}^{-1}(n) &= \mathbf{U}^{-1}(n-1) - \frac{\mathbf{U}^{-1}(n-1)\mathbf{d}_n^T\mathbf{d}_n\mathbf{U}^{-1}(n-1)}{1 + \mathbf{d}_n\mathbf{U}^{-1}(n-1)\mathbf{d}_n^T}
\end{aligned} \tag{4.15}$$

For convenience of purpose, we let $\mathbf{k}(n)$ as

$$\mathbf{k}(n) = \frac{\mathbf{U}^{-1}(n-1)\mathbf{d}_n^T}{1 + \mathbf{d}_n \mathbf{U}^{-1}(n-1)\mathbf{d}_n^T}. \tag{4.16}$$

Thus, (4.15) can be rewritten as

$$\mathbf{U}^{-1}(n) = \mathbf{U}^{-1}(n-1) - \mathbf{k}(n)\mathbf{d}_n\mathbf{U}^{-1}(n-1). \tag{4.17}$$

Now, multiplying both sides of (4.17) by the transmitted data $\mathbf{d}_n^T$, we have

$$\mathbf{U}^{-1}(n)\mathbf{d}_n^T = \mathbf{U}^{-1}(n-1)\mathbf{d}_n^T - \mathbf{k}(n)\mathbf{d}_n\mathbf{U}^{-1}(n-1)\mathbf{d}_n^T \tag{4.18}$$

Using (4.16) and (4.18), after some mathematical manipulation, we get the simple result

$$\mathbf{k}(n) = \mathbf{U}^{-1}(n)\mathbf{d}_n^T \tag{4.19}$$

According to the least-squares algorithm in previous Section, we have

$$\tilde{\mathbf{h}}(n) = \mathbf{U}^{-1}(n)\mathbf{V}(n). \tag{4.20}$$

Similarly define $\tilde{\mathbf{h}}(n-1)$. Substituting (4.14) and (4.17) into (4.20) with some algebraic manipulation, the recursive least squares algorithm is obtained by

$$\tilde{\mathbf{h}}(n) = \mathbf{U}^{-1}(n)\mathbf{V}(n-1) + \mathbf{k}(n)y_n \tag{4.21}$$

$$= \tilde{\mathbf{h}}(n-1) + \mathbf{k}(n)[y_n - \mathbf{d}_n\tilde{\mathbf{h}}(n-1)] \tag{4.22}$$

We thus see that the RLS algorithm only consist of first-order matrix difference equations and the inversion of matrix $\mathbf{U}(n)$ is replaced by the inversion of a scalar $1 + \mathbf{d}_n\mathbf{U}^{-1}(n-1)\mathbf{d}_n^T$.

4.3 Fast Fading Channel Estimation

4.3.1 EDGE Channel Characteristics

At the transmitter of the EDGE system, the modulated 8-PSK symbols $a_k \in \{\exp(j\frac{2\pi}{8}i); i = 0, 1, 2, \cdots, 7\}$ are placed in short slots, and a linearized Gaussian filter is used as the

transmit filter. The original slot structure of EDGE has 26 pilot symbols in the middle of each slot as shown in Fig. 4.1a. This slot structure is good enough to be used for estimating time-invariant channel state information of the entire slot. However, when the mobile subscriber is moving fast, the Doppler frequency is high, the fading within one slot is no longer constant, then the original slot structure of EDGE system cannot be used for estimating the time-varying channel fading with reasonable good accuracy. Therefore, in this chapter, the slot structure is slightly modified to facilitate the estimation of time-varying fading channels in 8-PSK system. We split the 26 pilot symbols into two groups, we shift the first group of 13 pilot symbols to the front of the data block and shift the second group of 13 symbols to the end of the data block, and keep the total number of symbols (and data) the same as those of the original slot structure. The modified slot structure is shown in Fig. 4.1b. The modified slot structure is used throughout this chapter.

3	58	26	58	3	8.25
Tail	Data	Training Sequence	Data	Tail	Guard

(a)

3	13	58	58	13	3	8.25
Tail	Training Sequence	Data	Data	Training Sequence	Tail	Guard

(b)
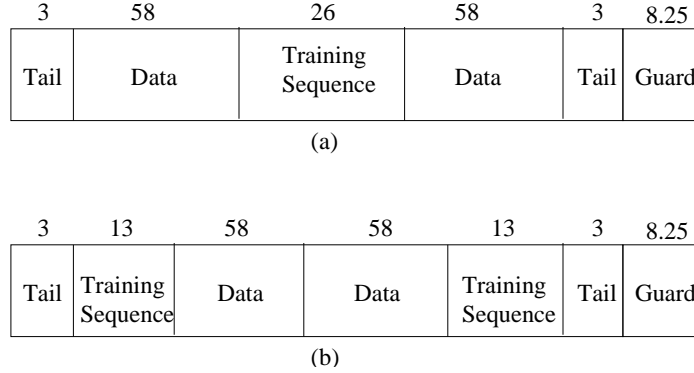
Figure 4.1: (a)The original EDGE slot structure, (b)The slightly modified slot structure

Assume that there is no timing error and frequency offset at the receiver, the baseband representation of the EDGE system shown in Fig. 2.1 can be written as

$$y_k = \sum_{l=0}^{L-1} h_k(l) d_{k-l} + n_k, \tag{4.23}$$

where d_k is the transmitted 8-PSK symbol, y_k is the symbol rate sampled output of the receive filter, n_k is the additive white Gaussian noise (AWGN), and $h_k(l)$, $0 \le l \le L-1$, is the time-varying CIR of the fading channel. $h_k(l)$ is the symbol rate sampled version

54

of the composite channel impulse response that is the convolution of the transmit filter $P_T(t)$, the receive filter $P_R(t)$, and the physical channel impulse response $g(t,\tau)$, which can be viewed as the response of the channel at time t to an impulse input at time $t-\tau$. The physical channel impulse response has the form

$$g(t,\tau) = \sum_i \varphi_i(t)\delta(\tau - \tau_i), \tag{4.24}$$

where $\varphi_i(t)$ for a certain value of i can be viewed as a time-varying flat fading process with average power $E[|\varphi_i(t)|^2]$ determined by the delay power profile of the channel. Now, we can define the discrete-time channel response $h_k(l)$ as

$$
\begin{aligned}
h_k(l) &= h(kT_s, lT_s) \tag{4.25} \\
h(t,\tau) &= P_t(\tau) \otimes g(t,\tau) \otimes P_r(\tau) \\
&= \sum_{i=0} \varphi_i(t) R_{P_t P_r}(t - \tau_i) \tag{4.26}
\end{aligned}
$$

where $R_{P_t P_r}(t)$ is the correlation of the transmitting and receiving filters.

In the EDGE system, linearized Gaussian filter and root raised cosine (RRC) filter are adopted as a transmit and receive filter, respectively. The linearized Gaussian filter [19],[12] is defined as following

$$
c_0(t) = \begin{cases} \Pi_{i=0}^3 q(t + iT), & 0 \le t \le 5T \\ 0, & \text{else} \end{cases} \tag{4.27}
$$

$$
q(t) = \begin{cases} \sin\left(\pi \int_0^t m(\tau)d\tau\right), & 0 \le t < 4T \\ \sin\left(\frac{\pi}{2} - \pi \int_0^{(t-4T)} m(\tau)d\tau\right), & 4T \le t < 8T \\ 0, & \text{else} \end{cases} \tag{4.28}
$$

where $g(t)$ is the Gaussian shaped frequency impulse of duration $4T$ and $T = 3.69\mu s$ is the symbol duration of the EDGE system. The implementation of linearized Gaussian filter will provide the approximately same transmit spectra between the EDGE and GSM systems [20],[12].

For the receiver input filter, we employ the RRC filter which belongs to the class of suboptimum input filters [12],[13]. In paper [12], the numerical analysis for the influence of the suboptimum filter RRC on the BER performance are provided. It has been shown that the suboptimum filter RRC has only small differences on BER performance at different profiles of the EDGE channel by comparing with the optimum filter whitened matched filter, which is individually design for each random channel realizations. The significant lower complexity and near-optimum performance offered by the RRC filter leads to choice as the receiver filter in EDGE system.

When the Doppler frequency, f_d, of the fading channel is in the range of $[0, 20]$ Hz, the multipath fading channels can be considered as time-invariant for one slot duration [12]-[21], thus the time variable k can be omitted in the representation of the CIR. Hence, the time-invariant CIR $h(l)$, $0 \leq l \leq L - 1$, can be reliably estimated with the conventional LS based algorithms. For typical fast fading channels,the CIR can no longer be treated as time-invariant. It will be shown next that the fading channel can be approximated as a linear function of the time variable.

According to [73], the ith-path of the fading channel can be written as

$$\varphi_i(t) \;=\; E_i \sum_{n=1}^{N} C_{ni} \exp[j(\omega_d t \cos \beta_{ni} + \phi_{ni})], \tag{4.29}$$

where E_i is a scaling constant, $\omega_d = 2\pi f_d$, β_{ni} and ϕ_{ni} are statistically independent random variables and they are uniformly distributed on $[-\pi, \pi)$. After some algebraic manipulations, we can get

$$\varphi_i(t) \;=\; \varphi_{ci}(t) + j\varphi_{si}(t) \tag{4.30}$$

$$\varphi_{ci}(t) \;=\; E_i \sum_{n=1}^{N} C_{ni} \left\{ \cos(\omega_d t \cos \beta_{ni}) \cos \phi_{ni} - \sin(\omega_d t \cos \beta_{ni}) \sin \phi_{ni} \right\} \tag{4.31}$$

$$\varphi_{si}(t) \;=\; E_i \sum_{n=1}^{N} C_{ni} \left\{ \sin(\omega_d t \cos \beta_{ni}) \cos \phi_{ni} + \cos(\omega_d t \cos \beta_{ni}) \sin \phi_{ni} \right\}. \tag{4.32}$$

While $f_d \leq 100$Hz, we have $|\omega_d t \cos(\beta_{ni})| \leq 0.3625$ radians for $0 \leq t \leq 576.92\mu$. As

a result, we can make the following approximations

$$\tilde{\varphi}_{ci}(t) \ = \ E_i \sum_{n=1}^{N} C_{ni}\{\cos \phi_{ni} - t\omega_d \cos \beta_{ni} \sin \phi_{ni}\} \qquad (4.33)$$

$$\tilde{\varphi}_{si}(t) \ = \ E_i \sum_{n=1}^{N} C_{ni}\{\sin \phi_{ni} + t\omega_d \cos \beta_{ni} \cos \phi_{ni}\}. \qquad (4.34)$$

by implementation of the small angle rule, $\cos \chi \approx 1$ and $\sin \chi \approx \chi$. It is apparent that $\varphi_i(t)$ can be approximated as a linear function of the time variable t, so as to $h_k(l)$, which is a linear function of $\varphi_i(t)$, while f_d has Doppler frequecy up to 100Hz. Now, we extend our discussion to the Doppler frequency with range up to 200Hz. It is clear that the channel impulse response is not necessary in linear form or constant from above derivations. According to [73], β_{ni} are assumed to be uniform distributed on $[-\pi, \pi)$. Therefore, there are some cases, the fading channel taps exhibit an parabolic/oscillatory behavior with the present of minimum or maximum peak. As a consequence, the bit error rate performance is degraded. In Section 4.5, we show that the new method combat the Doppler frequency effectively up to 300Hz, whereas the parabolic behavior exists.

These analysis are supported by Fig. 4.2, which shows the real part and imaginary part of one tap of a typical channel impulse response within one slot duration with Doppler frequency $f_d = 100$ Hz.

4.3.2 Channel Estimation

Having analyzed the characteristics of the Rayleigh fading channel, we can proceed to the estimation of the time-varying frequency-selective channel impulse response $h_k(l)$.

Based on the analysis in Section 4.3.1, we approximate the CIR $h_k(l)$ as a linear function of the time variable k,

$$h_k(l) = u_0(l) + ku_1(l), \qquad (4.35)$$

where $u_0(l)$ and $u_1(l)$ are parameters to be estimated. For a time-varying frequency-selective fading channel with channel length L, there are $2L$ parameters to be estimated
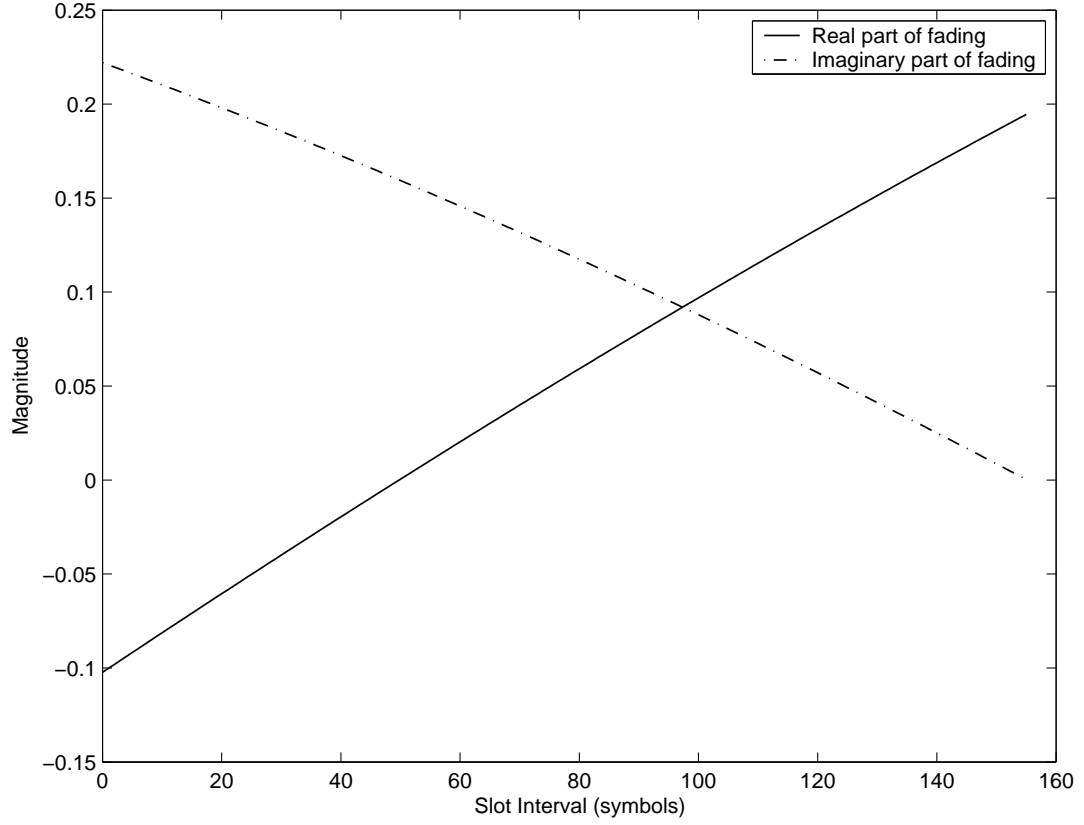
Figure 4.2: Real and imaginary part of the Rayleigh fading in one slot interval at f_d=100Hz

for each slot, and the channel impulse response of one slot can be linearly approximated by these parameters.

From (4.23) and (4.35), the kth received sample y_k can be represented as

$$y_k = \mathbf{d}_k(\mathbf{u}_0 + k \cdot \mathbf{u}_1) + n_k, \tag{4.36}$$

where $\mathbf{d}_k = [d_k, d_{k-1}, \cdots, d_{k-L+1}] \in \mathbb{C}^{1 \times L}$ are the transmitted symbols, and $\mathbf{u}_i = [u_i(0),$ $u_i(1), \cdots, u_i(L-1)]^T \in \mathbb{C}^{L \times 1}$, for $i = 0, 1$, with $(\cdot)^T$ representing the operation of transpose. With the known training symbols transmitted in the beginning and end of each slot, the received samples contributed exclusively by training symbols can be written

into matrix format

$$\mathbf{y} = \mathbf{A}\mathbf{u_0} + \mathbf{T} \cdot \mathbf{A} \cdot \mathbf{u_1} + \mathbf{n}, \tag{4.37}$$

$$= \begin{bmatrix} \mathbf{A} & \mathbf{T} \cdot \mathbf{A} \end{bmatrix} \begin{bmatrix} \mathbf{u_0} \\ \mathbf{u_1} \end{bmatrix} + \mathbf{n}, \tag{4.38}$$

where

$$\mathbf{y} = \begin{bmatrix} y_{L-1} & \cdots & y_{15} & y_{132+L-1} & \cdots & y_{147} \end{bmatrix}^T \in \mathbb{C}^{(34-2L)\times1} \tag{4.39}$$

$$\mathbf{n} = \begin{bmatrix} n_{L-1} & \cdots & n_{15} & n_{132+L-1} & \cdots & n_{147} \end{bmatrix}^T \in \mathbb{C}^{(34-2L)\times1} \tag{4.40}$$

$$\mathbf{A} = \begin{bmatrix} d_{L-1} & d_{L-2} & \cdots & d_1 & d_0 \\ \vdots & & \vdots & & \vdots \\ d_{15} & d_{14} & \cdots & d_{15-L+2} & d_{15-L+1} \\ d_{132+L-1} & d_{132+L-2} & \cdots & d_{133} & d_{132} \\ \vdots & & \vdots & & \vdots \\ d_{147} & d_{146} & \vdots & d_{147-L+2} & d_{147-L+1} \end{bmatrix} \in \mathbb{C}^{(34-2L)\times L} \tag{4.41}$$

and $\mathbf{T}$ is a diagonal matrix defined as

$$\mathbf{T} = \mathrm{diag}\{L-1, \cdots, 14, 15, 132+L-1, \cdots, 146, 147\}. \tag{4.42}$$

With (4.38), the cost function for LS criterion can be defined as follows

$$J_{LS} = (\mathbf{y} - \Phi\mathbf{u})^H(\mathbf{y} - \Phi\mathbf{u}), \tag{4.43}$$

where $\Phi = \begin{bmatrix} \mathbf{A} & \mathbf{T} \cdot \mathbf{A} \end{bmatrix}$, and $\mathbf{u} = \begin{bmatrix} \mathbf{u}_0^T & \mathbf{u}_1^T \end{bmatrix}^T$. The $\hat{\mathbf{u}}$ that minimizes J_{LS} can be obtained from the equation $\frac{\partial J_{LS}}{\partial \mathbf{u}^H} = 0$, and the solution is

$$\hat{\mathbf{u}} = \begin{bmatrix} \mathbf{A}^H\mathbf{A} & \mathbf{A}^H\mathbf{T}\mathbf{A} \\ \mathbf{A}^H\mathbf{T}\mathbf{A} & \mathbf{A}^H\mathbf{T}^2\mathbf{A} \end{bmatrix}^{-1} \begin{bmatrix} \mathbf{A}^H\mathbf{y} \\ \mathbf{A}^H\mathbf{T}\mathbf{y} \end{bmatrix}. \tag{4.44}$$

Next, we outline the recursive procedure for matrix Ψ, where $\Psi = \Phi^h\Phi$, using the same approach as the conventional recursive least square algorithm. From (4.36) and (4.38), the received samples at time k is expressed by

$$y_k = \Phi_k\mathbf{u} + n_k \tag{4.45}$$

59

where $\Phi_k \in \mathbb{C}^{1 \times L}$ is the kth row of the matrix Φ. From (4.45), the estimated $\hat{\mathbf{u}}$ at time k, namely $\hat{\mathbf{u}}(k)$ can be found by using the approach of minimizing the residual sum of squares defined by, $J(k) = \sum_{i=1}^{k} [y_i - \Phi_i \mathbf{u}]^2$. Thus the estimated $\hat{\mathbf{u}}(k)$ is derived as

$$\hat{\mathbf{u}}(k) = \left[\sum_{i=0}^{k} \Psi(i) \right]^{-1} \left[\sum_{i=0}^{k} \Phi_i^h \mathbf{y}_i \right] \tag{4.46}$$

where $\Psi(i) = \Phi_i^h \Phi_i \in \mathbb{C}^{L \times L}$ is the deterministic correlation matrix at time i. Define $\Psi(0) = c\mathbf{I}$, where is c is a small positive constant that added to the main diagonal matrix and thereby force the matrix $\Psi(k)$ be a positive definite matrix and $\mathbf{I} \in \mathbb{C}^{(L \times L)}$ is the identity matrix [24]. Now, using the matrix inversion lemma, the inverse of matrix $\Psi(k)$ can be computed recursively by

$$\Psi(k) = \Phi_k^h \Phi_k + \Psi(k-1) \tag{4.47}$$

$$\Psi^{-1}(k) = \Psi^{-1}(k-1) - \frac{\Psi^{-1}(k-1)\Phi_k^h}{1 + \Phi_k \Psi^{-1}(k-1)\Phi_k^h} \Phi_k \Psi^{-1}(k-1) \tag{4.48}$$

$$= \Psi^{-1}(k-1) - \kappa(k)\Phi_k \Psi^{-1}(k-1) \tag{4.49}$$

where $\kappa(n) = \frac{\Psi^{-1}(k-1)\Phi^h(k)}{1 + \Phi_k \Psi^{-1}(k-1)\Phi_k^h}$ is the gain vector. At last, substituting (4.49) into (4.46), the estimated $\hat{\mathbf{u}}$ at time k can be computed as follows,

$$\hat{\mathbf{u}}(k) = \hat{\mathbf{u}}(k-1) + \kappa(k)[\mathbf{y}_k - \Phi_k \hat{\mathbf{u}}(k-1)] \tag{4.50}$$

We thus see that the inversion of the correlation matrix Ψ^{-1} is now replaced by the inversion of scalar $\{1 + \Phi(k)\Psi^{-1}(k-1)\Phi^h(k)\}$ while estimating $\mathbf{u}$.

With the estimation of the parameters $\mathbf{u}_0$ and $\mathbf{u}_1$, the CIR of the entire slot can be easily obtained from (4.35). It is important to note that Ψ is deterministic and the noise is zero-mean white Gaussian noise, LS based algorithm estimator (4.44) and (4.50) is a linear unbiased estimator. The CIR information are then used in the equalizer to recover the original transmitted data.

4.4 Time-Varying Channel Equalization

For 8-PSK constellation in the frequency selective fading channel, where channel length $L > 4$, it is improper to use MLSE with VA as the equalizer due to its prohibitively computational complexity. It is shown in [12] that DDFSE and RSSE algorithms are promising equalization techniques for EDGE system. However, these algorithms can only be applied to systems with minimum phase CIR, otherwise, a dramatic performance degradation will occur. For system with time-invariant CIR, prefilter can be used to obtain an equivalent CIR with minimum phase [12],[22], but the prefilter approach is not applicable to systems with time-varying CIR without resorting to complex channel tracking. In this section, a Cholesky decomposition based method is introduced to obtain the equivalent minimum phase CIR for time-varying fading channels. For the purpose of simplicity, here we combine the first and second data block of one slot together, $i.e$,
$\bar{\mathbf{y}} = [y_{16}, y_{17}, \cdots, y_{131}]^T \in \mathbb{C}^{N_d \times 1}$, where $N_d = 116$ is the length of the entire data block.
    Based on the estimated time-varying CIR $\hat{h}_k(l)$ and (4.23), the input output relationship of the data block can be written into matrix format as

$$
\begin{bmatrix} y_{16} \\ y_{17} \\ \vdots \\ y_{130} \\ y_{131} \end{bmatrix} = \begin{bmatrix} \hat{h}_{16}(L-1) & \cdots & \hat{h}_{16}(1) & \hat{h}_{16}(0) & 0 & \cdots & \cdots & 0 \\ 0 & \hat{h}_{17}(L-1) & \cdots & \hat{h}_{17}(1) & \hat{h}_{17}(0) & 0 & \cdots & \cdots \\ \vdots & 0 & \ddots & \ddots & \ddots & \ddots & 0 & \cdots \\ 0 & \cdots & 0 & \hat{h}_{130}(L-1) & \cdots & \hat{h}_{130}(1) & \hat{h}_{130}(0) & 0 \\ 0 & \cdots & \cdots & 0 & \hat{h}_{131}(L-1) & \cdots & \hat{h}_{131}(1) & \hat{h}_{131}(0) \end{bmatrix}
$$

$$
\times \begin{bmatrix} d_{16-L+1} \\ d_{16-L+2} \\ \vdots \\ d_{130} \\ d_{131} \end{bmatrix} + \begin{bmatrix} n_{16} \\ n_{17} \\ \vdots \\ n_{130} \\ n_{131} \end{bmatrix}, \tag{4.51}
$$

or a compact form as

$$
\bar{\mathbf{y}} = \bar{\mathbf{H}} \cdot \bar{\mathbf{d}} + \bar{\mathbf{n}}. \tag{4.52}
$$

For typical channel profiles, such as the Typical Urban (TU) profile and Hilly Terrain (HT) profile [2], the impulse responses of the frequency-selective fading channels are usually not in their minimum phase state, $i.e.$, the power of $h_k(2)$ and $h_k(3)$ is larger

than that of $h_k(0)$ and $h_k(1)$. Hence the CIR matrix $\bar{\mathbf{H}} \in \mathbb{C}^{N_d \times (N_d+L)}$ formed with this CIR is not diagonally dominant, which may cause serious numerical instability problems when the DDFSE or RSSE equalizers are used.

Our objective is to find an equivalent system with minimum phase CIR, whose input-output relationship of the equivalent system can be represented as

$$\mathbf{W}\bar{\mathbf{y}} = \mathbf{B}\bar{\mathbf{d}} + \bar{\mathbf{e}}, \tag{4.53}$$

where $\mathbf{W} \in \mathbb{C}^{(N_d+L) \times N_d}$, $\mathbf{B} \in \mathbb{C}^{(N_d+L) \times (N_d+L)}$ and $\bar{\mathbf{e}} \in \mathbb{C}^{(N_d+L) \times 1}$ are the feedforward matrix, CIR feedbackward matrix and the noise vector of the equivalent system, respectively [23],[26]. In order to effectively equalize the time-varying frequency-selective fading channel using reduced state equalizers, the CIR matrix $\mathbf{B}$ should satisfy the following two conditions: (a) $\mathbf{B}$ should minimize the variance of the noise component of the system; (b) $\mathbf{B}$ should be an upper triangular matrix with most of the time-varying CIR energy concentrated in the first few taps. The first condition will improve the performance of the equalizer, and the second condition can guarantee a system with minimum phase CIR. Therefore, we implement the same approach as MMSE-DFE algorithm introduced by Al-Dhahir [26] to achieve our goal.

The variance of the noise component of the equivalent system is

$$\sigma_e^2 = \frac{1}{N_d} \text{trace}\{E[(\mathbf{B}\bar{\mathbf{d}} - \mathbf{W}\bar{\mathbf{y}})(\mathbf{B}\bar{\mathbf{d}} - \mathbf{W}\bar{\mathbf{y}})^h]\}, \tag{4.54}$$

where $\text{trace}(\cdot)$ will return the sum of the diagonal elements of a matrix. According to the orthogonality principle [13, pp.256-258], the matrix $\mathbf{B}$ minimizing σ_e^2 must satisfy $\mathbf{B} \cdot \mathbf{R}_{\bar{d}\bar{y}} = \mathbf{W} \cdot \mathbf{R}_{\bar{y}\bar{y}}$, where $\mathbf{R}_{\bar{d}\bar{y}} = E(\bar{\mathbf{d}} \cdot \bar{\mathbf{y}}^h)$. Thereby, the minimum value of σ_e^2 can be obtained as

$$\min(\sigma_e^2) = \frac{1}{N_d} \text{trace}\left[\mathbf{B}(\mathbf{R}_{\bar{d}\bar{d}} - \mathbf{R}_{\bar{d}\bar{y}}\mathbf{R}_{\bar{y}\bar{y}}^{-1}\mathbf{R}_{\bar{y}\bar{d}})\mathbf{B}^h\right], \tag{4.55}$$

$$= \frac{\sigma_n^2}{N_d} \cdot \text{trace}\left[\mathbf{B}(\frac{1}{\text{SNR}}\mathbf{I}_{N_d+L} + \bar{\mathbf{H}}^h\bar{\mathbf{H}})^{-1}\mathbf{B}^h\right], \tag{4.56}$$

$$= \frac{\sigma_n^2}{N_d} \cdot \text{trace}\left[\mathbf{B}\mathbf{U}^{-1}(\mathbf{U}^h)^{-1}\mathbf{B}^h\right]. \tag{4.57}$$

62

where $\mathbf{U} \in \mathbb{C}^{(N_d+L) \times (N_d+L)}$ is an upper triangular matrix from the Cholesky decomposition. The expression (4.56) is based on the assumption that the input data symbols d_k are independent, $i.e.$, $\mathbf{R}_{\bar{d}\bar{d}} = E_s \mathbf{I}_{N_d+L}$ with E_s being the symbol energy, σ_n^2 is the variance of the AWGN n_k, and SNR $= E_s/\sigma_n^2$.

Therefore, we find the equivalent CIR matrix $\mathbf{B}$ as

$$\mathbf{B} = \mathbf{U}, \tag{4.58}$$

$$\mathbf{W} = (\mathbf{U}^h)^{-1}\bar{\mathbf{H}}^h. \tag{4.59}$$

From above equations, the input-output relationship of the equivalent system can be written as

$$(\mathbf{U}^h)^{-1}\bar{\mathbf{H}}^h\bar{\mathbf{y}} = \mathbf{U}\bar{\mathbf{d}} + \bar{\mathbf{e}}, \tag{4.60}$$

where the matrix $\mathbf{U}$ has the time-varying CIR energy concentrated in the first few taps. The obtained equivalent CIR matrix can then be used in the DDFSE or RSSE equalizer to recover the original transmitted symbols. Follows, we summarize the proposed channel estimation and equalization algorithm in Table 1.

Table 4.1: Summary of proposed channel estimation and equalization algorithm

1. Perform channel estimation by recursive algorithm:
 Define $\Psi(0) = c\mathbf{I}$ and $\hat{\mathbf{u}}(0) = 0$
 Loop from i=0 to k
     Compute gain vector $\kappa(i)$
     Update $\hat{\mathbf{u}}(k)$:
         $\hat{\mathbf{u}}(k) = \hat{\mathbf{u}}(k-1) + \kappa(k)[\mathbf{y}_k - \Phi_k\hat{\mathbf{u}}(k-1)]$
 End of loop
 2. Generate the approximate CIR $h_k(l)$:
   $h_k(l) = u_0(l) + ku_1(l)$
 3. Calculate upper triangular matrix $\mathbf{U}$:
   $\mathbf{U}^h\mathbf{U} = \frac{1}{\text{SNR}}\mathbf{I}_{N_d+L} + \bar{\mathbf{H}}^h\bar{\mathbf{H}}$
 4. Apply reduced state equalizers for channel equalization:
   $(\mathbf{U}^h)^{-1}\bar{\mathbf{H}}^h\bar{\mathbf{y}} = \mathbf{U}\bar{\mathbf{d}} + \bar{\mathbf{e}}$

4.5 Simulation Results

In this section, simulations are carried out to evaluate the performance of the proposed channel estimation and equalization algorithms for EDGE systems with time-varying and frequency-selective fading channels, in terms of both estimation mean square error (MSE) and raw bit error rate (BER), which means the uncoded data are transmitted for BER calculation. The performance is evaluated under the Typical Urban and Hilly Terrain channel profiles shown in Fig.2.2 and 2.3 [2], and the simulation system is over-sampled 37 times to obtain a time resolution of $T_{sample} = T_{sym}/37 \approx 0.1\mu s$, which is the minimum differential delay of the multipath branches of the channel. The Rayleigh fading is generated according to the paper [25] and they are independent from slot to slot. For the perfect channel estimation in Figure 4.4, the receiver has all the information of the fading channels, which can be found by equation (4.26) and fed to the channel equalizer for demodulation and decision making under the noisy channel.

The MSE of the channel estimation algorithms under different maximum Doppler frequencies is shown in Fig. 4.3 for TU($L = 4$) and HT ($L = 7$) profiles. It can be seen from this figure that the Doppler frequency has very little influence on the MSE of the proposed estimation algorithm, while the MSE of the LS algorithm [12], [21] degrades dramatically with the increase of f_d. From the figure, we can conclude that the proposed algorithm can obtain a rather accurate estimation of the time-varying fading channel for a wide range of Doppler frequencies.

In Fig. 4.4 and 4.5, the BER performances of various channel estimation algorithms at different Doppler frequencies by employing MLSE and DDFSE equalizers are presented, respectively. In TU channel profile, effective length of $L = 4$ is sufficient and accurate to characterize the discrete-time CIR, which is suitable to be fed into MLSE equalizer with 8^3 states. The performance obtained from perfect channel estimation is shown as a lower bound reference. When the Doppler frequency is low, i.e. $f_d = 10$Hz, the LS and proposed algorithms have nearly the same BER performance which is 0.0038 at
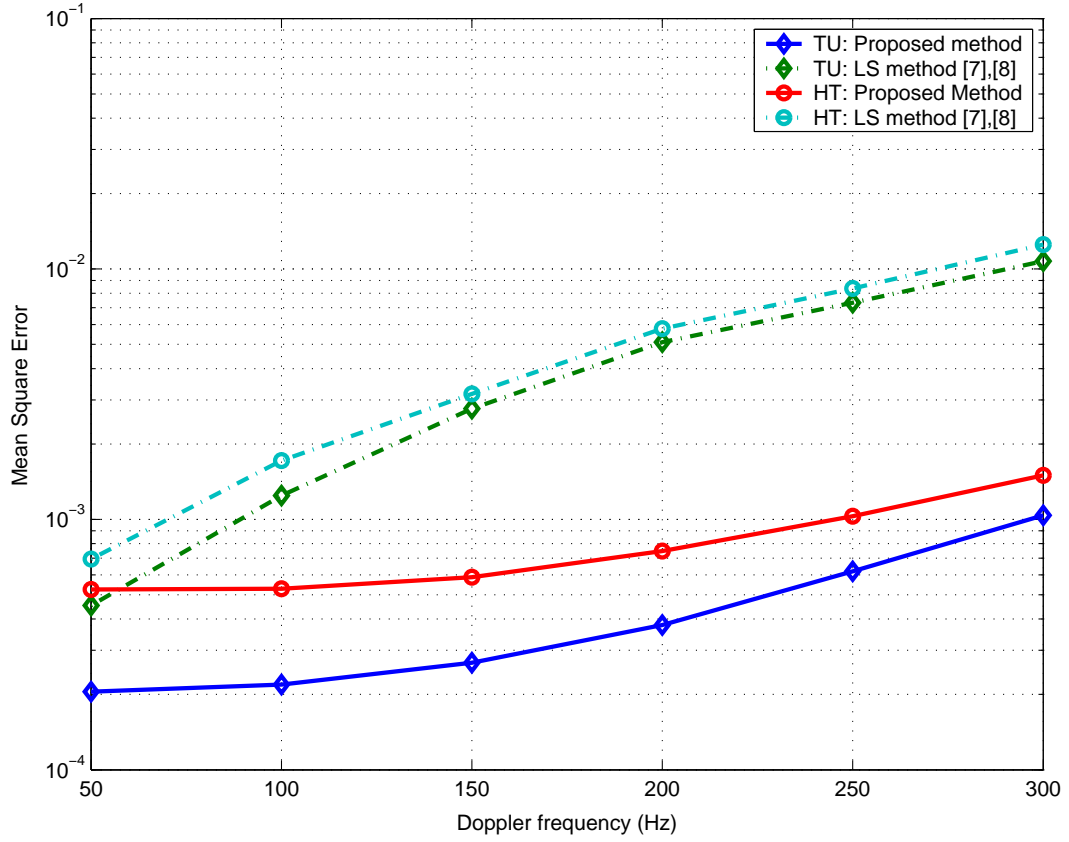
Figure 4.3: Mean-Square-Error at frequency range of 50-300Hz in TU and HT profiles

$E_b/N_o = 20$dB. With the increase of Doppler frequency to 100Hz, the BER performance based on LS algorithm degrades to 0.0087 at the same E_b/N_o. However, the BER performance for proposed algorithm still remains the same and thereby the proposed estimation method has about 2.5dB gain compared to the LS algorithm. While $f_d = 200$Hz, whereas the CIR exhibits the parabolic behavior, the BER performance of LS algorithm degrades dramatically to 0.027 at $E_b/N_o = 20$dB. Nevertheless, there is only a minor loss in the proposed estimation method. In Fig.4.5, in HT channel profile, the discre-time CIR with channel length $L = 7$ are estimated and performed Cholesky decomposition before fed into a DDFSE equalizer. For DDFSE equalizer, only the first 2 taps of CIR are used for trellis diagram with 8 states, whereas the remaining taps are implemented for metric calculations. It shows that the proposed method has the similar BER at Doppler frequency of $100Hz$ and $200Hz$, whereas the LS method

has the BER of 0.022 at $E_b/N_o = 20$dB and $f_d = 100Hz$, which is about 1.3dB loss compared to the proposed method. From above BER performance, it has shown that the proposed channel estimation method with Cholesky decomposition is a promising method to transform the estimated discrete-time CIR into a causal system with the CIR enery concentrated only on the first few taps, to combat the time-variant channels.
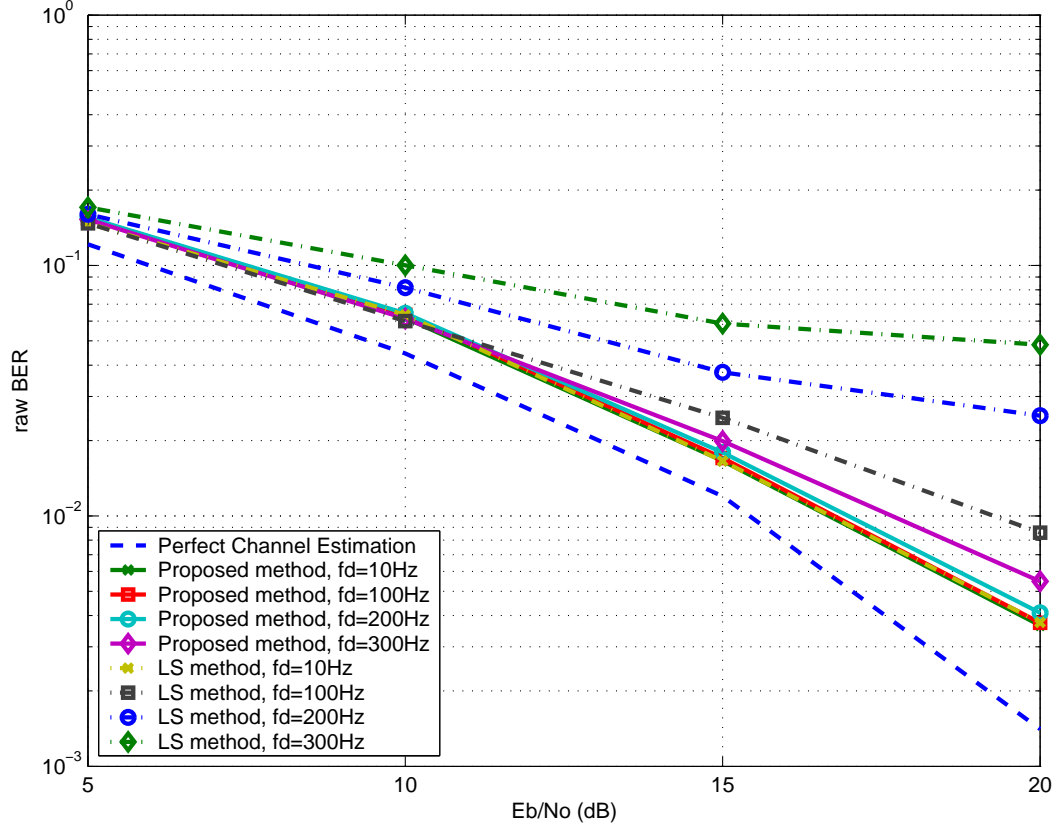
Figure 4.4: BER of LS and proposed channel estimation employing MLSE equalizer at f_d=10, 100, 200 and 300Hz in TU profile

4.6 Conclusion

In this chapter, a least-squares based algorithm was presented to estimate time-varying and frequency-selective fading channels of 8-PSK system. The proposed algorithm can accurately estimate various fading channels which have wide range of Doppler frequency
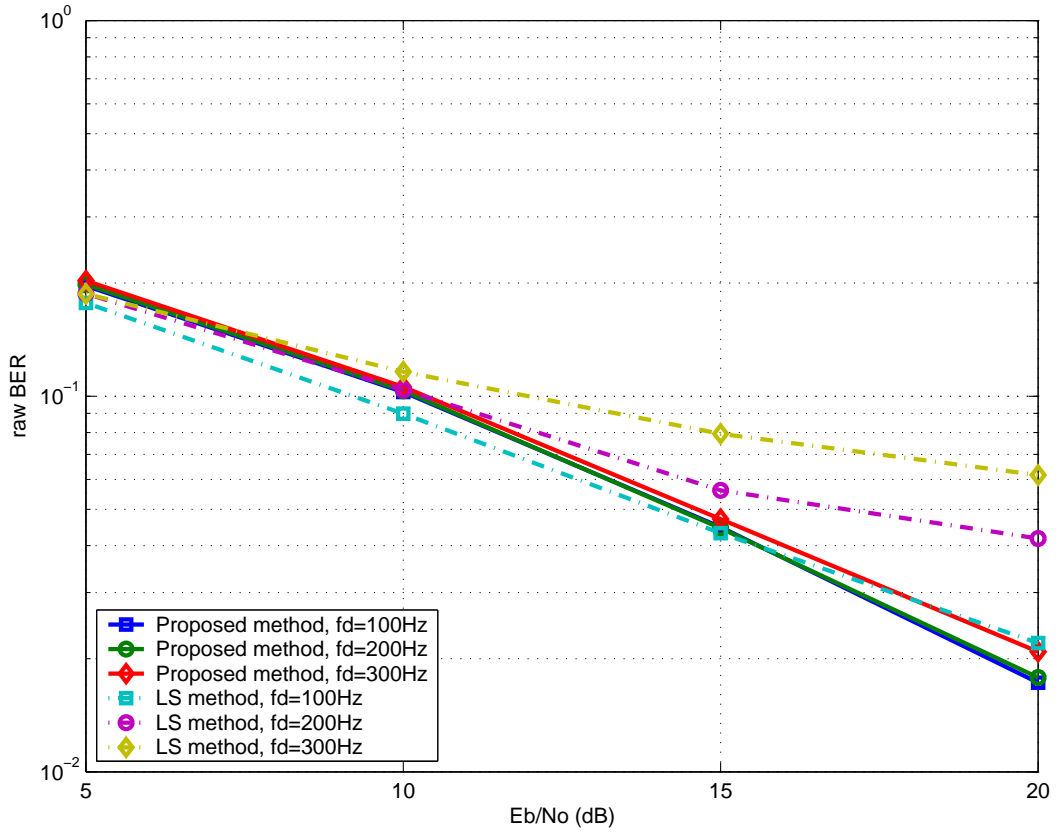
Figure 4.5: BER of LS and proposed channel estimation employing DDFSE ($\mu = 1$) equalizer at f_d=10, 100, 200 and 300Hz in HT profile

(up to 300 Hz). In terms of mean square error and bit error rate, it was shown via simulations that the proposed algorithm has much better performance than the least-squares algorithm, especially for Doppler frequency higher than 100 Hz. A reliable equalizer which employs the estimated time-varying channel impulse response is also discussed briefly.

Chapter 5

3-D Antennna Arrangement in MIMO Frequency Nonselective Rayleigh Fading Channel

5.1   Introduction

The multiple-input multiple-output communication technique has recently emerged as a new paradigm for high data rate wireless communications in rich multipath fading environments. By effectively exploiting the multipath fading utilizing the diversity scheme instead of mitigating them, the MIMO communication system shows greatly improved channel capacity potential far beyond that of traditional methods. According to [46, 47], the MIMO capacity scales linearly with the number of antennas assumed under the cases that some spatially uncorrelated, time quasi-static, and frequency flat Rayleigh fading channels. However, in practice, the optimum relative antenna separation and placement may not be feasible due to space limitations and other practical constraints. Consequently, subchannels of a MIMO system are usually correlated in both space and time. The correlation between the MIMO subchannels can substantially affect the performances of the MIMO systems and lead to decrement of system capacity [50, 51, 52]. Besides, the correlation functions are also served as a critical tool or guidelines for the

diversity schemes design and performance analysis, such as the design of space-time coding [53], the design of antenna arrays, and the analysis of optimum combining and equalization, etc. Therefore, further researches in modeling the physicals MIMO channels and developing the new correlation function are essential on providing accurate and in-depth understanding and estimation of the MIMO channels.

Recently, there have been many studies on the MIMO channel modeling, see [51]-[67] and the references therein. The most commonly used model is the 2-D Clarke's isotropic scattering model. This model assumes that all random scatterers are uniformly reflected via a ring surrounding the MS and no line-of-sight (LOS) component presents between the MS and the BS. In the literatures, there are also existing a large number of simulation models [56, 58, 59] based on this 2-D isotropic scattering. Later, Shiu proposed a 2-D MIMO abstract model based on the Clarke's 'one-ring' scattering model to study the impact of correlation of multiple antennas system against the capacity. The abstract model assumes that the multiple MS antennas are located in the same ring and receive the signals from all directions with equal probability. Excluding the isotropic scattering, Abdi argued that in many other circumstances, the MS receives the signals more likely from particular directions and it is convinced by the empirical measurements conducted in [48, 49]. Therefore, Abdi proposed the von Mises angular distribution to demonstrate the nonisotropic scattering scenario and further showed that the nonuniform distribution of the angle-of-arrival (AOA) at the MS can significantly affect the performance of the MIMO systems. Basically, the abstract models proposed above enable us to study the effect of fading correlation on the performance of the MIMO system whose received signals are assumed to travel on the plane.

Despite its wide acceptance in the area of wireless communications, the 2-D isotropic scattering model is argued by some three dimensional (3-D) models. A 3-D cylinder model was first proposed by Aulin [63] based on the fact that, in highly urbanized areas, the locations of the random scatterers may be better described by a cylinder rather than

69

a ring. Later, the cylinder model has been improved and analyzed for single-input single-output (SISO), single-input multiple-output (SIMO) and multiple-input single output (MISO) channels in [64, 65]. The simulation results show that the fading correlation estimated by the 3-D model are significantly difference well compared to the 2-D isotropic model especially the antennas are not placed on the plane. For instance, the two MS antennas are placed vertically (along the z-axis), there is always no diversity gain in 2-D model; 3-D model shows increment in diversity gain while the relative distance of the antennas increased, assume other parameters remain the same. Experimental measurements reported in the literatures have shown good agreement with the 3-D cylinder model. The cylinder model includes the 2-D scattering model as a special case by letting the maximum elevation angle (or the height) of the cylinder to zero.

In this chapter, to facilitate us in the derivation of new space-time correlation functions and the analysis of the impact of antenna arrangements in various models, we construct a new simple generic 3-D model for MIMO frequency nonselective Rayleigh fading channels. Different from others derived in the references, by clarifying the widely accepted limitation of correlation models, the proposed generic model consists of multiple antennas in 3-D isotropic or nonisotropic scattering environments. We assume that the BS antennas are located at the top of the building and receive the signals through the small angle spread. The MS antennas are located in the 3-D scattering model and might receive the signals from all directions with equal probability or mainly from particular directions. The closed form, mathematically tractable space-time correlation functions between the subchannels of the MIMO system where the BS and MS antennas may be arranged in 3-D space are derived. The effect of the mobility (the Doppler) of the MS is also considered in our derivation. The new fading correlation functions are very useful especially in the 3-D antenna arrangement. For example, while no extra diversity gain is obtained due to the relative distance on the plane is restricted, the vertically or diagonally antenna arrangements are the alternative methods to improve the diversity gain.

The new 3-D MIMO abstract model can easily simplified to different kind of models such as SIMO, MISO, SISO in isotropic or nonisotropic scattering for analysis purposes. Our simulation results in later section further show that the nonisotropic scattering affect the system performance dramatically in the 3-D case. In this paper, the key role is to develop a generic space-time correlation function using simple 3-D MIMO abstract model, which enable us to analyze the fading correlation of MIMO system in frequency nonselective Rayleigh fading channel and the impact of multiple antennas arrangements in in various 3-D scenarios.

5.2   Propagation Modeling

When a propagation path exists, it carries equal energy in both directions but the spatial distribution of arriving plane waves may be significantly different in each direction. For instance, the BSs in macrocells are relatively free from local scatterers and the plane waves thus arrive from one direction with a fairly small angle of arrival spread. Typically, the MSs located in macrocellular environment are usually surrounded by local scatterers so that the plane waves arrive from all directions with equal probability and without line-of-sight. For this type of scattering environment in the forward channel, the received envelope is Rayleigh distributed and is said to exhibit Rayleigh fading [73].

5.2.1   Frequency Non-Selective (Flat) Fading

When we assume that the distance between BS and MS is sufficiently large, the propagation model environment can be modeled as two-dimensional. In Fig. 5.1, the MS is moving along the x-axis with velocity v and is encircled by scatterers. Denote θ_k is the angle of incidence by the kth plane wave at the MS antenna. The movement of MS introduces a Doppler shift into the incident plane wave. The Doppler shift is defined as

$$f_{D,k} = f_m \cos \theta_k \text{ Hz} \tag{5.1}$$

where $f_m = v/\lambda_c$ and λ_c is the wavelength of the arriving plane. f_m is maximum Doppler frequency when $\theta_k = 0$. In this case of 2-D plane, a simple model that commonly referred as Clarke's 2-D isotropic scattering model assumes that the plane waves arrive at the MS from all directions is uniform distributed among 0 and 2π, i.e, $p(\theta) = 1/(2\pi), \theta \in [-\pi, \pi)$. Consider the transmission of the band-pass signal

$$s(t) = \text{Re}[\tilde{s}(t)e^{j2\pi f_c t}] \tag{5.2}$$

where $\tilde{s}(t)$ is the complex envelope of the transmitted signal, f_c is the carrier frequency and $\text{Re}[z]$ is the real part of z. Given that the channel is comprised of N propagation paths, the received band-pass waveform is

$$r(t) = \text{Re}\left[\sum_{k=1}^{N} C_k e^{j2\pi[(f_c+f_{D,k})(t-\tau_k)]}\tilde{s}(t - \tau_k)\right] \tag{5.3}$$

where C_k and τ_k are, respectively, the amplitude and time delay associated with the kth propagation path. Extracting from (5.3), the channel can be modeled by a linear time-variant filter having the complex low-pass impulse response given by

$$h(t,\tau) = \sum_{k=1}^{N} C_k e^{j2\pi[(f_c+f_{D,k})\tau_n - f_{D,k}t]}\delta(t - \tau_k) \tag{5.4}$$

where $\delta(\cdot)$ is the dirac delta function. If the differential path delays $\tau_i - \tau_j$ are small compared to sampling time period, then τ_k are all approximated to $\hat{\tau}_k$ for all the case. In this situation, the received signal is said to exhibit **flat fading**. Moreover, the received complex envelope $g(t) = g_I(t) + jg_Q(t)$ can be treated as a wide-sense stationary complex Gaussian Random process. Under the assumption of $g_I(t)$ and $g_Q(t)$ are independent identically distributed zero-mean Gaussian random variable, the magnitude $|g(t)|$ fo the received complexed envelope has a Rayleigh distribution. Thus, this type of fading is called **Rayleigh fading**.

5.2.2 2-D MIMO Propagation Model

The "one-ring" model was first employed by Jakes [56] to model the Rayleigh fading channel for one MS antenna. It has been shown that if the fades connecting pairs of
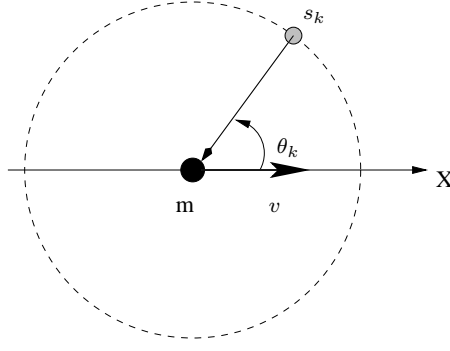
Figure 5.1: Doppler shift of MS antenna

transmit and receive antennas are independently, identically distributed, the MIMO system offer a large increase in capacity well compared to single antenna systems. To further investigate the effects of fading correlation in multiple antennas communication systems, Shiu extended the "one-ring" model for MIMO system.

Fig. 5.2 depicts the simple 2×2 abstract model, which the BS and MS antennas are placed on the X-Y plane and the MS antennas are surrounded by the same isotropic scattering environment. Based on far-field assumption and this abstract model, Shiu derived an approximated cross-correlation for the subchannels h_{lp} and h_{mq}.
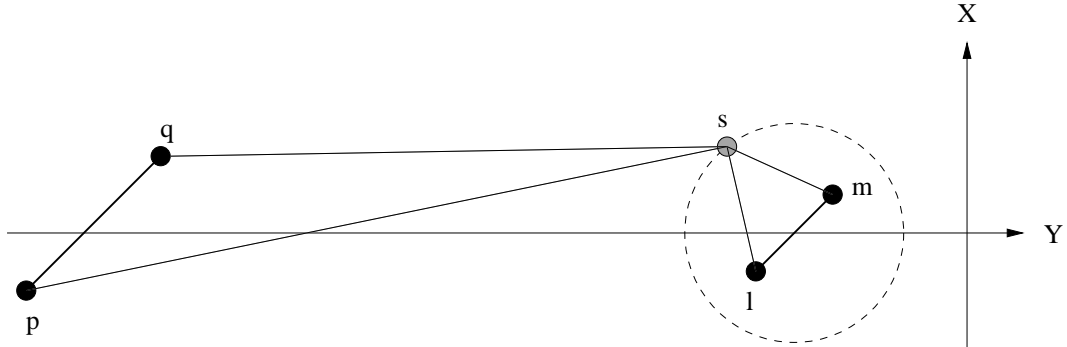
Figure 5.2: 2-D isotropic scattering for 2×2 abstract model

5.2.3   3-D Propagation Model

In previous subsection 5.2.1, we introduced the 2-D Clarke's isotropic scattering model that the incoming waves are assumed to be independent and uniformly distributed in

the interval $(0, 2\pi)$. Later, Aulin proposed a generalisation of the Clarke's model so that the received signals are not necessarily travel horizontally. Thus, a three-dimensional model is introduced. Based on this generic model, Parsons introduced a more realistic expression for the pdf of elevation angle β based on data derived from experimental observations. In Fig. 5.3(a), the 3-D scattering geometry for mobile reception is depicted. It shows the MS is encircled by scatterers distributed on the cylinder model.

Furthermore, Turkmani and Parsons introduced a 3-D model to study the cross-correlation between the signals received by two spatially separated antennas at BS. The scattering geometry is depicted in Fig. 5.3(b). They derived the integral form of cross-correlation function between the signals on two spatially separated antennas is given with respect to the movement of MS and the distribution of the scatterers surround the MS.

PSfrag replacements

(a)   (b)
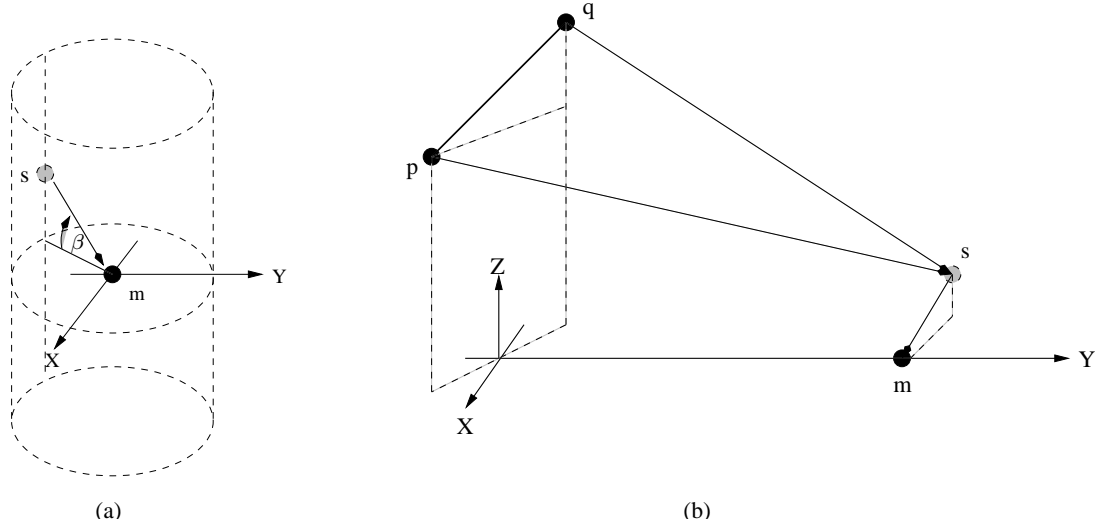
Figure 5.3: (a) 3-D "cylinder" model on MS antenna. (b) 3-D arrangement of BS antennas

5.3   3-D MIMO Channel Model

5.3.1   The MIMO Frequency Nonselective Rayleigh Channel

We assume the MIMO system is time-invariant during the downlink transmission; thereby the scatterers on the cylinder are fixed during a burst transmission. The complex envelope signal $s_p(t)$ transmitted by pth antenna, follows different paths and coincides at lth antenna. At the mobile station, the received signal $r_l(t)$ comprises of different paths' signal from the surrounding scatterers S_k and the corresponding complex lowpass equivalent channel impulse response that connecting the antenna elements p and l is denoted as h_{lp}. In proceed, the baseband input-output relationship of the discrete-time MIMO system can be written as following matrix notations:

$$\mathbf{r}(t) = \mathbf{H}(t)\mathbf{s}(t) + \mathbf{u}(t), \tag{5.5}$$

where the input vector $\mathbf{s}(t) = [s_1(t)s_2(t)\cdots s_{n_{BS}}(t)]^T \in \mathbb{C}^{1\times n_{BS}}$, the output vector $\mathbf{r}(t) = [r_1(t)r_2(t)\cdots r_{n_{MS}}(t)]^T \in \mathbb{C}^{1\times n_{MS}}$, the additive white Gaussian noise (AWGN) $\mathbf{u}(t) = [u_1(t)u_2(t)\cdots u_{n_{MS}}(t)]^T \in \mathbb{C}^{1\times n_{MS}}$, and $[\cdot]^T$ denotes the transpose operator. Assume that the MIMO channel is frequency nonselective, then the channel $\mathbf{H}(t)$ is an $n_{MS} \times n_{BS}$ matrix whose (l,p)th element is the subchannel fading coefficient connecting the antenna elements p and l, that is $[\mathbf{H}(t)]_{lp} = h_{lp}(t)$.

Suppose there are N effective scatterers, where all rays reach the lth antenna with equal power; without line of sight component, the subchannel impulse response $h_{lp}(t)$ can be expressed as

$$h_{lp}(t) = \lim_{N\to\infty} \frac{1}{\sqrt{N}} \sum_{k=1}^{N} g_k$$
$$\cdot \exp\left\{-j\frac{2\pi}{\lambda}(D_{p,S_k} + D_{S_k,l}) + j2\pi f_d t \cos(\xi - (\theta + \sigma)) + j\phi_k\right\} \tag{5.6}$$

where j is $\sqrt{-1}$, $D_{x,y}$ is the distance of the two points x and y, g_k and ϕ_k are, respectively, the amplitude and random phase shift of the k scatterer, λ is the wavelength of the carrier

frequency, $f_d = \nu/\lambda$ is the maximum Doppler frequency given that ν is the motion speed of users in direction ξ. When the gain h_{lp} is normalized and $N \to \infty$, the total power of the scatterers is $N^{-1} \sum_{k=1}^{N} E[g_k^2] = 1$, where $E[\cdot]$ is the expectation operator. Thus the channel is assumed to be unit power transferred, i.e. $E[|h_{lp}(t)|^2] \leq 1$. According to central limit theorem, when $N \to \infty$, the subchannel impulse response $h_{lp}(t)$ can be modeled as a lowpass zero mean complex Gaussian process [73], which implies that its envelop $|h_{lp}(t)|$ is Rayleigh distributed and its phase ϕ_k is independent and identically distributed (iid) and uniform over $[0, 2\pi)$.

5.3.2 Probability Density Function of AOA

From the aforementioned paragraphs, the MS antenna receives the signal from the surrounding scatterers S_k. When S_k is assumed only distributed uniformly over $[0, 2\pi)$ ('one-ring' model) on the X-Y plane, its pdf is given as $p_\theta(\theta) = 1/2\pi$. Nevertheless, this ideal case is not always valid. In some scenarios, the signals only travel in certain range of angles from particular direction; the nonuniform pdf of AOA at the MS is given in different models such as quadratic pdf [75], Laplace pdf [77], cosine [76], von Mises pdf [61] and other geometrically based pdfs. In order to clearly describe the nonisotropic scattering environments with a clean and closed form mathematical correlation functions, we adopt von Mises pdf for the azimuth angle θ in this paper. The von Mises pdf plays a key role in statistical modeling and analysis of angular variables in a 2-D nonisotropic scattering environment. The temporal correlation function applied with this pdf for a single receive antenna is derived and shown that the predicted data is successfully fitted to the measured data. Later, it is further extended to spatio-temporal model in multielement system [61]. The von Mises pdf $p_\theta(\theta)$ is given as

$$p_\theta(\theta) \quad = \quad \frac{\exp[\kappa \cos(\theta - \theta_p)]}{2\pi I_0(\kappa)}, \qquad \theta \in [-\pi, \pi) \qquad (5.7)$$

where $I_0(\cdot)$ is the zero-th order modified Bessel function, $\theta_p \in [-\pi, \pi)$ and $\kappa \geq 0$ are the mean direction and the width of the AOA scatterer, respectively. According to equation

(5.7), when $\kappa = 0$, we obtain $p_\theta(\theta) = 1/2\pi$, which is an one-ring isotropic scattering. If $\kappa \neq 0$, it forms a unidirectional shape and the width of of the AOA of the scatterer is approximately equal to $2/\sqrt{\kappa}$ [61].

In many references, 2-D scattering models are assumed while the performance of the multielement antenna systems are evaluated. Even though it is true that the 2-D scattering model is well enough to demonstrate the channel model for the MIMO systems in some scenarios, it might not accurate enough for all the cases. Later in the study case of next section, we show that in several special cases, the 3-D scattering models are required in order to demonstrate the scattering environments accurately. However, some channel models can be simplified to a 2-D scattering model without any loss. In general, the signals are not necessary traveling on the plane to the receiver. The simulation and experimental results presented in [64, 65, 68] clearly show that the existing of vertical angle could affect the correlation dramatically. Therefore, 2-D scattering model is only the ideal and simplest case to estimate the correlation of the multielement antenna system. In order to form a 3-D MIMO model, we adopt the distribution of the AOA β in the vertical plane from papers [64]. Its pdf $p_\beta(\beta)$ is given by

$$p_\beta(\beta) \;\; = \;\; \frac{\pi}{4|\beta_m|} \cos\left(\frac{\pi}{2}\frac{\beta}{\beta_m}\right), \qquad |\beta| \leq |\beta_m| \leq \frac{\pi}{2} \tag{5.8}$$

where $p_\beta(\beta)$ is a flexible function of the degree of the urbanization, and its parameter β_m is in the range of $0°$ to $15°$, according to the experimental results reported in [68].

Various of scattering environments could be obtained with different combination of κ and β. For instance, when κ and β_m are zero, a general 2-D one ring scattering model is obtained. If $\kappa \neq 0$ and $\beta_m = 0$, it becomes a 2-D nonisotropic scattering model; on the other hand, when $\kappa = 0$ and $\beta_m \neq 0$, it forms an 3-D isotropic scattering in a cylinder fashion.

77

5.4 New 3-D Space-Time Correlation Functions

Consider a MIMO system where the BS and MS employ n_{BS} transmit and n_{MS} receive antennas, respectively. All antennas are assumed to be omnidirectional without beamforming. Without loss of generality, the antenna elements are numbered as $1 \leq p \leq q \leq n_{BS}$ and $1 \leq l \leq m \leq n_{MS}$. In Figure 5.4, a basic structure of MIMO system is depicted, which consists of $n_{BS} = n_{MS} = 2$ uniform linear arrays. For the sake of simplicity, we define a Cartesian coordinate system as follow: first define the X-Y plane to contain the center of the linear arrays l and m, which denoted as O'. Next, project the BS antennas p and q to the X-Y plane as $\tilde{p}$ and $\tilde{q}$, then choose the center between $\tilde{p}$ and $\tilde{q}$ as the coordinate origin O. The line that connects the coordinate origin O and the center of the MS arrays O' is defined as Y-axis and the distance between them is denoted as D. Let R as the radius of the cylinder, $H = D_{q,\tilde{q}}$ as the elevation of the BS antenna q and $V = D_{p,\tilde{p}} - D_{q,\tilde{q}}$ as the vertically displacement between the two BS antennas. Obviously, in Figure 5.4, the orientation of the BS linear arrays p and q is a function of variables $D_{\tilde{p},\tilde{q}}$, H and V. Assume the MS antennas l and m enclosed by the same cylinder and connected by the line $D_{l,m}$. While $D_{l,m}$ decreases to zero, then there is only one receive antenna located at the center O' of the ring. Suppose there are N effective scatterers impinging on the MS antennas from a random position S_k on the cylinder. The elevation angle of S_k relative to the cylinder center O' is β and the azimuth angle is θ. The height of the cylinder is computed by the maximum elevation angle β_m given by $2R \tan \beta_m$. The geometry of the MS antennas l and m is based on the angle ρ, which is the elevation angle of MS antennas relative to the cylinder center O'. Other parameters are better depicted in Figure 5.5 which is the projection on the X-Y plane.

Figure 5.4: The 3-D MIMO model.

5.4.1 New Space-Time Correlation Function

Based on 3-D model configuration given above, let us define the space-time cross-correlation function between two arbitrary subchannels $h_{lp}(t)$ and $h_{mq}(t)$ as $\zeta_{lp,mq}(\tau) = E[h_{lp}(t)h_{mq}^*(t+\tau)]$, where * is the complex conjugate operator. According to (5.6), we obtain

$$\zeta_{lp,mq}(\tau) = \lim_{N\to\infty} \frac{1}{N} \sum_{k=1}^{N} E[g_k^2]$$
$$\exp\left\{-\frac{2\pi j}{\lambda}[D_{p,S_k} - D_{q,S_k} + D_{l,S_k} - D_{m,S_k}] - j2\pi f_d\tau\cos(\xi - (\theta + \sigma))\right\} \quad (5.9)$$

Assume that N is large and all rays have equal power, the infinitesimal power $E[g_k^2]/N$ contributed by the kth scatterer equals to differential angles from $d\theta$ and $d\beta$, respectively, with probability $p(\theta)$ and $p(\beta)$. Therefore, (5.9) can further be written into the integral
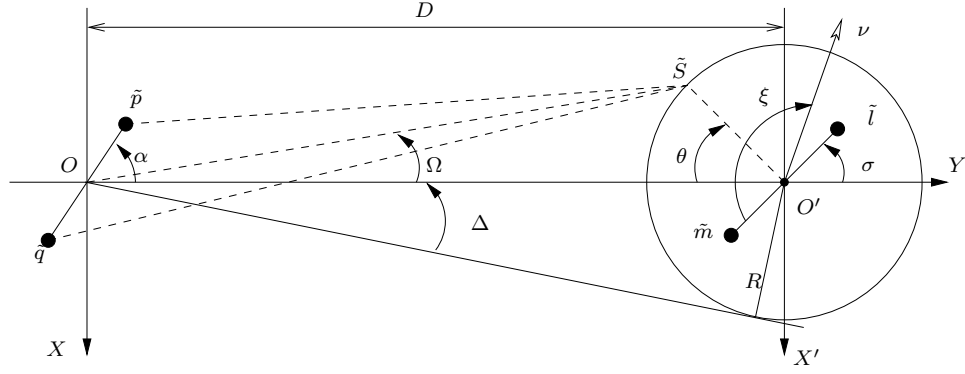
Figure 5.5: Projection of the 3-D MIMO model on the $X - Y$ plane, where ν is the motion speed of the MS at ξ direction. The narrow angle of spread is $\Delta = \arcsin(R/D)$ when $D \gg R \gg \max(D_{pq}, D_{lm})$.

form given by

$$
\zeta_{lp,mq}(\tau) = \int_{-\beta_m}^{+\beta_m} \int_0^{2\pi} p_\theta(\theta) p_\beta(\beta)
$$
$$
\exp\left\{ -\frac{2\pi j}{\lambda}[D_{p,S_k} - D_{q,S_k} + D_{l,S_k} - D_{m,S_k}] - j2\pi f_d \tau \cos(\xi - (\theta + \sigma)) \right\} d\theta d\beta \quad (5.10)
$$

Generally, the BS antennas are usually place well above the city building and seldom obstructed, while the MS antennas are alway encircled by the buildings and reflectors. Thus BS receives the signal through a narrow angle spread $\Delta = R/D$, while MS receives the signal from the surrounding scatterers. According to experimental conducted to the channels at different locations [69, 71, 78], the angle spread Δ is often less than $15°$ for macrocells in urban and suburban. Thereby, the far field propagation assumption is held in practical case of wireless MIMO communication systems given that $D \gg R \gg \max(D_{p,q}, D_{l,m})$. We may approximate the relative distances in (5.10) as

$$
D_{p,S_k} - D_{q,S_k} \approx D_{p,q} \cos\gamma, \quad (5.11)
$$

$$
D_{l,S_k} - D_{m,S_k} \approx D_{l,m} \cos\psi. \quad (5.12)
$$

where γ and ψ are the AOAs at BS and MS antennas in 3-D space, respectively. Apparently, it is necessary to express $\cos\gamma$ and $\cos\psi$ in terms of the random variable θ and β and other measurable parameters. For a given scatterer S_k, we obtain the following

useful relationships from the appropriate triangles by applying the law of cosine and Pythagoras' theorem.

$$D^2_{p,S_k} = D^2_{p,q} + D^2_{q,S_k} - 2D_{p,q}D_{q,S_k}\cos\gamma \tag{5.13}$$

$$D^2_{p,S_k} = D^2_{\tilde{p},\tilde{S}_k} + (H + V - R\tan\beta)^2 \tag{5.14}$$

$$D^2_{q,S_k} = D^2_{\tilde{q},\tilde{S}_k} + (H - R\tan\beta)^2 \tag{5.15}$$

$$D^2_{p,q} = V^2 + D^2_{\tilde{p},\tilde{q}} \tag{5.16}$$

$$D^2_{l,S_k} = D^2_{m,S_k} + D^2_{l,m} - 2D_{m,S_k}D_{l,m}\cos\psi \tag{5.17}$$

$$D^2_{l,S_k} = (D_{m,S_k}\sin\beta - D_{l,m}\sin\rho)^2 + D^2_{\tilde{l},\tilde{S}_k} \tag{5.18}$$

$$D^2_{\tilde{p},\tilde{S}_k} = D^2_{\tilde{p},\tilde{q}} + D^2_{\tilde{q},\tilde{S}_k} - 2D_{\tilde{p},\tilde{q}}D_{\tilde{q},\tilde{S}_k}\cos(\alpha - \Omega) \tag{5.19}$$

$$D^2_{\tilde{l},\tilde{S}_k} = (D_{m,S_k}\cos\beta)^2 + (D_{l,m}\cos\rho)^2 + 2D_{m,S_k}D_{l,m}\cos\beta\cos\rho\cos(\theta + \sigma). \tag{5.20}$$

Substitute (5.19) to (5.14) and (5.20) to (5.18) after some mathematical manipulation using other expressions above, we obtain the following key relationship

$$D^2_{p,S_k} = D^2_{p,q} + D^2_{q,S_k} - 2D_{q,S_k}\left[\frac{D_{\tilde{q},\tilde{S}_k}D_{\tilde{p},\tilde{q}}\cos(\alpha - \Omega) - (H - R\tan\beta)V}{\sqrt{D^2_{\tilde{q},\tilde{S}_k} + (H - R\tan\beta)^2}}\right], \tag{5.21}$$

$$D^2_{l,S_k} = D^2_{m,S_k} + D^2_{l,m} - 2D_{m,S_k}D_{l,m}(\sin\beta\sin\rho - \cos\beta\cos\rho\cos(\theta + \sigma)) \tag{5.22}$$

According to far field assumptions above, which are generally held for many practical cases, imply that $D_{\tilde{p},\tilde{S}_k} \approx D_{\tilde{q},\tilde{S}_k} \approx D$. Furthermore, we use the approximate relationships $\sqrt{1 + \chi^2} \approx \chi$ and $1/\chi^2 \approx 0$, when χ is large; $\sin\chi \approx \chi$ and $\cos\chi \approx 1$, when χ is small. We obtain $\sin\Omega \approx \Delta\sin\theta$. Compare (5.13) to (5.21) and (5.17) to (5.22), the distances (5.11) and (5.12) can be approximated as follows,

$$D_{p,q}\cos\gamma \approx D_{\tilde{p},\tilde{q}}\cos(\alpha - \Omega) - V/\Pi \tag{5.23}$$

$$\approx D_{\tilde{p},\tilde{q}}(\cos\alpha + \Delta\sin\alpha\sin\theta) \tag{5.24}$$

$$D_{l,m}\cos\psi \approx D_{l,m}(\sin\beta\sin\rho - \cos\beta\cos\rho\cos(\theta + \sigma)) \tag{5.25}$$

where $\Pi = D/(H - R\tan\beta)$. When $D \gg V \times H$ is valid, for practical case of interest, it is reasonable to assume the last term $V/\Pi \approx 0$ and lead to (5.24). Substitute (5.24)

and (5.25) into (5.10), the integral form of space-time cross-correlation MIMO system in term of θ and β can be written as

$$
\zeta_{lp,mq}(\tau) \approx \exp\left(\frac{-j2\pi D_{\tilde{p},\tilde{q}}\cos\alpha}{\lambda}\right) \int_{-\beta_m}^{\beta_m} \int_0^{2\pi} p_\theta(\theta)p_\beta(\beta) \cdot \exp\left\{-\frac{2\pi j}{\lambda}\right.
$$
$$
\cdot[D_{\tilde{p},\tilde{q}}\Delta\sin\alpha\sin\theta + D_{l,m}(\sin\beta\sin\rho - \cos\beta\cos\rho\cos(\theta+\sigma))]
$$
$$
\left. -2\pi f_D\tau\cos[\xi-(\theta+\sigma)]\right\} d\theta d\beta. \tag{5.26}
$$

According to experimental data reported in [68], the maximum elevation angle β_m is usually small and falls in the range of $0°$ to $15°$. This empirical observation later simplifies (5.26) into a useful approximation function in a tidy closed form solution. Given in [74], the integral of exponential function is

$$
\int_{-\pi}^{\pi} \exp(x\sin z + y\cos z)dz = 2\pi I_0\left(\sqrt{x^2+y^2}\right), \tag{5.27}
$$

where $I_0(jx) = J_0(x)$, and $J_0(\cdot)$ is the zero-th order Bessel function of the first kind. Consequently, (5.10) can be further simplified as follows

$$
\zeta_{lp,mq}(\tau) \approx \frac{\cos(\beta_m b_{MS}\sin\rho)\exp(-ja_{BS}\cos\alpha)}{\left[1-(\frac{b_{MS}\sin\rho}{d})^2\right]I_0(\kappa)}
$$
$$
\cdot I_0\left(\ \{\kappa^2 - (a_{BS}\Delta\sin\alpha)^2 - (b_{MS}\cos\rho)^2 - c^2\right.
$$
$$
-2a_{BS}\Delta\sin\alpha[b_{MS}\cos\rho\sin\sigma + c_f\sin(\xi-\sigma)] + 2b_{MS}c_f\cos\rho\cos\xi
$$
$$
\left. -j2\kappa[b_{MS}\cos\rho\cos(\theta_p+\sigma) + c_f\cos(\theta_p-\xi+\sigma) + a_{BS}\Delta\sin\theta_p\sin\alpha]\}^{\frac{1}{2}}\ \right) \tag{5.28}
$$

where the simplified notations are $a_{BS} = 2\pi D_{\tilde{p},\tilde{q}}/\lambda$, $b_{MS} = 2\pi D_{l,m}/\lambda$, $c_f = 2\pi f_d\tau$, and $d = \pi/(2\beta_m)$. Note that the new approximated 3-D MIMO frequency nonselective fading channel correlation function (5.28) valid under the assumption of Δ and β_m are small for all the cases.

The correlation function derived above is based on the assumption $D \gg H \times V$ for all the cases. Despite of this assumption, we investigate the case that the distance $V \times H$ are not neglected ($V/\Pi \neq 0$). Substituting (5.23) into (5.26) and follows the same derivation steps above, we have the correlation function between the subchannels

$h_{lp}(t)$ and $h_{mq}(t)$ as

$$G(\Lambda, +e) = \frac{d^2}{2(d^2 - j(b_{MS} + e)^2)} \exp\left(\frac{jeH}{R}\right) \left[\sin(d\Lambda) \exp\{-j(b_{MS} + e)\Lambda\} \right.$$
$$\left. -\frac{j(b_{MS} + e)}{d} \cos(d\Lambda) \exp\{-j(b_{MS} + e)\Lambda\} \right] \qquad (5.29)$$

$$\rho_{lp,mq}(\tau) \approx \exp(-ja_{BS}\cos\alpha) \left[G(\Lambda, +e) \Big|_{\Lambda=-\beta_m}^{\Lambda=H/R} + G(\Lambda, -e) \Big|_{\Lambda=H/R}^{\Lambda=\beta_m} \right]$$
$$\times I_0 \left(\{\kappa^2 - (a_{BS}\Delta\sin\alpha)^2 - (b_{MS}\cos\rho)^2 - c^2 \right.$$
$$-2a_{BS}\Delta\sin\alpha[b_{MS}\cos\rho\sin\sigma + c_f\sin(\xi - \sigma)] + 2b_{MS}c_f\cos\rho\cos\xi$$
$$\left. -j2\kappa[b_{MS}\cos\rho\cos(\theta_p + \sigma) + c_f\cos(\theta_p - \xi + \sigma) + a_{BS}\Delta\sin\theta_p\sin\alpha\}^{\frac{1}{2}} \right) / I_0(\kappa) (5.30)$$

where $e = 2\pi V\Delta/\lambda$ and $\chi|_{\chi=y}^{\chi=x} = x - y$. (5.28) and (5.30) include all the relevant parameters of MIMO system, which facilitate us in mathematical analysis and computational advantages over the simulation based correlation model. Moreover, the general formulas obtained above can be further simplified for the special cases of SIMO and MISO channels. In the next subsection, the correlations functions in Case I to Case IV are simplified from (5.28) and those of in Case V are simplified from (5.30).

5.4.2 Case Study

CASE I: In 2-D channel models, the simplest special case Clarke's temporal correlation model [73] consists of single BS antenna and single MS antenna in an isotropic scattering, can be obtained by letting $a_{BS} = b_{MS} = \kappa = \beta_m = 0$ in (5.28) and given as $J_0(2\pi f_D\tau)$. If $\kappa \neq 0$ and $\xi = 180° + \sigma$, the temporal correlation model in a nonisotropic scattering around MS is simplified from (5.28) as $I_0(\sqrt{\kappa^2 - c_f^2 + 2j\kappa c_f\cos\theta_p})/I_0(k)$. This closed-form solution agrees with the results in [61].

 CASE II: In MISO channels with two BS antennas and single MS antenna, if $f_D = \kappa = 0$, then the correlation function between the subchannels $h_{lp}(t)$ and $h_{lq}(t)$ is simplified as $\exp\{-ja_{BS}\cos\alpha\} J_0(a_{BS}\Delta\sin\alpha)$. Notice that the expression only consists of distance a_{BS} on the X-Y plane and the angle α. The same closed-form equation can be found

in [72]. While κ is no longer zero, the spatio correlation function of nonisotropic scattering is given as $\zeta_{lp,lq}(\tau) \approx \frac{\exp(-ja_{BS}\cos\alpha)}{I_0(\kappa)} I_0\left(\sqrt{\kappa^2 - (a_{BS}\Delta\sin\alpha)^2 - j2\kappa a_{BS}\Delta\sin\alpha\sin\theta_p}\right)$. The same equation can be derived by letting $a_{BS} = b_{MS} = 0$ in (12) of [52]. Obviously, variable β does not exists in any case of MISO channel model. Thereby, a commonly used 2-D channel correlation function proposed in many literatures are well enough to describe the MISO channel model for the all the cases. The same assumption can be found in many literatures [51, 52] and [73] etc.

CASE III: In SIMO channels, when the BS has one transmit and MS has two receive antennas placed on the X-Y plane ($\rho = 0°$), (5.28) can be derived to several existing equations. Assume that a 2-D one-ring isotropic scattering is considered, where $\beta_m = 0°$ and $\kappa = f_D = 0$, (5.28) is simplified as $J_0\left(\sqrt{b_{MS}^2 + c_f^2 - 2b_{MS}c_f\cos\xi}\right)$. The same result can be found in Lee's paper [70]. According to [64], when the two MS antennas are placed on the X-Y plane ($\rho = 0°$) and the scattering consists of β_m that forms a cylinder model, the correlation function is given by $\int_{-\beta_m}^{\beta_m} p_\beta(\beta) J_0(b\cos\beta)d\beta$. Nevertheless, the approximation derived from (5.28) using the small angle relationship, where β_m falls in the range of $0°$ to $15°$, is given as $J_0(2\pi D_{l,m}/\lambda)$. The correlation values computed by the new approximation has only slightly difference compare to the integration model, but improves the computational dramatically. Based on the derivation above, a conclusion can be drawn to the two MS antennas, which are placed on the X-Y plane ($\rho = 0°$), that the influence of β_m can be neglected and lead to 2-D scattering model around the MS antennas. In addition, $\rho = 0°$ and $\kappa \neq 0$ simplify (5.28) to a 2-D nonisotropic scattering, whose approximated correlation function is given as $I_0\left(\sqrt{\kappa^2 - b_{MS}^2 - j2\kappa b_{MS}\cos(\theta_p + \sigma)}\right)/I_0(k)$ by letting $a_{BS} = c_f = 0$. The same approximation is originally given by simplifying (12) of [61] under the same condition given as above.

CASE IV: In SIMO channel, with one BS antenna and two MS antenna antennas not on the X-Y plane ($\rho \neq 0°$). Consider the case where $\kappa = f_D = 0$, the new correlation

function between the subchannels $h_{lp}(t)$ and $h_{mp}(t)$ is simplified to

$$\zeta_{lp,mp}(\tau) \;=\; \frac{\cos(b_{MS}\beta_m \sin\rho)\,J_0(b_{MS}\cos\rho)}{1 - \left(\frac{b_{MS}\sin\rho}{d}\right)^2} \tag{5.31}$$

The equation (5.31) shows that β_m and ρ have a big impact on the crosscorrelation function. Apparently, when the angle of ρ is fixed to a certain value larger than zero, the term $\cos(b_{MS}\beta_m \sin\rho)$ in numerator of (5.31) is inversely proportional to the elevation angle β_m. Consequently, when β_m increments, the subchannels have smaller correlation values lead to better diversity gain. In a simple case $\rho = 90°$, the two MS antennas are placed vertically to each other. The equation (5.31) is further simplified to $\cos(b_{MS}\beta_m)/[1 - (b_{MS}/d)^2]$. In next section, the simulation result shows that while β_m increase to $20°$, the correlation of the two vertically placed antenna decreases dramatically. Follows, the next spatio model is the extension of (5.31), when the MS antennas encounter the nonisotropic scattering, i.e, $\kappa \neq 0$. The new approximated correlation function is given by

$$\zeta_{lp,mp}(\tau) = \frac{\cos(b_{MS}\beta_m \sin\rho)}{\left[1 - \left(\frac{b_{MS}\sin\rho}{d}\right)^2\right] I_0(\kappa)}$$
$$\times I_0(\sqrt{\kappa^2 - (b_{MS}\cos\rho)^2 - j2\kappa b_{MS}\cos\rho\cos(\theta_p + \sigma)}) \tag{5.32}$$

It is important to note here while the two antennas are placed vertically ($\rho = 90°$), the $I_0(k)$ will cancel out each other from the numerator and denominator and simplified the equation (5.32) to (5.31). We prove that the two vertically placed antennas are not affected by the azimuth AOA. Besides, the expression (5.32) hasr larger correlation when compared to (5.31). The outcome is truth because the signals only travel in a small range of angle from particular direction while arriving to the MS antennas. Thereby, the signals are more correlated.

CASE V: To study the key difference between the new correlation functions (5.28) and (5.30), we setup the BS antennas in a "triangle" shape. Assume that in MISO case, there are three multiple BS antennas and one MS antennas enclosed by a cylinder

85

model, the pth and qth antennas are placed at the same height H and the rth antenna has a distance V above the qth antenna. The distance $D_{p,q}$ and $D_{q,r}$ is perpendicular to each other. Thus it forms a "right angle triangle" shape with the diagonal distance $D_{p,r} = \sqrt{D_{p,q}^2 + D_{q,r}^2}$. Consider a case where two vertically placed antennas are at the BS, $\kappa = a_{BS} = b_{MS} = c_f = 0$, simplifies (5.30) to a new stationary correlation function given as

$$
\begin{aligned}
\zeta_{lq,lr}(\tau) \approx{} & \frac{d^2}{2(d^2 - e^2)} \exp\left(\frac{jeH}{R}\right) \\
& \times \left[\sin(d\Lambda)\exp\{-je\Lambda\} - \frac{je}{d}\cos(d\Lambda)\exp\{-je\Lambda\}\right] \Big|_{\Lambda=-\beta_m}^{\Lambda=H/R} \\
& + \frac{d^2}{2(d^2 - je^2)} \exp\left(-\frac{jeH}{R}\right) \\
& \times \left[\sin(d\Lambda)\exp\{je\Lambda\} + \frac{je}{d}\cos(d\Lambda)\exp\{je\Lambda\}\right] \Big|_{\Lambda=H/R}^{\Lambda=\beta_m}
\end{aligned}
\tag{5.33}
$$

The relationship above is in term of the distances H, V at BS, R and the AOA β_m at MS. Given that those parameters are fixed, the simplified correlation function $\zeta_{lq,lr}$ is a constant. Thus, the AOA α of BS does not effect the correlation between the two subchannels. Nevertheless, the correlation of the horizontally (refer to expression in CASE II) and diagonally placed antennas vary significantly according to the AOA α and will be depicted in the simulation result in next section. The correlation of the two diagonally placed antennas p and r is the smallest for all the cases due to their largest separation distance $D_{p,r}$.

5.5 Antennas arrangement and their impact

Extensive simulations have been carried out to the derived space-time correlation functions of the 3-D models and following by the analysis of the correlations for various antenna arrangements. Firstly, several examples are presented here to show the effect of the new 3-D model and its difference from the conventional 2-D model. In what

follows, the impacts of antenna spacing and arrangement of BS antennas and MS antennas in isotropic/nonisotropic scattering are demonstrated. In all examples, except they are stated separately, we define the following parameters: the distance between the BS and MS antennas is $D = 1200$ meter, the radius of the cylinder is $R = 100$ meter, the placement of MS antennas is aligned on Y-axis ($\sigma = 0°$). The angle spread is $\Delta = \arcsin(R/D) \approx 5°$ and the elevation of lower BS antennas is $H = 30$ meters.

In the first examples, the correlation of SIMO channel with one BS antenna and two MS antennas in isotropic scattering is depicted in Figure 5.6. Noted in CASE IV, we show that the correlation of two vertically placed antennas are not affected by the azimuth AOA. Therefore, the nonisotropic models are neglected here. We analyze the correlation of the special case which the two MS antennas are placed vertically and enclosed by the cylinder model and β_m varies from 0° (one-ring model) to 20°. The reader might have noted that $\rho = 90°$, the elevation angle β_m has a significant impact on the correlation between the two MS antennas. It has been shown that the degradation in capacity is small with fading correlation correlation coefficient as high as 0.5 while maximal-ratio combining is employed [50, 51]. According to Figure 5.6, we can attain 0.5 at $D_{lm} = 1.17\lambda$ when β_m is given as 20°. However, the same correlation value 0.5 can only be achieved at $D_{lm} = 2.35\lambda$ for smaller $\beta_m = 10°$. If β_m is zero, the vertically placed antennas always have the correlation $\zeta_{lp,mp} = 1$ that is completely correlated and no diversity gain available. However, the new 3-D isotropic channel model shows that vertically placed MS antennas can have small correlations and are able to provide considerable diversity gain. This is in good agreement with field measurements. Figure 5.7 depicts the effect of the MS 3-D antenna placement in SIMO channel. The simulation results are carried at the angles $\rho = 0°$, 75° and 90° and $\kappa = 0, 3$. Providing that $\beta_m \leq 20°$, the correlation function of MS antennas on the X-Y plane is only a simple 2-D spatial correlation function given in Case III. Thereby, the 2-D Clark's model is sufficient and accurate enough to describe the SIMO channels with horizontally placed

MS antennas. Figure 5.7 shows that the correlation of smaller ρ reduces much faster than that of the larger ρ. For instances, when $\rho = 0°$, the correlation $\zeta_{lp,mp} = 0.5$ is achieved at distance $D_{l,m} = 0.24\lambda$. But MS antennas placed at $\rho = 75°$ and $90°$, respectively, require farther distance $D_{l,m} = 0.89\lambda$ and 2.35λ. Figure 5.7 also depicts the scenario where the MS antennas are enclosed in a 3-D nonisotropic scattering model. It is obvious that the correlations increase dramatically compare to that of isotropic models. Even though the $\rho = 0°$ antenna placement provides the smallest correlation well compared to the others, the antenna placement might not be feasible all the time due to space limit. Thus, the 3-D antenna placements may be the alternative methods to achieve better diversity gain and the new correlation function is a good guidance for the analysis and setup process.

Figure 5.8 shows the impact of κ and β over the correlation of SIMO channel in an isotropic and nonisotropic scattering. Assume the MS antennas are placed at $\rho = 75°$ in an isotropic scattering. It is apparent that the exist of $\beta_m = 20°$ provides the smaller correlation well compared to $\beta_m = 0°$. The second lobe of $\kappa = 0, \beta_m = 20°$ has the maximum value less than 0.05 but that of $\kappa = 0, \beta_m = 0°$ can be as high as 0.4. When $\kappa = 3$, the correlations reduce much slower than that of $\kappa = 0$. Apparently, the correlation increases dramatically when we consider 2-D nonisotropic scattering ($\kappa = 3, \beta_m = 0°$). However, the existence $\beta_m = 20°$ in the nonisotropic scattering decreases the correlation at the same distance and lead to better diversity gain. For instance, when $D_{lm} = 2\lambda$, the correlation given by $\beta_m = 0°, \kappa = 3$ and $\beta_m = 20°, \kappa = 3$ are 0.795 and 0.058, respectively. According to Figure 5.8, 3-D isotropic model is considered as the best case while 2-D nonisotropic model is the worst case in sense of the correlation values. In Figure 5.9, the isometric view of the effect of β_m and κ on the correlations of the SIMO channel at distance $D_{lm} = 1\lambda$ and $\rho = 75°$ is depicted. Obviously, while $\beta_m = 0°$, the correlation value is increasing dramatically with κ. Given that $\kappa \geq 5$, the correlations close to 1 and there are no diversity gain. Fortunately, existence of β_m

can decrease the correlation between the two subchannels. Given that we measure the $\beta_m = 15°$ in the nonisotropic scattering, we can set up the two MS antennas at the distance $D_{lm} = 1\lambda$ and angle $\rho = 75°$. As a consequence, the correlation falls into the "valley" and the two subchannels are totally uncorrelated.

The next example is a MISO channel with three BS antennas and one MS antenna. The BS antennas are arranged in the structure described in CASE V. The pth and qth antennas are placed at the height $H = 30$ meters, and the rth antenna is $V = 30$ meters above the q antenna so that $V/\Pi \neq 0$. The MS antenna enclosed in the isotropic scattering with $R = 300$ meters and the $\beta_m = 10°$. Apparently, the AOA α affects the correlation value dramatically in some cases. As shown in Figure 5.10, the correlation of two vertically placed antennas q and r is always constant regardless of α. While considering the '*inline*' case ($\alpha = 0°$), the horizontally placed antennas are totally correlated but the correlation of the diagonally placed antennas is only 0.522. It is important to note that the vertically placed antennas require larger distance V and R to achieve low correlation. The diagonally placed antennas p and r has the largest distance separation while compared to the previous two antenna arrangements. Therefore, it always has the smallest correlation.

The example of a MIMO channel is presented at last. The Figure 5.11 depicts the correlations of vertically placed MS antennas in 3-D isotropic model whose $\beta_m = 20°$. It is clear that the correlations are significantly effected by the arrangement of the MS antennas and apparently different from the 2-D models when other relevant channel parameters remain the same. Low correlations can be achieved by carefully arranging the MS and BS antennas such that their correlation falls in the "valleys" of the plots. For instance, when $D_{BS}/\lambda = 4.5$, the correlation of the MIMO system always falls in the first "valley" for any spacing of the MS antennas.
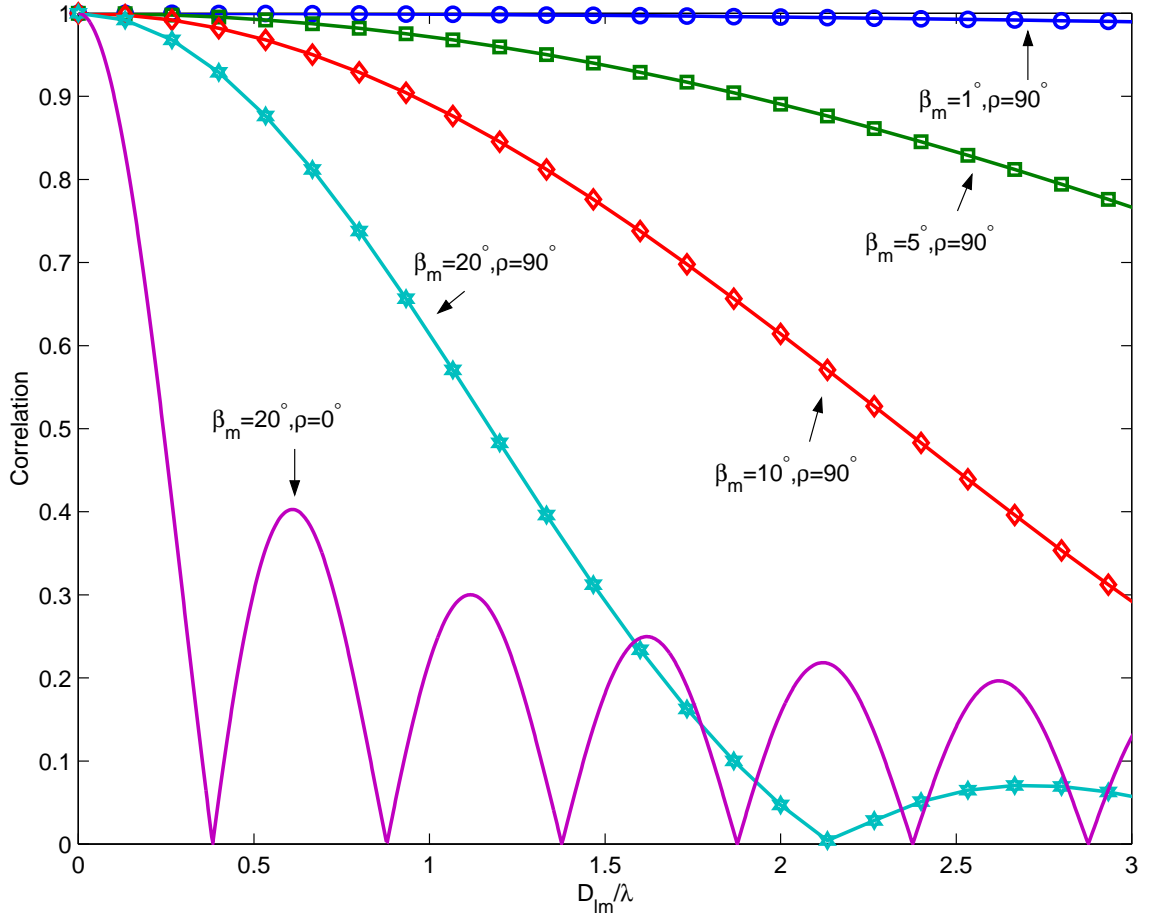
Figure 5.6: The correlation of a SIMO channel with one BS and two MS antennas, placed with $\rho = 0°$ and $90°$.

5.6   Conclusion

In this paper, we have derived the generic flexible and mathematically tractable space-time crosscorrelation functions for 3-D MIMO frequency nonselective Rayleigh fading channel. In our model, we employed the elevation angle β_m to extend the 2-D one-ring scattering model to 3-D cylinder model, and the von Mises distribution to characterize the nonuniform distribution for the angle of arrival around the MS antennas. Other relevant parameters of interest such as the height of BS antennas, the 3-D arrangement of BS and MS antennas and the Doppler spread of MS antennas are taken in account. We also analyze the correlation functions of the conventional 2-D and new 3-D model
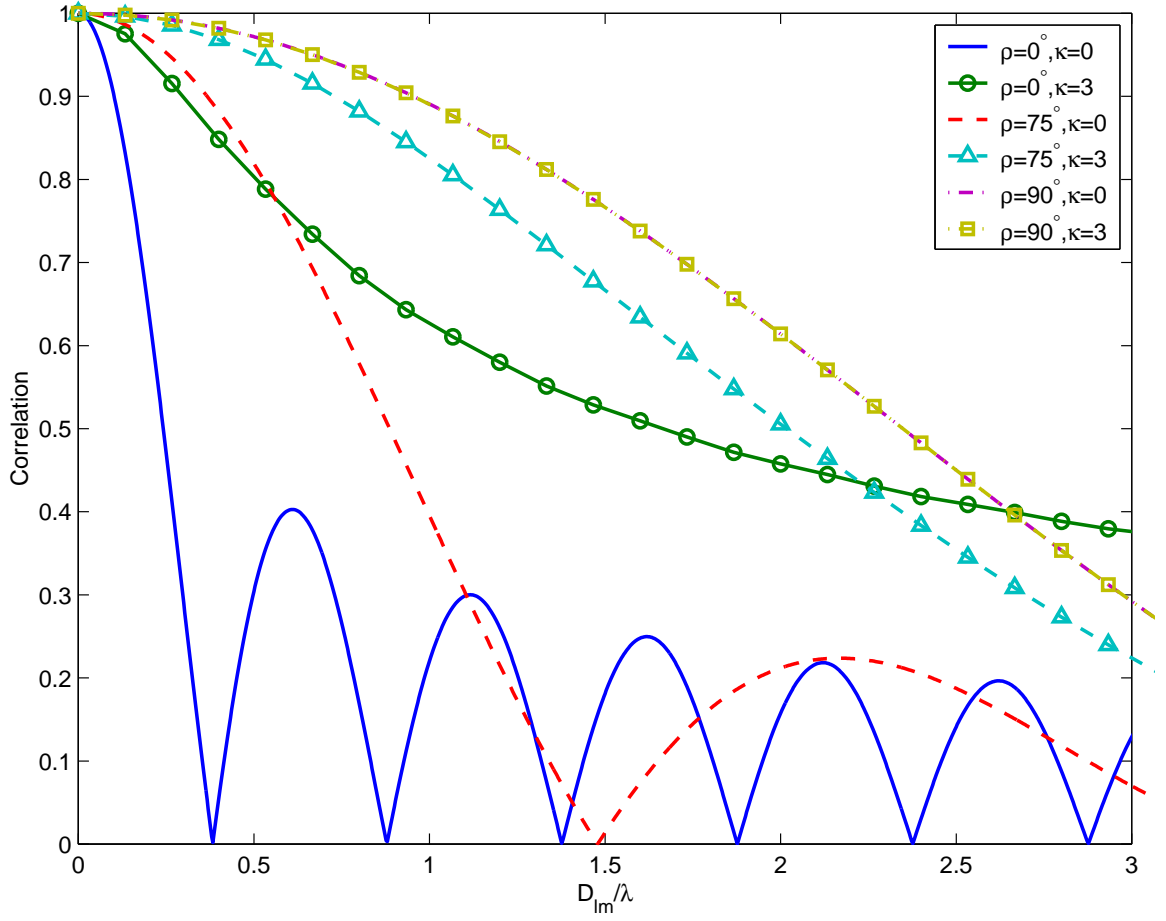
Figure 5.7: The correlation of a SIMO channel with one BS and two MS antennas with 3-D antenna arrangements in isotropic nonisotropic scattering models. The maximum elevation angle of the fading cylinder is $\beta_m = 10°$.

in different antenna arrangements enclosed by isotropic/nonisotropic scattering. It is shown that the proposed closed form function can easily reduced to different well-known cases for SISO, SIMO and MISO fading channels. The simulation results have verified our formulas and further shown that the correlation computed by the proposed function are significantly different from the conventional 2-D one-ring scattering model.
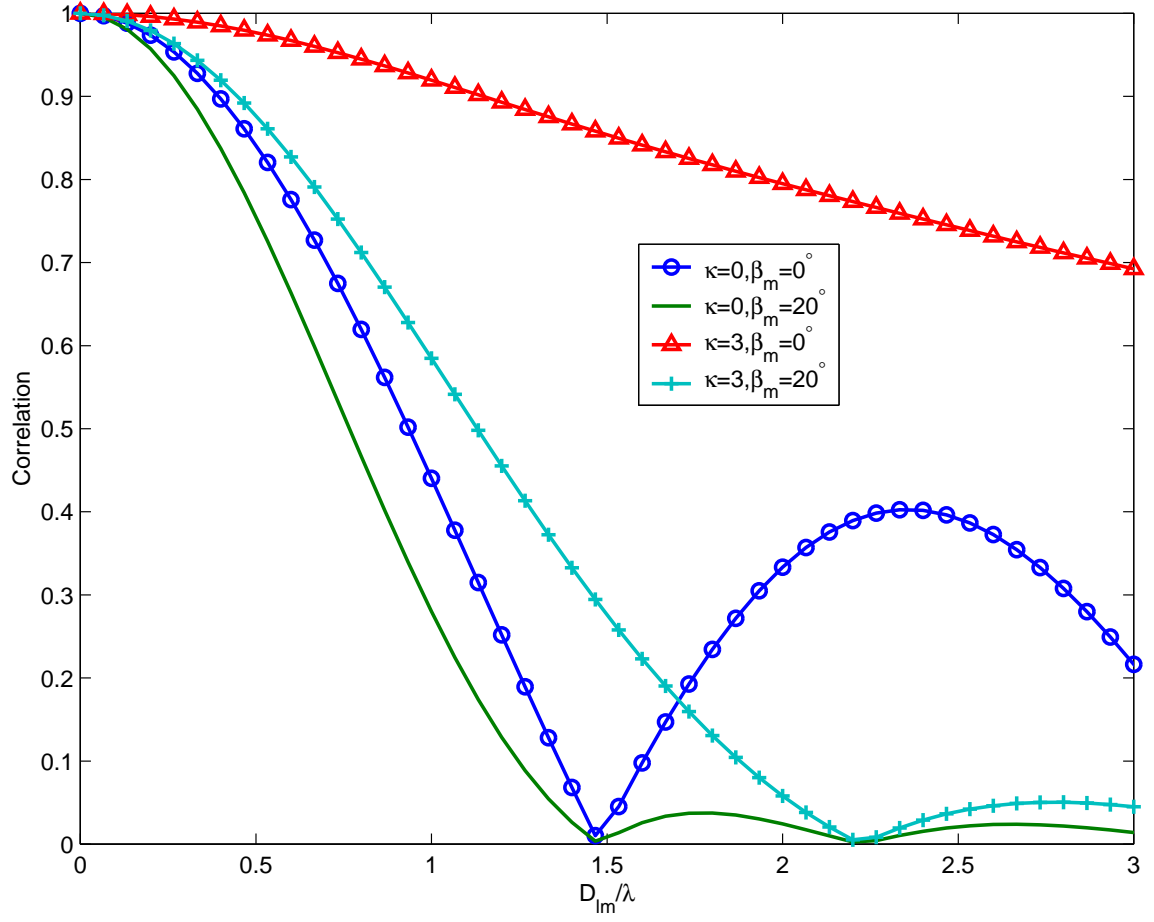
Figure 5.8: The correlation of a SIMO channel with one BS and two MS antennas, placed with $\rho = 75°$.
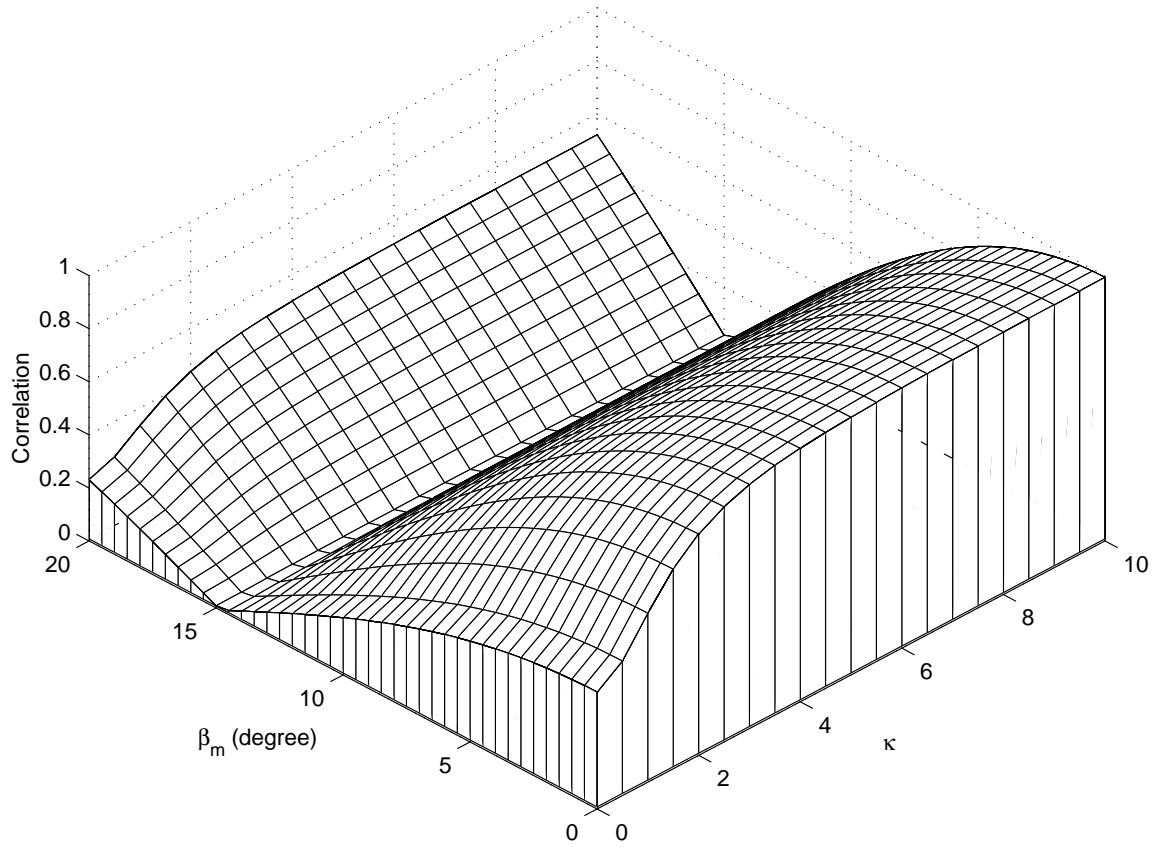
Figure 5.9: Isometric view of the correlation of a 1x2 channel with the two MS antennas placed at $\rho = 75°$.
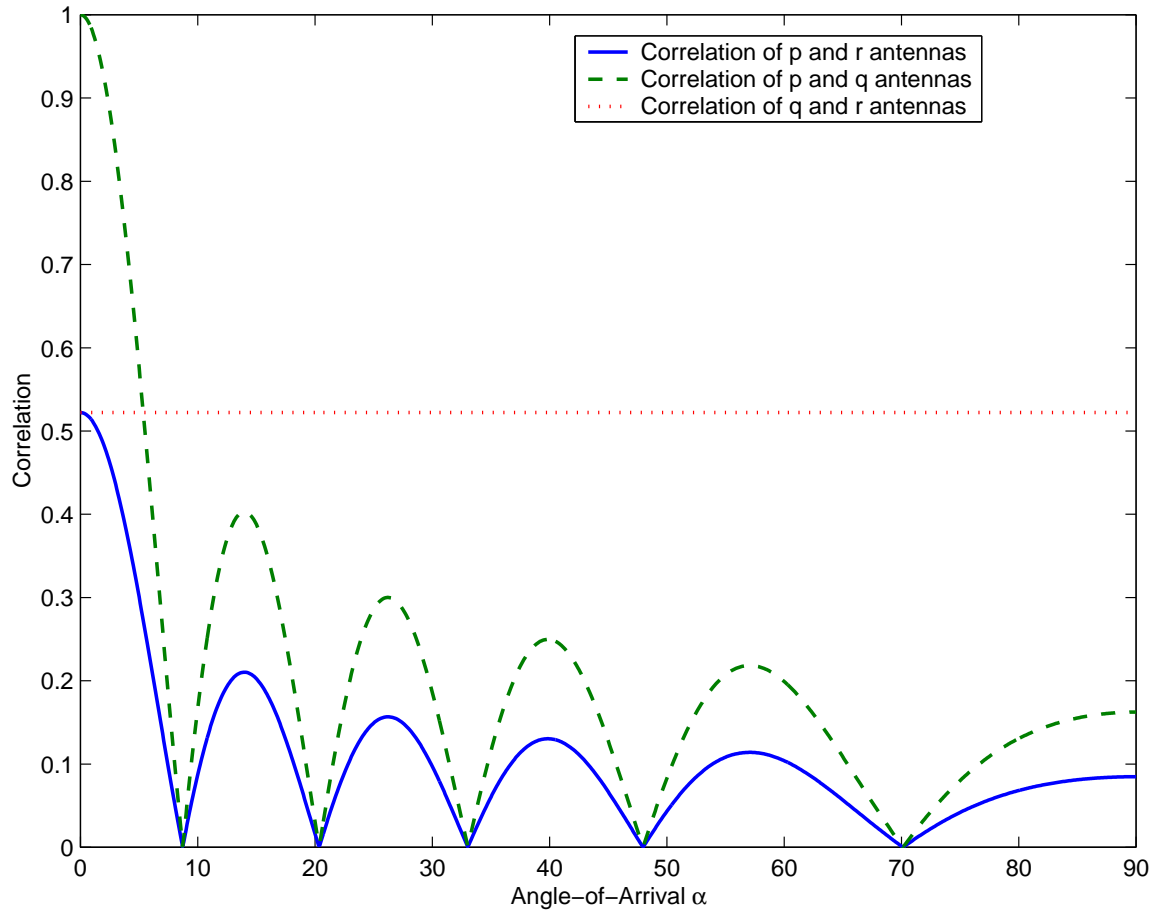
Figure 5.10: The correlation of a MISO channel with one MS and three BS antennas, placed in a right-angled triangle shape.
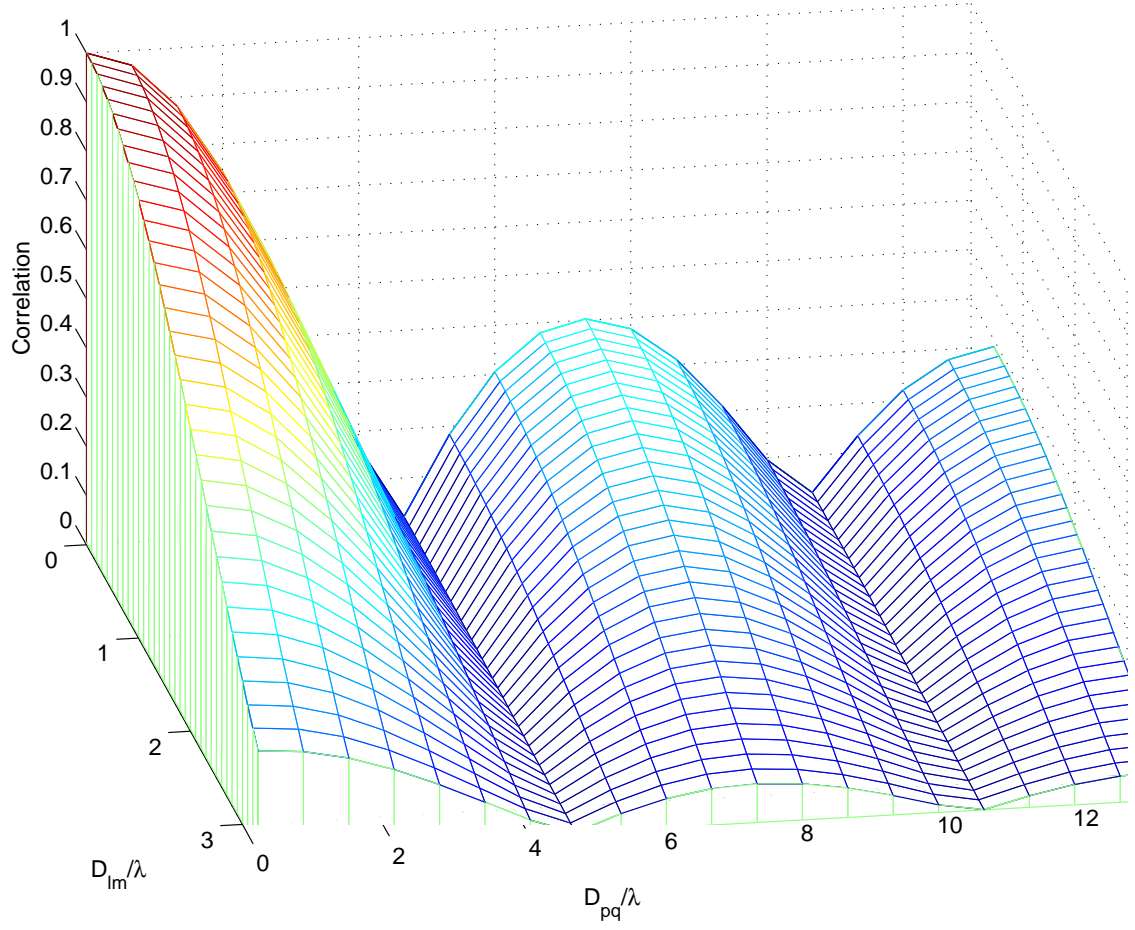
Figure 5.11: Isometric view of the cross-correlation of a 2x2 channel with vertically placed MS antennas ($\rho = 90°$) and $\beta_m = 10°$.

Chapter 6

Conclusion

As was highlighted, the research on the physical layer of wireless communication has been done. Basically, the research areas can be divided into three main categories: channel modeling, channel estimation and channel equalization An overview of each topic is first introduced at the beginning of the chapters. Follows, the relevant informations and necessarily mathematical derivations are illustrated. Finally, we propose the new algorithms or model to improve the system performance of the communication system. Basically, the chapters can be summarized in the following structure.

In Chapter 2, we introduce the 3G 8-PSK EDGE equalization and symbol detection. First of all, the optimum equalizer MLSE based on Viterbi algorithm and near-optimum equalizer DDFSE and RSSE are described in details. To reduce the computational complexity of the equalizer in the system with large signal constellation size and long channel impulse response, we proposed a new method based on minimizing the Euclidean distance between the detected and received signal sequence. Simulation were carried at the EDGE typical channel profiles TU and HT to test the new equalizer. The simulation results show that the new method contributes good performance well compared to RSSE2 and RSSE8 equalizers. Apparently, the new method outperforms the RSSE2 in decoded BER when strong coding is implemented. Although there is a small loss in BER while comparing to RSSE8, we show that our new equalizer only requires approximately quarter of computational complexity of RSSE8. Moreover, the proposed method can be

further implemented in higher constellation system.

In Chapter 3, a novel low complexity decision feedback equalizer is proposed for turbo equalization. The chapter begins with the principle of turbo equalization using trellis-based BER optimal channel equalizer and channel decoder. When the higher modulation signals are used with severely distorted multipath channels, the computational complexity of the MAP equalizer grows exponentially. Moreover, the inefficiency of the conventional low complexity DFE algorithm reduces the gain of BER performance in iterative equalization. To increase the performance gain with low computational complexity, our new method computes the extra metric r_{n+1} using the feedback symbols from previous iteration and combining it with *a priori* information of the symbols. After each iteration, the hard detected symbols are saved in the memory as *a priori* data for next iteration. We verified the proposed algorithm for BPSK and 8PSK modulation. The promising simulation results indicate that the proposed low complexity DFE algorithm always has better BER performance when compared to conventional DFE throughout the iterations in turbo equalization.

Chapter 4 discusses the channel estimation of EDGE system in fast fading channel. According to other researches, the CIRs are always defined as time-invariant while the mobile system travels in slow speed. However, in fast fading channel, the original proposed least-squares algorithm does not provide good estimation in the sense of MSE and BER. So, we proposed a new least-squares based channel estimation algorithm to estimate the time-varying channel. As shown in simulation results, the new algorithm can accurately estimate various of fading channel in wide range of Doppler frequency. In terms of mean square error and bit error rate, the proposed channel estimation algorithm has much better performance especially while Doppler frequency higher than 100Hz. Moreover, we introduce the Cholesky decomposition in brief details to transform the CIR energy to the first few taps for reliable equalization.

We investigate the correlation of the subchannels of MIMO system in Chapter 5.

Based on the researches of the abstract models in multiple antennas systems, we proposed a new 3-D MIMO Rayleigh fading channel model. A closed-form cross-correlation function of the subchannels in 3-D MIMO system is derived to analyze various of channel models such as SIMO, MISO and MIMO. In some special cases, our new correlation function can easily be simplified to other existing equations that were first proposed by other researchers. Simulation have been carried intensively to verify our formula.

6.1   Future Research

This dissertation has covered the basic issues of the physical layer in wireless communication. In order to implement the algorithms successfully in the future wireless communications, further researches into the development is required. The new equalizer proposed in Chapter 2 can be developed and implemented to the MIMO system or turbo equalization system for further improvement in system performance. Also, the iterative equalization introduced in Chapter 3 is a powerful receiver. The proposed low computational complexity algorithm can be further improved and developed into the multiuser detection such as WCDMA or UMTS systems. Although the 3-D Rayleigh fading channel model proposed in Chapter 5 is well enough to describe the channel where the scatterer forms a "cylinder" model or located in certain direction. Research on the abstract model in the dispersive channel can be extended to investigate the correlation of the subchannels where the mobile station antennas received the signals that interfered by the multipath channels.

Bibliography

[1] A. Furuskar, S. Mazur, F. Muller, and H. Olofsson, "EDGE: Enhanced Data Rates for GSM and TDMA/136 Evolution," *IEEE Personal Communications*, vol.6, pp.56-66, June 1999.

[2] ETSI. GSM 05.05, "Radio transmission and reception," ETSI EN 300 910 V8.5.1, Nov. 2000.

[3] P. Stuckman, "The GSM evolution: mobile packet data services," First Edition, John Wiley & Sons, Ltd., 2002.

[4] C.A. Belfiore and J.H. Park, "Decision-feedback equalization," *Proc. IEEE*, vol.67, pp.1143-1156, Aug. 1979.

[5] G. D. Forney, "Maximum Likelihood Sequence Estimation of digital sequences in the presence of intersymbol interference," *IEEE Trans. Inform. Theory*, vol. IT-18, pp. 363-378, May 1972.

[6] V. M. Eyuboglu and S.U. Quereshi, "Reduced-state sequence estimation with set partitioning and decision feedback," *IEEE Trans. Commun.*, vol. 36, pp. 13-20, Jan 1988.

[7] V. M. Eyuboglu and S.U. Quereshi, "Reduced-state estimation for coded modulation on intersymbol interference channels," *IEEE J. Select. Areas Commun.*, vol.7, pp.989-995, 1989.

[8] A. Duel-Hallen and C. Heegard, "Delayed decision-feedback sequence estimation," *IEEE Trans. Commun.*, vol. 37, pp.428-436, May 1989.

[9] G. Foschini, "A reduced state variant of maximum likelihood sequence detection attaining optimum performance for high signal-to-noise ratios," *IEEE Trans. Inform. Theory*, vol.IT-23, pp.605-609, Sept. 1977.

[10] P. Monsen, "Feedback equalization for fading dispersive channels," *IEEE Trans. Info. Theory*, vol.IT-17, pp.56-64, Jan. 1971.

[11] V. Franz and J.B. Anderson, "Concatenated decoding with a reduced-search BCJR algorithm", *IEEE Journal on Selected Areas in Communications*, vol.16, pp.186-195, Feb. 1998.

[12] W.H. Gerstacker and R. Schober, "Equalization Concepts for EDGE," *IEEE Trans. on Wireless Commun.*, vol.1, pp.190-199, Jan. 2002.

[13] J. Proakis, *Digital Communications*, Fourth Edition, McGraw-Hill, 2001.

[14] W. Gerstacker and J. Huber, "Improved equalization for GSM mobile communications," in *Proc. Int. Conft. Telecommunications*, Istanbul, Apr. 1996, 128-131.

[15] M. Schmidt and G.P. Fettweis, "FIR prefiltering for near minimum phase target channels," in *Proc. 6th Canadian Workshop Information Theory*, June 1999.

[16] B. Yang, "An improved fast algorithm for computing the MMSE decision feedback equalizer," *Int. J. Electron. Commun.*, vol.53, no.1, pp.1-6, 1999.

[17] N. Zhou and N. Holte, "Least squares channel estimation for a channel with fast time variation," in *Proc. IEEE ICASSP*, vol. 5, Mar. 1992, pp.165-168.

[18] J. Chen and Y. Wang, "Adaptive MLSE equalizers with parametric tracking for multipath fast fading channels," *IEEE Trans. Commun.*, vol. 49, pp.655-663, 1992.

[19] P. Jung, "Laurent's representation of binary digital continuous phase modulated signals with modulation index 1/2 revisited," *IEEE Trans. Commun.*, vol. 42, No. 2/3/4 pp. 221-224, Apr. 1994.

[20] H. Olofsson and A. Furuskar, "Aspects of introducing EDGE in existing GSM networks," in *Proc. IEEE Int. Conf. Universal Personal Commun.*, vol. 1, 1998, pp. 421-426.

[21] J.C. Olivier, S.Y. Leong, C. Xiao and K.D. Mann, "Efficient Equalization and Symbol Detection for 8-PSK EDGE Cellular System," *IEEE Trans. Veh. Technol.*, vol. 52, pp.525-529, May 2003.

[22] J.C. Olivier and C. Xiao, "Joint optimization of FIR prefilter and channel estimate for sequence estimation," *IEEE Trans. Commun.*, vol.50, pp.1401-1404, Sept. 2002.

[23] A. Klein, G.K. Kaleh, and P.W. Baier "Zero forcing and minimum mean-square-error equalization for multiuser detection in code-division multiple-access channels ," *IEEE Trans. Veh. Technol.*, vol. 45, pp.276-287, May 1996.

[24] S.S. Haykin, *Introduction to adaptive filters*, Macmillan Publishing Company, Canada, pp.129-143, 1984.

[25] Y.R. Zheng and C. Xiao, "Improved models for the generation of multiple uncorrelated Rayleigh fading waveforms," *IEEE Commun. Lett.*, vol.6, pp.256-258, June 2002.

[26] N. Al-Dhahir, J.M. Cioffi, "MMSE decision-feedback equalizers:finite-length results," *IEEE Trans. Inform. Theory*, vol.41, No.4, pp.961-975, Jul. 1995.

[27] N. Al-Dhahir, J.M. Cioffi, "Fast computation of channel-estimate based equalizers in packet data transmission," *IEEE Trans. Signal Processing*, vol. 43, No. 11, pp.2462-2473, Jul. 1995.

[28] C. Douillard *et al.*, "Iterative correction of intersymbol interference: Turbo-equalization," *Euro Trans. Telecommun.*, vol. 6, no. 5, pp.507-511, Sept.-Oct. 1995.

[29] C. Berrou, A. Glavieux, and P. Thitimajshima, "Near Shannon limit error-correcting and decoding: Turbo codes (1)," in *Proc. IEEE Int. Conf. Commun.*, vol. 2, May, 1993, pp. 1064-1070.

[30] L.R. Bahl, J. Cocke, F. Jelinek, and J. Raviv, "Optimal decoding of linear codes for minimizing symbol error rate," *IEEE Trans. of Inform. Theory*, vol. IT-20, pp.284-287, Mar. 1974.

[31] X. Wang and H.V. Poor, "Iterative (Turbo) soft interference cancellation and decoding for coded CDMA," *IEEE Trans. Commun.*, vol. 47, no. 7, pp. 1046-1061, July 1999.

[32] M. Tuchler, A.C. Singer, and R. Koetter, "Minimum mean squared error equalization using a priori information," *IEEE Trans. on Signal Processing*, vol 50, no. 3, pp. 673-683, Mar. 2002.

[33] M. Tuchler, R. Koetter and A.C. Singer, "Turbo equalization: principles and new results," *IEEE Trans. Commun.*, vol. 50, no. 5, May 2002.

[34] M.J. Lopez, K. Zangi, and J. Cheng, "Reduced-complexity MAP equalizer for dispersive channels," in *Proc. IEEE Veh. Technol. Conf.*, Sept. 2000, pp.1371-1375.

[35] R. Otnes and M. Tuchler, "Low-complexity turbo equalization for time-varying channels," in *Proc. IEEE Veh. Technol. Conf.*, May 2002, pp.140-144.

[36] P. Strauch *et al.*, "Turbo equalization for an 8-PSK modulation scheme in a mobile TDMA communication system," in *Proc. IEEE Veh. Technol. Conf.*, vol. 3, Sept. 1999, pp. 1605-1609.

[37] X. Tang and Z. Diang, "Turbo equalization for EDGE system with DDF-SOVA," in *Conf. Rec. 35th Asilomar Conf. Signals, Systems & Computers*, Nov. 2001, pp.295-299.

[38] A. Berthet, R. Visoz, and P. Tortelier, "Sub-optimal turbo-detection for coded 8-PSK signals over ISI channels with application to EDGE advanced mobile system," in *Proc. IEEE PIMRC*, Sept. 2000, pp.151-157.

[39] W.H. Gerstacker, R.R. Muller, and J.B. Huber, "Iterative equalization with adaptive soft feedback," *IEEE Trans. on Commun.*, vol. 48, no. 9, pp.1462-1466, Sept. 2000.

[40] G. Bauch and V. Franz, "A comparison of soft-in/soft-out algorithms for 'Turbo detection'," in *Proc. Int. Conf. Telecomm.*, June 1998, pp. 259-263.

[41] J. Hagenauer, "A Viterbi algorithm with soft-decision outputs and its application," in *Proc. IEEE GLOBECOM '89*, Nov. 1989, pp. 1680-1686.

[42] J. Hagenauer and L. Papke, "Decoding "Turbo"-codes with the soft output Viterbi algorithm," in *Proc. IEEE Inform. Theory*, Jul. 1994, pp. 164.

[43] C. Berrou, P. Adde, E. Angui, and S. Faudeil, "A low complexity soft-output Viterbi decoder architecture," in *Proc. IEEE Int. Conf. Commun.*, May 1993, pp. 737-740.

[44] A. Dejonghe and L. Vandendorpe, "Turbo-equalization for multilevel modulation: an efficient low complexity scheme," in *Proc. IEEE Int. Conf. Commun.*, May. 2002, pp. 1863-1867.

[45] S.L. Ariyavisitakul and Y. Li, "Joint coding and decision feedback equalization for broadband wireless channels," *IEEE J. Select. Areas Commun.*, vol. 16, no. 9, pp. 1670-1678, Dec. 1998.

[46] I.E. Telatar, "Capacity of multi-antenna Gaussian channels," *Eur. Trans. Telecom.*, vol.10, pp.585-595, Nov. 1999.

[47] G.J. Foschini and M.J. Gans, "On limits of wireless communications in a fading environment when using multiple antennas," *Wireless Personal Communications*, vol.6, pp.311-335, 1998.

[48] J. Fuhl, J. P. Rossi, and E. Bonek, "High resolution 3-D direction-of-arrival determination for urban mobile radio," *IEEE Trans. Antennas Propagat.*, vol. 45, pp. 672-682, 1997

[49] P. C. Fannin and A. Molina, "Analysis of mobile radio channel sounding measurements in inner city Dublin at 1.808GHz," in *Proc. Inst. Elect. Eng. Commun.*, vol. 143, 1996, pp.311-316.

[50] J. Salz and J.H. Winters,

"Effect of fading correlation on adaptive arrays in digital mobile radio," *IEEE Trans. Veh. Techno.*, vol. 43, No.4, pp.1049-1057, Nov. 1994

[51] D.S. Shiu, G.J. Foschini, M.J. Gans and J. M. Kahn, "Fading correlation and its effect on the capacity of multielement antenna systems," *IEEE Trans. Commun.*, vol. 48, No.3, pp.502-513, Mar. 2000

[52] T.A. Chen, M.P. Fitz, W.Y. Kuo, M.D. Zoltowski, and J.H. Grimm, "A space-time model for frequency nonselective rayleigh fading channels with applications to space-time modems," *IEEE J. Select. Areas Commun..*, vol. 18, No. 7, pp.1175-1190, July 2000.

[53] S.M. Alamouti, "A simple transmit diversity technique for wireless communication," *IEEE J. Select. Areas Commun.*, vol.16, No.8, pp.1451-1458, Oct. 1998.

[54] R.D. Murch and K.B. Letaief, "Antenna systems for broadband wireless access," *IEEE Commun. Mag.*, Vol. 40, No. 4, pp. 76-83, April 2002.

[55] M.C. Jeruchim, P. Balaban, and K.S. Shanmugan, *Simulation of Communication Systems: modeling, methodology, and techniques*, 2nd Ed., Kluwer Academic Publisher, 2000.

[56] W.C. Jakes, "Microwave Mobile Communication," New York: Wiley, pp.60-65, 1974

[57] K.W. Yip and T.S. Ng, "Efficient simulation of digital transmission over WSSUS channels," *IEEE Trans. Commun.*, vol.43, pp.2907-2913, Dec. 1995.

[58] M.F. Pop and N.C. Beaulieu, "Limitations of sum-of-sinusoids fading channel," *IEEE Trans. Commun.*, vol.49, pp.699-708, Apr. 2001.

[59] Y.R. Zheng and C. Xiao, "Simulation models with correct statistical properties for Rayleigh fading channels," *IEEE Trans. Commun.*, vol.51, pp.920-928, June 2003.

[60] A. Abdi and M. Kaveh, "A versatile spatio-temporal correlation function for mobile fading channels with nonisotropic scattering," in *Proc. IEEE Workshop Stat. Signal Array Processing* Pocono Manor,PA, 1994, pp.58-62.

[61] A. Abdi and M. Kaveh, "A space-time correlation model for multielement antenna systems in mobile fading channels," *IEEE J. Select. Areas Commun.*, vol. 20, No. 3, pp.550-560, Apr. 2002.

[62] A. Abdi, J. A. Barger, and M. Kaveh, "A parametric model for the distribution of the angle of arrival and the associated correlation function and power spectrum at the mobile station," *IEEE Trans. Veh. Technol.*, vol. 51, pp. 425-434, May 2002.

[63] T. Aulin, "A modified model for the fading at a mobile radio channel," *IEEE Trans. Veh. Techno.*, vol. VT-28, pp. 182-203, 1979.

[64] J.D. Parsons and A.M.D. Turkmani, "Characterization of mobile radio signals: model description," *IEE Proc.-I*, vol. 138, No. 6, pp.549-556, Dec. 1991.

[65] A.M.D. Turkmani and J.D. Parsons, "Characterization of mobile radio signals: base station crosscorrelation," *IEE Proc.-I,*vol.138, No. 6, pp.557-565, Dec. 1991.

[66] H.L. Bertoni, *Radio Propagation for Modern Wireless Systems*, Prentice Hall, 2000.

[67] J.P. Kermoal, L. Schumacher, K.I. Pedersen, P.E. Mogensen, and F. Frederiksen, "A stochastic MIMO radio channel model with experimental validation," *IEEE J. Select. Areas Commun.*, vol.20, pp.1211-1226, Aug. 2002.

[68] Y. Yamada, Y. Ebine, and N. Nakajima, "Base station/vehicular antenna design techniques employed in high capacity land mobile communications system,"*Rev. Elec. Commun. Lab.*, NTT, 1987, pp.115-121.

[69] F. Adachi, M.T. Feeney, A.G. Williamson and J.D. Parsons, "Cross-correlation between the envelopes of 900 MHz signals received at a mobile radio base station site," *IEE Proc. F. Commun., Radar and Signal Process*, pp.506-512, 1986.

[70] W.C.Y. Lee, "Level crossing rates of an equal-gain predetection diversity combiner," *IEEE Trans. Commun. Technol.*, vol. 18, pp. 417-426, 1970.

[71] W.C.Y. Lee, "Effect of correlation between two mobile radio base-station antennas," *IEEE Trans. Commun.*, vol.COM-21, No.11, pp.1214-1224, Nov. 1973.

[72] T. Fulghum and K. Molnar, "The Jakes fading model incorporating angular spread for a disk scatterers," in *Proc. IEEE Veh. Technol. Conf.*, Ottawa, ON, Canada, 1998, pp. 489-493.

[73] G.L. Stuber, "Principle of mobile communication," 2nd Edition, Boston, MA:Kluwer, 2001.

[74] I.S. Gradshteyn and I.M. Ryzhik, "Table of integrals, series, and products," 6th Ed., Edited by A. Jeffrey, Academic Press, 2000.

[75] K. Anim-Appiah, "Complex envelope correlations for nonisotropic scattering," *Electron. Lett.*, vol. 34, pp. 918-919, 1998.

[76] M.D. Austin and G.L. Stuber, "Velocity adaptive handoff algorithms for microcellular systems," *IEEE Trans. Veh. Technol.*, vol. 43, pp. 549-561, 1994.

[77] Q. Spencer, M. Rice, B. Jeffs, and M. Jensen, "A statistical model for angle of arrival in indoor multipath propagation," in *Proc. IEEE Veh. Technol. Conf.*, Atlanta, GA, 1996, pp. 160-164.

[78] P. Pajusco, "Experimental characterization of D.O.A at the base station in rural and urban area," in *Proc. IEEE Veh. Technol. Conf.*, Ottawa, ON, Canada, 1998, pp. 993-997.

PUBLICATIONS

[1] J.C. Olivier, S.Y. Leong, C. Xiao, and K.D. Mann, "Efficient equalization and symbol detection for 8-PSK cellular system," *IEEE Trans. on Vehic. Tech.*, vol.52, no.3, May 2003.

[2] C. Xiao, J. Wu, S.Y. Leong, Y.R. Zheng, and K.B. Letaief, "A discrete-time Model for triply selective MIMO Rayleigh fading channels," *IEEE Trans. on Wireless Commun.*, vol. 3, pp. 1678-1688, Sept. 2004.

[3] S.Y. Leong, J. Wu, J.C. Olivier and C. Xiao, "Fast time-varying channel estimation and equalization for 8-PSK system," submitted to *IEEE Trans. on Vehicular Technology*, 2003.

[4] S.Y. Leong, K.P. Lee, and C. Xiao, J.C. Olivier, "Improved DFE algorithm using *a priori* information," submitted to *IEEE Trans. on Vehicular Technology*, 2004.

[5] S.Y. Leong, Y. Zheng, and C. Xiao, "3-D antenna arrangement in MIMO frequency nonselective Rayleigh fading channel," prepared for submission to *IEEE Trans. on Wireless Commun.*

[6] C. Xiao, J. Wu, and S.Y. Leong, Y.R. Zheng, and K.B. Letaief, "A discrete-time model for spatio-temporally correlated frequency-selective MIMO radio channels," in *Proc. IEEE Wireless Communications and Networking WCNC*, vol.1 , March 2003, pp.16-20.

[7] S.Y. Leong, J. Wu, J.C. Olivier, and C. Xiao, "Fast time-varying dispersive channel estimation and equalization for 8-PSK cellular system," in *Proc. IEEE Global Telecommunications Conference 2003 Globecomm'03*, vol. 5, Dec. 2003, pp.2421-2425.

[8] S.Y. Leong, Y. Zheng, and C. Xiao, "Space-time fading correlation function of a 3-D MIMO channel models," in *Proc. IEEE Wireless Communications and Networking WCNC*, vol.2, March 2004, pp.1127-1132.

[9] S.Y. Leong, K.P. Lee, C. Xiao, and J.C. Olivier, "Improved DFE algorithm using *a priori* information," in *Proc. IEEE Vehic. Tech. Conference VTC'F04*, 2004.

VITA

Sang-Yick Leong was born June 28, 1977 in Melaka, Malaysia. After finishing his college in Malaysia, he received his B.S in Electrical Engineering (1999); M.S in Electrical Engineering (2001) at the University of Missouri-Columbia. He will receive the Ph.D. in Eletrical Engineering from University of Missouri-Columbia in May 2005. He is married to Kah-Ping Lee in January 3rd, 2004 and his baby boy named Yick-Ren Leong is born on Oct. 1, 2004.